NOTE TO USERS

The original manuscript received by UMI contains pages with indistinct, light, broken, and/or slanted print. Pages were microfilmed as received.

This reproduction is the best copy available

UMI

Hydrogenation of Crotonaldehyde in a Trickle-bed Reactor with Forced On-Off Liquid Flow

by

David A. Stradiotto

A thesis
presented to the University of Waterloo
in fulfillment of the
thesis requirement for the degree of
Doctor of Philosophy
in
Chemical Engineering

Waterloo, Ontario, Canada, 1998

© David Stradiotto 1998



National Library of Canada

Acquisitions and Bibliographic Services

395 Wellington Street Ottawa ON K1A 0N4 Canada Bibliothèque nationale du Canada

Acquisitions et services bibliographiques

395, rue Wellington Ottawa ON K1A 0N4 Canada

Your file Votre référence

Our file Notre référence

The author has granted a nonexclusive licence allowing the National Library of Canada to reproduce, loan, distribute or sell copies of this thesis in microform, paper or electronic formats.

The author retains ownership of the copyright in this thesis. Neither the thesis nor substantial extracts from it may be printed or otherwise reproduced without the author's permission.

L'auteur a accordé une licence non exclusive permettant à la Bibliothèque nationale du Canada de reproduire, prêter, distribuer ou vendre des copies de cette thèse sous la forme de microfiche/film, de reproduction sur papier ou sur format électronique.

L'auteur conserve la propriété du droit d'auteur qui protège cette thèse. Ni la thèse ni des extraits substantiels de celle-ci ne doivent être imprimés ou autrement reproduits sans son autorisation.

0-612-32859-7



The University of Waterloo requires the signatures of all persons using or photocopying this thesis. Please sign below, and give address and date.

ABSTRACT

In many trickle-bed reactors, thorough wetting of the external catalyst surface is important for successful operation. Since the transport of a non-volatile liquid phase reactant to the catalyst surface occurs by liquid-solid contact only, incomplete catalyst external wetting could reduce reactor performance. Incomplete catalyst external wetting, documented in the literature, can occur in trickle-bed reactors as liquid flow rate is decreased. A possible remedy for incomplete catalyst external wetting is the introduction of large liquid flow pulses to the bed. This pulsing technique constitutes on-off liquid flow or periodic operation. This approach was studied for the hydrogenation of crotonaldehyde in water in a trickle-bed reactor packed with Pd/γ -Al₂O₃ catalyst.

Steady operation of the trickle-bed experiments provided data from which a reaction rate law was developed along with an estimate of the kinetic parameters. The activation energy estimate suggested that the kinetic parameters were obtained under conditions of minimal mass transfer resistance. Further analysis revealed that the rate of hydrogenation was largely controlled by surface kinetics.

Periodic operation of the trickle-bed reactor consisted of periodic interruption of liquid flow, while maintaining a constant hydrogen flow rate. This method was applied to the trickle-bed reactor operating at different combinations of temperature, pressure, period duration and split (fraction of the period with liquid flow). Periodic operation, under some conditions, enhanced conversion compared with steady liquid flow (i.e. steady state), while under other conditions, it did not.

Tracer experiments established the response of catalyst external wetting with liquid flow rate. These experiments show a reduction in catalyst external wetting with decreased liquid flow rate, consistent with the literature.

The improvement was based on more complete catalyst external wetting under periodic operation. The observed poor performance was due to depletion of the liquid phase reactant during the no-liquid-flow portion of the period, suggesting that an optimum period duration and split exist.

A model for both steady-state and periodic operation were proposed and tested against the experimental data.

ACKNOWLEDGEMENTS

I am very grateful to Dr. Robert R. Hudgins and Dr. Peter L. Silveston for their guidance, patience, and for their generous financial support of my project. Working with them has been a truly stimulating and pleasurable learning experience.

The help of the various support staff in the Department of Chemical Engineering is also greatly appreciated.

I would like to thank the many friends I have made at the University and with whom I have shared and continue to share many enjoyable times.

Finally I would like to thank Caralyn, my parents, sister and brother-in-law for their support and constant words of encouragement.

to my parents Mary and Emilio

CONTENTS

1	Introduction	1
2	Literature Review	5
2.1	Outline	5
2.1.1	Flow Regimes of Operation	5
	Trickle-bed Reactors - Qualitative Characteristics and the	6
	Development Steady Operation Models	
2.1.3	Catalyst External Mass Transfer	14
2.1.4	Liquid Holdup	17
2.1.5	Catalyst Wetting	19
2.1.6	Axial Dispersion	20
	Trickle-bed Model Classifications	23
2.2	Periodic Operation	25
2.2.1	Background	25
2.2.2	Reactor Studies	28
2.2.3	Trickle-Bed Reactor Studies	31
2.3	Reaction System	3 <i>5</i>
2.4	Summary	37
3	Experimental Work	39
3.1	Outline	39
3.2	Trickle-Bed Reactor Steady And Periodic Operation Experiments	39
3.2.1	Experimental Equipment	39
3.2.2	Experimental Procedure	41
3.2.3	Planning Trickle-bed Experiments	47
3.3	Hydrodynamic Experiments	48
4	Trickle-Bed Reactor Experimental Results	53
4.1	Outline	53
4.2	Trickle-bed Reactor Steady Operation Experiments	53
4.2.1	Estimation of Kinetic Rate Law and Kinetic Parameters from Steady	53
	Operation Data at 1.1 MPa	33
4.2.2	Estimation of Kinetic Rate Law and Kinetic Parameters from Steady	61
	Operation Data at 0.1 MPa	
4.3	Comparison of Steady and Periodic Operation	69
4.3.1	Comparison of Steady and Periodic Operation Data at 25°C and 1.1	69
	MPa	

4.3.2	Comparison of Steady and Periodic Operation Data at 50°C and 1.1 MPa	84
4.3.3	Comparison of Steady and Periodic Operation Data at 50°C and 0.1 MPa	91
4.4		98
5	Hydrodynamic Experiments	101
5.1	Objective	101
5.2	Liquid Holdup	101
5.3	Catalyst External Wetting	104
6	Application of Periodic Operation to Trickle-Bed Reactors	108
6.1	The Case for Periodic Operation of Trickle-Bed Reactors	108
6.2	Experimental Investigation of a Potential Application	109
7	Modeling	117
7.1	Outline	117
7.2	Trickle-bed reactor models	117
7.2.1	Steady-operation trickle-bed models	117
7.2.2	Steady-operation model A	118
7.2.3	Steady-operation model B	120
7.2.4	Trickle-bed reactor model parameters	121
7.2.5	Periodic operation trickle-bed models	122
7.2.6	Periodic operation models A and B	124
7.2.7	Trickle-bed Reactor System Classification	125
7.2.8	Numerical solution of trickle-bed models	126
7.3	Simulation results	129
7.3.1 7.3.2	Steady operation simulation results at 25°C and 1.1 MPa	129
7.3.3	Periodic operation simulation results at 25°C and 1.1 MPa Steady operation simulation results at 50 °C and 1.1 MPa	134
.3.3 7.3.4	Periodic operation simulation results at 50°C and 1.1 MPa	138 140
7.3.5	Steady and periodic operation simulation results at 50°C and 0.1	143
	MPa	143
7.4	Summary of simulation results	146
8	Conclusions and Recommendations	148
8.1	Conclusions	148
8.2	Recommendations	149
	Appendices	
Α	Crotonaldehyde Feed Concentration and Mole Flow Rates	150
	,	-50

В	Hydrogen Feed Concentration and Mole Flow Rates	151
C		154
D	Three-phase Catalytic Reactor Overall Resistance Derivation	155
E	Sample Calculation of the Surface Reaction Rate Constant	160
	Estimation of k and E ₂ Using the CSTR Form of the Reaction	
	Equation	
F	Sample Calculation of the Surface Reaction Rate Constant	162
	Estimation of k and E _a Using the Integral Form of the Reaction	
	Equation	
G	Trickle-bed reactor resistance analysis to determine the contribution	167
	of various processes to the overall rate of reaction	
H	Axial Dispersion Sample Calculation	170
I	Catalyst External Wetting Correlations	173
J	Estimation of Binary Liquid Diffusion Coefficients at Infinite	176
	Dilution Using the Wilke-Chang Correlation	
K	Experimental Results for Trickle-bed Experiments with Light	178
	Distillate	
L	Experimental Results for Trickle-bed Experiments with Water	181
M	Sample Gas Chromatograph Analysis Data and Calculations	187
N	Reaction Thermodynamics	190
0	Simulation Code Listings	191
P	Liquid Holdup Data	200
Q	Statistical Analyses for First Order Plug Flow Models for Steady and	202
	Periodic Operation	
R	Classification of Trickle-bed Reactor System and Periodic Operation	205
S	Calculation of Catalyst External Wetting from Tracer Experimental	208
	Data	
	Reference List	210
	Nomenclature	214

LIST OF TABLES

2.1	Summary of the dependence of several trickle-bed models on liquid velocity	12
2.2	Parameters used in the gas-liquid mass transfer coefficient of Goto and Smith (Goto et. al., 1975a)	15
2.3	Parameters used in the liquid-solid mass transfer coefficient of Goto and Smith (Goto et. al., 1975a)	16
2.4	Correlations for predicting the liquid phase Peclet number under trickle flow conditions	21
2.5	Bailey's four classes of periodic operation	26
2.6	Classification of periodic operation control problems	29
2.7	Periodic operation reactor studies	31
2.8	Catalytic hydrogenation of crotonaldehyde, temperature: 25°C; pressure: 50 psig; iron was added as ferrous chloride, zinc as zinc acetate, and silver as silver nitrate (from Rylander, 1967).	36
2.9	Reaction rate constants for crotonaldehyde hydrogenation in a slurry reactor	37
3.1	Trickle-bed reactor experiment design	47
3.2	Matrix of liquid flow rates and experimental sets with anticipated controlling mechanism	48
4.1	Trickle-bed reactor steady operation data for estimation of kinetic rate parameters	54
4.2	Ratio of dissolved hydrogen and crotonaldehyde concentrations (mol H ₂ /mol crotonaldehyde)	55
4.3	Estimates of the kinetic rate constant of equation (4.2) from trickle- bed steady operation experimental data (1.1 MPa hydrogen pressure)	56
4.4	Estimates of the activation energy for the reaction rate constants of Table 4.3	56
4.5	Reaction rate constant estimates for steady operation at 25°C and 50°C and 1.1 MPa	60
4.6	Activation energy estimates for steady operation at 1.1 MPa	61
4.7	Kinetic rate constants for equation (4.8)	64
4.8	Fluid flow ranges for Goto-Smith liquid solid mass transfer coefficient correlation	66
4.9	Apparent rate constants for steady operation at 25°C and 1.1 MPa	73
1.10	Comparison of Apparent Rate Constants for Steady and Periodic Operation at 25°C and 1.1 MPa	82
1.11	Comparison of Apparent Rate Constants for Steady and Periodic Operation at 25°C and 1.1 MPa, based on the highest apparent k value observed	83
6.1	Typical hydrodesulphurization operating conditions (Gianetto and Silveston, 1986)	109

6.2 Hydrodesulphurization LHSVs converted to equivalent space times and liquid flow rates for the reactor used in this study

LIST OF ILLUSTRATIONS

2.1	Concentration profiles for trickle-bed reactors (Fogler, 1986)	13
2.2		17
	flow rate	
2.3	Mears criterion for neglecting axial dispersion as a function of conversion and liquid volumetric flow rate for the experimental trickle-bed (L/d_p is the ratio of catalyst bed length to catalyst particle diameter)	23
2.4	Output vs. input for a hypothetical process	27
2.5	Typical square wave used in periodic operation	30
2.6	Comparison of steady state and time-average AMS conversion under periodic operation (Lange et al., 1995)	33
3.1	Experimental trickle-bed reactor process flow diagram	40
3.2		42
3.3	Catalyst bed detail	42
3.4	•	43
3.5	Prepacking section	43
3.6	•	44
3.7	Outlet section rotated 90°	44
3.8	Catalyst bed cross-section	45
3.9		45
3.10	Hydrodynamic packed bed flow diagram (S = solenoid actuated valve)	50
4.1	Contributing resistances to overall reaction rate as a function of liquid flow rate for steady operation experiments at 25 °C, 1.1 MPa and 50	58
	°C, 1.1 MPa	
4.2	than 100 mL/min) for 25°C and 1.1 MPa	59
4.3	First order plot of steady-state data at high liquid flow rates (greater than 100 mL/min) for 50°C and 1.1 MPa	60
4.4	Steady-state crotonaldehyde conversion vs. liquid flow rate data for 25°C, 1.1 MPa, 50°C, 1.1 MPa, and 50°C, 0.1 MPa	62
4.5	First order plot of steady-state data at high liquid flow rates (greater than 100 mL/min) for 50°C and 0.1 MPa	65
4.6		66
	flow rate for steady operation experiments at 50 °C, 0.1 MPa	00
4.7	Contributing resistances to overall reaction rate as a function of liquid	68
	flow rate for steady operation at 25°C and 50 °C, 1.1 MPa, assuming a	•
	liquid-solid mass transfer coefficient twice that predicted by the Goto-	
	Smith correlation	
4.8	Contributing resistances to overall reaction rate as a function of liquid	68
	flow rate for steady operation at 25°C and 50 °C, 1.1 MPa, assuming a	
	liquid-solid mass transfer coefficient half that predicted by the Goto-	
	Smith correlation	

4.9	Crotonaldehyde conversion vs. liquid flow rate under steady operation, 25 °C, 1.1 MPa, liquid flow rate range: 0 to 450 mL/min	70
4.10	First order rate law plot for steady operation, 25 °C, 1.1 MPa, liquid	71
	flow rate range: 0 - 450 mL/min	
4.11	First order rate law plot for steady operation, 25 °C, 1.1 MPa	71
	Comparison of experimental data, liquid flow rate range: 50 - 450	
	mL/min with first order model fitted over entire flow rate range (5 -	
	450 mL/min)	
4.12	Steady operation first order plug flow model 25 °C, 1.1 MPa, liquid	72
	flow rate range: 0 - 50 mL/min	
4.13	Steady operation first order plug flow model, 25°C, 1.1 MPa, liquid	72
	flow rate range: 50 - 450 mL/min	
4.14	Steady and periodic operation (5 min period, 0.5 split) first order rate	74
	law plot, 25 °C, 1.1 MPa, liquid flow rate range: 50 - 500 mL/min	
4.15	Steady and periodic operation (5 min period, 0.5 split) crotonaldehyde	75
	conversion vs. liquid flow rate, 25 °C, 1.1 MPa	, ,
4.16	Steady and periodic operation (5 min period, 0.1 split) first order rate	76
	law plot, 25 °C, 1.1 MPa, liquid flow rate range: 0 - 50 mL/min	70
4.17	Steady and periodic operation (5 min period, 0.1 split), 25 °C, 1.1	76
1.17	MPa, Conversion vs. Liquid flow rate	70
4.18	Comparison of catalyst external wetting under steady and periodic	78
7.10	operation as a function of time-average liquid flow rate	70
4.19	Ratio of external catalyst wetting under periodic operation (5 minute	79
7.17	period) to that under steady operation as a function of time-average	19
	liquid flow rate	
4.20	Steady and periodic operation (20 min period, 0.5 split), first order	80
7.20	rate law plot, 25 °C, 1.1 MPa, liquid flow rate range: 50 - 450 mL/min	80
4.21	Steady and periodic operation (20 min period, 0.5 split), 25 °C, 1.1	80
7.21		80
4 22	MPa, Conversion vs. Liquid flow rate	0.1
4.22		81
4 2 2	rate law plot, 25 °C, 1.1 MPa, liquid flow rate range: 0 - 50 mL/min	0.4
4.23	Steady and periodic operation (20 min period, 0.1 split), 25 °C, 1.1	81
4 2 4	MPa, Conversion vs. liquid flow rate	0.5
4.24	Steady operation crotonaldehyde conversion vs. liquid flow rate, 50°C, 1.1 MPa	85
4.25		0.5
4.26	Steady operation first order plot, 50°C, 1.1 MPa	85
4.20	Steady and periodic operation 5 min period, 0.1 split Crotonaldehyde	87
4 27	conversion vs. Liquid flow rate, 50°C, 1.1 MPa	00
4.27	Steady and periodic operation 5 min period, 0.5 split Crotonaldehyde	88
4 20	conversion vs. liquid flow rate, 50°C, 1.1 MPa	
4.28	Steady and periodic operation 20 min period, 0.1 split Crotonaldehyde	88
4 20	conversion vs. liquid flow rate, 50°C, 1.1 MPa	
4.29	Steady and periodic operation 20 min period, 0.5 split crotonaldehyde	89
	conversion vs. liquid flow rate, 50°C, 1.1 MPa	

4.30	Conversion ratios for periodic to steady operation, 0.1 split, 0 - 50 mL/min, 50°C, 1.1 MPa	90
4.31	Conversion ratios for periodic to steady operation, 0.5 split, 0 - 450	91
	mL/min, 50°C, 1.1 MPa	
4.32	Steady operation crotonaldehyde conversion vs. liquid flow rate, 50°C, 0.1 MPa and 50°C, 1.1 MPa	92
4.33	Conversion ratio for steady operation at 50°C, 1.1 MPa and 50°C, 0.1	93
	MPa	
4.34	Steady and periodic operation (5 min period, 0.1 split) crotonaldehyde conversion vs. liquid flow rate, 50°C, 0.1 MPa	95
4.35	Steady and periodic operation (5 min period, 0.5 split) crotonaldehyde conversion vs. liquid flow rate, 50°C, 0.1 MPa	95
4.36	Comparison of periodic operation at 25°C and 50°C, 1.1 MPa for a 5 min period and 0.1 split	96
4.37	Comparison of periodic operation at 25°C, 1.1 MPa and periodic operation at 50°C, 0.1 MPa for a 5 min period and 0.5 split	96
4.38	Steady and periodic operation (20 min period, 0.1 split)	97
	crotonaldehyde conversion vs. liquid flow rate, 50°C, 0.1 MPa	
4.39	Steady and periodic operation (20 min period, 0.5 split)	97
	crotonaldehyde conversion vs. liquid flow rate, 50°C, 0.1 MPa	
5.1	Total static liquid holdup and external static liquid holdup as a	102
	function of gas flow rate	
5.2	Time response of dynamic liquid holdup drainage from the catalyst	103
	bed as a function of gas flow rate	
5.3	Dynamic liquid holdup as a function of liquid and gas flow rate	104
5.4	Catalyst external wetting efficiency as a function of liquid flow rate	105
5.5	Catalyst external wetting as a function of liquid flow rate with experimental data shifted	106
6.1	Crotonaldehyde conversion as a function of liquid flow rate, gas flow rate and bed depth	111
6.2	First order plot of steady operation data at different gas/liquid ratios	112
6.3	Comparison of steady and periodic operation crotonaldehyde conversion - effect of cycle period	114
6.4		114
6.5	Comparison of quasi-steady and steady crotonaldehyde conversion	115
6.6	Comparison of quasi-steady and periodic operation crotonaldehyde conversion - effect of cycle period	115
6.7		116
U. /	Conversion - Effect of Flush Duration	110
7.1	Gas-liquid-solid contact at the particle level for Model A	120
7.2	Gas-liquid-solid contact at the particle level for Model B	121
7.3	• •	130
	and complete catalyst wetting $(f = 1)$	

7.4	Steady operation Model B assuming variable catalyst external wetting	131
	with experimental data (Mills-Dudukovic wetting correlation used)	
	and complete catalyst wetting $(f = 1)$	
7.5	,	131
7.6	,	132
7.7	Bulk liquid phase crotonaldehyde concentrations as predicted by simulation Model A under steady operation at 25°C and 1.1 MPa	133
7.8	Crotonaldehyde concentrations at the catalyst outer surface as predicted by simulation Model A under steady operation at 25°C and 1.1 MPa	133
7.9	Comparison of periodic and steady operation model with experimental data at 25°C and 1.1 MPa; periodic operation parameters: 0.1 split 5 minute period	135
7.10	Comparison of periodic and steady operation model with experimental data at 25 °C and 1.1 MPa; periodic operation parameters: 0.5 split 5 minute period	135
7.11	Comparison of periodic and steady operation model with experimental data at 25 °C and 1.1 MPa; periodic operation parameters: 0.1 split 20 minute period	136
7.12	Comparison of periodic and steady operation model with experimental data at 25 °C and 1.1 MPa; periodic operation parameters: 0.5 split 20 minute period	137
7.13	Steady operation Model A assuming variable catalyst external wetting with experimental data (Mills-Dudukovic wetting correlation used) and complete catalyst wetting $(f = 1)$	138
7.14	Steady operation Model B assuming variable catalyst external wetting with experimental data (Mills-Dudukovic wetting correlation used) and complete catalyst wetting $(f = 1)$	139
7.15	Steady Model A normal deviate for complete and variable wetting	139
7.16	Steady Model B normal deviate for complete and variable wetting	140
7.17	Comparison of periodic and steady operation model with experimental data at 50°C and 1.1 MPa; periodic operation parameters: 0.1 split 5 minute period	141
7.18	Comparison of periodic and steady operation model with experimental data at 50°C and 1.1 MPa; periodic operation parameters: 0.5 split 5 minute period	141
7.19	Comparison of periodic and steady operation model with experimental data at 50°C and 1.1 MPa; periodic operation parameters: 0.1 split 20 minute period	142
7.20	Comparison of periodic and steady operation model with experimental data at 50°C and 1.1 MPa; periodic operation parameters: 0.5 split 20 minute period	142
7.21	Steady operation Model A assuming variable catalyst external wetting with experimental data (Mills-Dudukovic wetting correlation used) and complete catalyst wetting $(f = 1)$	143

7.22	Steady operation Model B assuming variable catalyst external wetting with experimental data (Mills-Dudukovic wetting correlation used) and complete catalyst wetting $(f = 1)$	144
7.23	Comparison of periodic and steady operation model with experimental data at 50°C and 0.1 MPa; periodic operation parameters: 0.1 split 5 minute period	144
7.24	Comparison of periodic and steady operation model with experimental data at 50°C and 0.1 MPa; periodic operation parameters: 0.5 split 5 minute period	145
7.25	Comparison of periodic and steady operation model with experimental data at 50°C and 0.1 MPa; periodic operation parameters: 0.1 split 20 minute period	145
7.26	Comparison of periodic and steady operation model with experimental data at 50°C and 0.1 MPa; periodic operation parameters: 0.5 split 20 minute period	146

CHAPTER

ONE

INTRODUCTION

Trickle-bed reactors are used for a wide range of chemical processes. Some of these processes include general hydrogenation, oxidation, and several important petroleum processes including hydrodesulphurization, hydrodenitrogenation and hydrotreatment. These last three processes are significant not only because they are used to raise the quality of finished products such as diesel fuel and gasoline but also they are used to treat the feedstocks which are then sent to other process units, especially catalytic units. Without treatment of these feedstocks, catalyst poisoning of a unit further downstream is always a threat. A comprehensive list of these and other applications for trickle-bed reactors is given by Mills and Dudukovic (1984) and Ramachadran (1983).

This project is a study of the effect of periodic operation on trickle-bed reactor (TBR) performance. The study attempts to explain observed phenomena mechanistically and to suggest when periodic operation may be beneficial or detrimental to TBR performance. While the literature abounds with studies of conventional TBR operation, TBR periodic-operation literature is sparse. The study by Haure et.al. (1989) represents one of the first studies of periodic TBR operation. However the system studied differed in several key ways from the one in this project. First, in the Haure study, the two reactants were in both the gas and liquid phases while in this study one reactant is only in the gas and one is in the liquid phase. In the former, the reaction can occur when the liquid reactant meets the gas-covered catalyst as well as when the gaseous reactant meets liquid-covered catalyst. Second, the Haure system exhibited exothermicity due to the concentrations of reactants, and the heats of reaction and dilution. These considerations fundamentally change the way in which the system can behave as compared to the system studied in this project.

More recent studies of the effect of periodic operation on TBR performance were those of Lange (1992) and Castellari and Haure (1995). In both studies α -methylstyrene was hydrogenated to cumene. However the reaction system of those authors differed from the one used in this project in that the liquid phase concentrations of α -methylstyrene were large enough to cause significant exothermicity in the system.

A motivation for studying this system was to emulate a process involving the reaction of a dilute non-volatile liquid phase component with a weakly soluble gas reactant. Hydrodesulphurization, hydrodenitrogenation, and aqueous-phase oxidation of organic pollutants are reactor systems falling into this category. Crotonaldehyde was chosen for its ease of hydrogenation at ambient temperature and mild pressure (about 10 atm). The hydrogenation of crotonaldehyde can proceed according to the following reactions

$$CH_3CH = CHCHO + H_2 \xrightarrow{k_1} CH_3(CH_2)_2CHO$$

 $CH_3CH = CHCHO + H_2 \xrightarrow{k_2} CH_3CH = CHCH_3OH$

The main objectives of this project are:

- 1. To test if periodic operation influences conversion.
- 2. To determine the relationship between the experimentally observed conversion under periodic operation and the regime of operation which is defined in terms of measurable trickle-bed reactor parameters.
- 3. To find a mechanistic explanation of the observed experimental behaviour.
- 4. To recommend how periodic operation can be applied.

To accomplish these objectives, experiments were conducted. Additional information regarding the analysis and behaviour of trickle-bed reactors was either obtained experimentally or from the research literature. This information included the important aspects of characterizing trickle-bed reactors such as mass transfer, external

catalyst wetting and liquid holdup. The fundamentals of periodic operation from the literature are presented with emphasis on the those studies implementing periodic operation for trickle-bed reactors. The literature review is presented in Chapter 2.

The original hypothesis of this project was that gas-liquid mass transfer could be enhanced by periodic operation, as shown by the Haure study even though the reactants were distributed between gas and liquid phases differently in the present study. However, hydrogenation rates are not necessarily diffusion controlled; for example, hydrodesulfurization is often surface-reaction controlled (Shah, 1979). What does commonly occur under steady-operation in trickle-beds is poor catalyst wetting, especially under low liquid flow rates. As a result, catalyst utilization is reduced and the potential occurs for hot spots on the dry zones of catalyst surface if the liquid phase reactant is volatile. Both effects are undesirable. Periodic operation in the form of onoff liquid pulses present an alternative to steady liquid-flow operation. The higher liquid flow pulse should improve external catalyst wetting since at higher liquid flow rates, external catalyst wetting is greater as has been demonstrated in the literature (Mills and Dudukovic, 1981). Therefore the second hypothesis is that periodic operation can improve hydrogenation rates as compared to steady operation since effective external catalyst wetting with the liquid phase is increased.

The equipment, operational methods, and an experimental plan are outlined in Chapter 3. Experiments to test the hypothesis were attempted. First, crotonaldehyde hydrogenation experiments under steady operation were performed. Estimates of kinetic parameters suggested which steps in the hydrogenation of crotonaldehyde were rate determining. The first set of experiments were determined to be in a regime of operation where surface reaction of crotonaldehyde was rate controlling. Periodic-operation experiments were then designed, conducted and compared with comparable steady-operation experiments. Next, two other sets of experiments were conducted in different regimes of operation. In one set, the hydrogenation of crotonaldehyde was

controlled largely by liquid-solid mass transfer. In another set, the crotonaldehyde hydrogenation rate was controlled by the transport of hydrogen to the catalyst surface.

In Chapter 4, the observed results are discussed and a mechanistic explanation for the observed behaviour is suggested. Kinetic parameters results are also presented. The suitability of periodic operation as an alternative for operating trickle-bed reactors is discussed also. Chapter 5 presents the results of hydrodynamic experiments. In Chapter 6, a test application of the hydrogenation of crotonaldehyde diluted in naptha is presented with some results. Chapter 7 is a presentation of steady-operation and periodic-operation mathematical models. The details of numerical solution of the mathematical models are outlined. Finally, steady-operation and periodic-operation simulation results are compared with experimental data. In the last chapter, Chapter 8 conclusions and recommendations are presented.

LITERATURE REVIEW

2.1 Outline

The literature covering the steady operation of trickle-bed reactors is vast. Reviews of the state of knowledge of trickle-bed reactors include Satterfield (1975), Koros (1976), Herskowitz and Smith (1983), and most recently Gianetto and Specchia (1992). While these papers span almost 40 years (the earliest paper cited by Satterfield is dated 1952), the papers focus on common elements such as the flow regimes of operation, and the characteristics of trickle-bed reactors including catalyst wetting, interphase mass transfer, and liquid holdup, all of which are highly coupled phenomena. Many papers also present the quantitative prediction of trickle-bed behavior by appropriate mathematical models. This chapter will review the state of understanding of trickle-bed reactor behavior under steady and periodic operation.

2.1.1 Flow Regimes of Operation

Fundamentally, two processes occur simultaneously in a trickle-bed reactor: mass transfer and chemical reaction. Mass transfer occurs externally on catalyst particles as well as within the catalyst pores, the former process being convective, the latter being primarily diffusive. Chemical reaction in heterogeneous catalytic systems includes adsorption of reactants on the catalyst surface, chemical reaction of the adsorbed species, and subsequent desorption of the products. It is the sum of the rates of mass transfer and chemical reaction which determine how the trickle-bed reactor performs. If the overall rate of product formation is limited by mass transfer, then the system can be said to be mass transfer limited. Similarly, if the rate of product formation is limited by chemical reaction, then the system can be said to be reaction limited. Of course it is also possible to find situations where

both processes are significant in limiting the rate of product formation. To gauge whether a trickle-bed reactor will be mass transfer limited, reaction limited, or somewhere between the two extremes requires a knowledge of reaction kinetics and of the various mass transfer coefficients in the system. The latter are determined by the flow regime within the reactor.

Conventional trickle-bed reactors packed with catalyst operate with liquid and gas flowing cocurrently over the catalyst. Cocurrent flow is used since lower pressure drop can be achieved compared with counter-current flow. The term trickle-bed implies that the reactor is operating in the trickling regime. This regime is characterized by relatively low liquid and gas flows compared to some of the highly interacting flow regimes. As a consequence, the hydrodynamic parameters of the trickle-regime such as external catalyst wetting, gas-liquid and liquid-solid mass transfer coefficients, and liquid dynamic and static holdups will be different from those in other flow regimes. All hydrodynamic parameters discussed in this chapter will be with reference to the trickle-flow regime. The reason for focusing on the trickle-flow regime is that most industrial reactors operate in this regime (Frye and Mosby, 1967; Satterfield, 1975).

2.1.2 Trickle-Bed Reactors - Qualitative Characteristics and the Development of Steady Operation Models

Several physical parameters appear to influence the behavior of a trickle-bed reactor under steady operation. These include reaction kinetic rate constants, catalyst effectiveness factors, dynamic and static liquid holdups, gas-gas, gas-liquid, and liquid-solid mass transfer coefficients, external and internal catalyst wetting, and the radial spread of liquid in the reactor. These parameters arise from the mathematical models derived to explain observed behavior. One approach to modeling a trickle-bed reactor is to start with the most comprehensive model and then simplify it by making assumptions about the physical behavior of the system to

which it applies. Ideally the simplest model should be used to explain observed behavior, provided the assumptions are justified.

One of the most comprehensive trickle-bed reactor models is given by Gianetto and Silveston (1986) and also more recently by Gianetto and Specchia (1992). The model consists of a mass balance for each species in each phase, an energy balance, and a momentum balance:

Reaction:
$$v_A A + v_B B \rightarrow products$$
 (2.1)

Gas Phase Mass Balance (assuming non-volatile B)

$$-D_{A,Gas} \frac{d^{2}C_{A,Gas}}{dz^{2}} + u_{Gas} \frac{dC_{A,Gas}}{dz} + k_{L}a_{LA}(HC_{AG} - C_{AL}) = 0$$
 (2.2)

Liquid Phase

$$-D_{A,L}\frac{d^{2}C_{A,L}}{dz^{2}}+u_{L}\frac{dC_{A,L}}{dz}-k_{L}a_{LA}(HC_{AG}-C_{AL})+k_{S}a_{SA}(C_{AL}-C_{AS})=0$$
 (2.3)

$$-D_{B,L}\frac{d^{2}C_{B,L}}{dz^{2}}+u_{L}\frac{dC_{B,L}}{dz}+k_{S}a_{SB}(C_{BL}-C_{BS})=0$$
(2.4)

Solid Phase

$$\frac{k_{s}a_{sA}(C_{AL}-C_{AS})}{v_{A}} = \frac{k_{s}a_{sB}(C_{BL}-C_{BS})}{v_{B}} = (1-\varepsilon_{B})k_{v}\eta_{C}\eta(C_{AS})^{m}(C_{BS})^{n}$$
(2.5)

Energy (Heat) Balance

$$-\lambda_{eff} \frac{d^2T}{dz^2} + (u_L \rho_L C_{PL} + u_G \rho_G C_{PG}) \frac{dT}{dz} = (1 - \varepsilon_B) k_v \eta_C \eta (C_{AS})^m (C_{BS})^n (-\Delta H_R)$$
(2.6)

Momentum

$$\frac{dP}{dz} = f(\varepsilon_B, \psi, d_P, D_T, \rho_L, u_L, \rho_G, u_G, \mu_L, \sigma_L, \dots)$$
 (2.7)

A few notes on the above equations:

- 1. The first term in each fluid mass balance is an axial dispersion term, the second is a convective transport term, and the remaining terms are accumulation/depletion terms in the form of mass transfer terms. Radial dispersion is neglected. Both dispersion terms can be neglected if mass transfer by diffusion is small compared to convective mass transfer or chemical reaction.
- 2. Since B is assumed to be nonvolatile, a gas phase mass balance does not exist. Secondly B is transferred only to the solid phase (catalyst).
- 3. Since the model describes a steady-state liquid phase, the mass transfer rates of A and B are equal to each other and to the rate of formation of products.
- 4. The energy balance ignores no mechanical energy terms. Also it treats the gas and liquid phases as a pseudo-homogeneous phase.
- 5. The momentum balance in trickle-bed reactors is usually described by a pressure drop correlation.

Gianetto and Silveston (1986) and Gianetto and Specchia (1992) suggest the following simplifying assumptions to make the model easier to work with:

- 1) For large deep beds liquid axial dispersion D_L , gas axial dispersion D_G , and effective thermal conductivity λ_{eff} can be neglected.
- 2) If one reactant is in large excess, its mass balance may be dropped because its concentration should be constant throughout the bed.

- 3) Good catalyst wetting means the contacting efficiency η_c can be set to unity.
- 4) If the gaseous reactant is very soluble, pressure drop will have little influence on conversion in the reactor, allowing the momentum balance to be neglected.
- 5) For sufficiently low chemical reaction rates, interparticle and intraparticle mass transfer do not affect the apparent reaction rate, eliminating the solid phase mass balance equation.
- 6) For isothermal operation, the heat balance can be neglected.

With the assumptions listed above, and assuming A is in large excess, only a mass balance on component B, the liquid phase reactant remains. If the reaction is first order and by substitution of equation (2.5) into simplified equation (2.4) gives

$$u_{L} \frac{dC_{B,L}}{dz} + (1 - \varepsilon_{B})k_{v}\eta C_{B,L} = 0$$
 (2.8)

Integration of (2.8)

$$\int_{C}^{C_{o}} \frac{dC_{B,L}}{C_{B,L}} = \frac{k_{v}(1 - \varepsilon_{B})\eta}{u_{L}} \int_{0}^{L} dz$$
 (2.9)

gives

$$ln\frac{C_i}{C_o} = \frac{k_v(1 - \varepsilon_B)\eta L}{u_L} \qquad (2.10)$$

The conversion X is defined as

$$X = \frac{C_i - C_o}{C_i} \tag{2.11}$$

and thus,

$$ln\frac{1}{1-X} = \frac{k_{\nu}(1-\varepsilon_B)\eta L}{u_L} = \frac{k'_{\nu}\eta}{SV}$$
 (2.12)

where SV is space velocity. The constant k'_{*} is defined as

$$\dot{k_{v}} = k_{v}(1 - \varepsilon_{B}) \tag{2.13}$$

This model has been termed a pseudo-homogeneous model and it is also a plugflow model (see also Shah, 1979). If the trickle-bed system is not reaction controlled but rather mass transfer controlled, k_v may be replaced by an apparent rate constant $k_{\rm app}$. Therefore equation (2.12) would become

$$ln\frac{1}{1-X} = \frac{k_{app}(1-\varepsilon_B)\eta L}{u_L} = \frac{k'_{app}\eta}{SV}$$
 (2.14)

where, analogously to equation (2.13), k'_{app} is defined as

$$k'_{app} = k_{app}(1 - \varepsilon_B) \tag{2.15}$$

To account for the effect of incomplete catalyst wetting two models were developed. Henry and Gilbert (1973) suggested that the reason for less effective catalyst wetting at low liquid flow rates was a result of inadequate liquid holdup. The model is a modification of equation (2.12) taking the following form

$$ln\frac{1}{1-X} = \frac{k_{\nu}(1-\varepsilon_B)\eta\varepsilon_L}{SV}$$
 (2.16)

where ε_L is the liquid holdup, which is a measure of the saturation of the void space with liquid.

A second model incorporating partial catalyst wetting, using a wetting coefficient f $(0 \le f \le 1)$ is its range, produces equation (2.17)

$$ln\frac{1}{1-X} = \frac{k_{\nu}(1-\varepsilon_B)\eta f}{SV}$$
 (2.17)

While both equations (2.16) and (2.17) are identical in form, the distinguishing constant in each equation is a hydrodynamic parameter which describes a different physical phenomenon although the hydrodynamic constants in each equation are related to the other by their common dependence on liquid velocity. If the system is not reaction controlled but rather mass transfer controlled, k_v in equations (2.16) and (2.17) can be replaced by k_{app} , generating equations (2.18) and (2.19) for the liquid holdup model and the external catalyst wetting model.

$$ln\frac{1}{1-X} = \frac{k_{app}(1-\varepsilon_B)\eta\varepsilon_L}{SV}$$
 (2.18)

$$ln\frac{1}{1-X} = \frac{k_{app}(1-\varepsilon_B)\eta f}{SV}$$
 (2.19)

The models defined by equations (2.13), (2.14), and (2.16) through (2.19) are linear equations. These models are useful since experimental conversion data can be plotted (via the mapping of conversion to ln(1/1-X) which is the ordinate) and reciprocal space velocity as abscissa. The slope of each equation is equal to the numerator of the right-hand side of each equation. Hence the slope determined

from the experimental data either by graphical or numerical analysis can be compared with any of the models. Interestingly, the slope can be a function of liquid velocity. Table 2.1 summarizes how liquid velocity can affect the slope of each model.

	Equation Slope Parameters		
Equation/Model	Surface Reaction	External Mass Transfer	
Pseudo-homogeneous Eqn. (2.13) & (2.14)	$k_v \neq k_v(u_L)$ $\therefore slope \neq slope(u_L)$	$k_{app} = k_{app}(u_L)$ $\therefore slope = slope(u_L)$	
Liquid Holdup Eqn. (2.16) & (2.17)	$k_{v} \neq k_{v}(u_{L}) \varepsilon_{L} = \varepsilon_{L}(u_{L})$ $\therefore slope = slope(u_{L})$	$k_{app} = k_{app}(u_L) \varepsilon_L = \varepsilon_L(u_L)$ $\therefore slope = slope(u_L)$	
External Wetting Eqn. (2.18) & (2.19)	$k_v \neq k_v(u_L)$ $f = f(u_L)$ $\therefore slope = slope(u_L)$	$k_{app} = k_{app}(u_L)$ $f = f(u_L)$ $\therefore slope = slope(u_L)$	

Table 2.1 Summary of the dependence of several trickle-bed models on liquid velocity

Table 2.1 reveals two important facts. First it is possible to have a situation where the slope is independent of liquid velocity, but this occurs only in one of six possible cases. Second it is possible to have situations where the dependence of the slope on the liquid velocity arises from one or two hydrodynamic parameters. In the latter case, one of the parameters is an external mass transfer coefficient while the other can be either liquid holdup or external wetting of the catalyst.

The implications are that if experimental data are obtained over a sufficiently large liquid velocity interval, then it should be expected that the slope of the transformed experimental data should change in value within the interval. Where the system exhibits a constant slope would indicate the reaction limited sub-interval. Likewise another sub-interval will exist where the slope of experimental data will not be

constant with liquid velocity. In this sub-interval it is possible to have a system where overall reaction rate is either surface reaction controlled or external mass transfer controlled as shown in Table 2.1. The challenge is then to determine which and how many hydrodynamic parameters are contributing to the change in slope with liquid velocity.

One of the simplest models of trickle-bed reactor design can be found in Fogler (1986). It provides a reasonable description of the processes occurring under certain assumptions. Schematically the model is given in Figure 2.1. The figure shows a single catalyst particle completely surrounded by a film of liquid, and the liquid film is completely surrounded by gas.

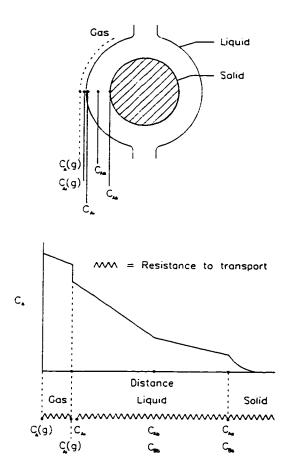


Figure 2.1 Concentration profiles for trickle-bed reactors (Fogler 1986)

2.1.3 Catalyst External Mass Transfer

Interphase and intraphase mass transfer, often limit the rate of reactant consumption and consequently product formation. If the reactant is in the liquid phase, then the reactant must move from the bulk liquid (if not pure reactant) to the catalyst surface and then, if the catalyst is porous, diffuse through the pores to the active sites within the particle. If the reactant is in the gas phase, it must move from the bulk gas phase (if not pure) to the gas-liquid interface, be absorbed into the liquid phase and then proceed in the same manner as the liquid phase reactant. To quantify these mass transfer processes, mass transfer coefficients have been developed. The most commonly used are the gas-liquid mass transfer coefficient, $k_L a_i$, and the liquid-solid mass transfer coefficient, $k_S a_S$. Numerous authors have proposed correlations for the prediction of the above mass transfer coefficients. Some have a mechanistic basis while others are more empirical in nature. However, the correlations have some common features. First they usually have parameters which are specific to a given system including packing characteristics (size, shape, and composition), fluid properties (density, viscosity, surface tension, although some correlations do include variables for fluid properties), and regime of operation (such as trickle, pulse, or spray flow regimes). Secondly, most express the direct dependence of mass transfer coefficient on liquid velocity for the trickle flow regime. A comprehensive list of correlations from several authors is given by Gianetto and Silveston (1986). For this study an estimate of the gas-liquid and liquid-solid mass transfer coefficients is needed for both data analysis and reactor simulation. The mass transfer correlations of Goto and Smith (1975a) were chosen. These correlations were chosen, since the system used to develop these correlations was similar the system used in this study. For gas-liquid mass transfer, the Goto and Smith (1975a) correlation is

$$k_L a = D_L \alpha_L \left(\frac{G_L}{\mu_L}\right)^{n_L} \left(\frac{\mu_L}{\rho_L D_L}\right)^{\frac{1}{2}}$$
(2.20)

where $k_L a$ [s⁻¹] is the gas-liquid mass transfer coefficient, G_L [g/(cm² s)] is the superficial liquid flow rate or the mass flux of liquid, μ_L [g/(cm s)] is the dynamic viscosity of the liquid, ρ_L [g/cm³] is the liquid density and D_L [cm²/s] is the molecular diffusivity in the liquid phase. The constants α_L and n_L are characteristic of the specific packing used in the study. These values are listed in Table 2.2. Note that the units of the variables in the correlation were listed above since the constants are not dimensionless.

Particles	$\alpha_L,[(cm)^{n_L-2}]$	n_L
Glass beads (0.413 cm)	2.8	0.40
CuO·ZnO (0.291 cm)	6.0	0.41
CuO·ZnO (0.0541 cm)	7.8	0.39

Table 2.2 Parameters used in the gas-liquid mass transfer coefficient of Goto and Smith (Goto and Smith, 1975a)

For liquid-solid mass transfer, the (Goto and Smith, 1975a) correlation is

$$k_S a = D_L \alpha_S \left(\frac{G_L}{\mu_L}\right)^{n_S} \left(\frac{\mu_L}{\rho_L D_L}\right)^{\frac{1}{3}}$$
 (2.21)

The correlation above is of almost identical form as equation (2.20) with the exception that the constants are of different values as listed in Table 2.3. The experiments conducted to generate the data for both correlations used water as the liquid phase and oxygen as the gas phase. The experiments to produce liquid-solid mass transfer data used β -naphthol particles which are slightly soluble in water.

In both correlations, it is interesting to note the strong dependence of both mass transfer coefficients on the physical properties of the liquid and the liquid velocity only. Notable is the absence of any effect of gas velocity on the mass transfer coefficients. The explanation may be that these correlations are applicable to the trickle flow regime, which is a low interaction regime. Low interaction means a minimal exchange of momentum between the flowing phases and hence gas flow should not affect liquid flow significantly.

$β$ -Naphthol Particles Sizes, d_p	$\alpha_{S},[(cm)^{n_{S}-2}]$	n_{s}
0.241	45	0.56
0.0541	153	0.67

Table 2.3 Parameters used in the liquid-solid mass transfer coefficient of Goto and Smith (1975a)

Figure 2.2 shows the response of the volumetric mass transfer coefficients to liquid flow rate. The flow rate range corresponds to the range covered in this study. From the figure it is evident that the liquid-solid mass transfer coefficient is much greater than the gas-liquid mass transfer coefficient. This suggests that of the two mass transfer resistances, gas-liquid mass transfer will usually dominate, except at only very low liquid flow rates, where both mass transfer coefficient curves ultimately converge at the origin. In fact, the gas-liquid mass transfer coefficient is most sensitive to liquid flow rate at very low liquid flow rates (less than 5 mL/min) whereas the liquid-solid mass transfer coefficient, while sensitive in the very low liquid flow rate region, remains sensitive to liquid flow rate over the entire liquid flow rate range, and the liquid-solid mass transfer coefficient does not appear to level off at higher liquid flow rates as compared to the gas-liquid mass transfer coefficient.

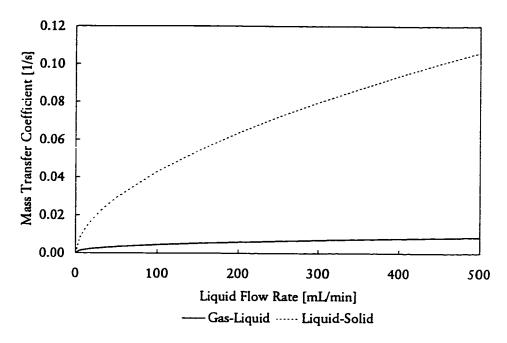


Figure 2.2 Response of mass transfer coefficients (Goto and Smith, 1975a) to liquid flow rate

2.1.4 Liquid Holdup

In a three-phase reactor like a trickle bed, each phase occupies a fraction of the total volume of the reactor. Mathematically this is expressed by

$$\varepsilon_{\rm B} = \varepsilon_{\rm C} + \varepsilon_{\rm L} \tag{2.22}$$

where ε_B is the bed voidage (fraction of reactor volume not occupied by catalyst), ε_G is the gas phase holdup (fraction of reactor volume occupied by gas), and the liquid phase holdup (fraction of reactor volume occupied by liquid). Ramachandran (1983) states that the liquid holdup is affected by such trickle bed parameters as

- 1) liquid flow rate (large effect)
- 2) liquid inlet distributor in large columns
- 3) shape and size of particles
- 4) wetting characteristics of packing and fluids
- 5) gas flow rate

The liquid holdup can be subdivided into two parts: the static liquid holdup and the dynamic liquid holdup. Mathematically this is described by

$$\varepsilon_{L} = \varepsilon_{LS} + \varepsilon_{LD} \tag{2.23}$$

where ε_{LS} is the static liquid holdup and ε_{LD} is the dynamic liquid holdup. The dynamic liquid holdup represents the portion of the liquid holdup present with liquid flow. When liquid flow is stopped, the remaining liquid in the reactor is the static liquid holdup. The static liquid holdup can be subdivided further into the external static holdup and the internal static holdup (Gianetto and Silveston, 1986). The external static holdup is the fraction of the static liquid holdup between the solid particles in the bed. The internal static holdup is the fraction of the static liquid holdup contained within the pores of a catalyst. (Obviously this would not exist for a nonporous catalyst.) Mathematically this is represented by

$$\varepsilon_{LS} = \varepsilon_{LSE} + \varepsilon_{LSI} \tag{2.24}$$

Combining equations (2.5) through (2.7) gives

$$\varepsilon_{\rm B} = \varepsilon_{\rm C} + \varepsilon_{\rm LD} + \varepsilon_{\rm LSE} + \varepsilon_{\rm LSI} \tag{2.25}$$

The importance of the liquid holdup depends on types of reactions occurring in the trickle bed. If the reaction of a nonvolatile species in the liquid phase is required, then the liquid holdup should be sufficiently high to ensure adequate wetting of the catalyst. Otherwise the catalyst surface will remain unwetted and not utilized. However if the reaction can occur in the gas phase as well as the liquid phase, then additional liquid holdup may provide a barrier (via diffusion resistance) for gas phase reactants from reaching the active sites on the surface of the catalyst (Hofmann, 1986).

2.1.5 Catalyst Wetting

The reactant from the liquid phase in a trickle-bed reactor has two possible ways of reaching the catalyst active sites. If the liquid phase reactant is volatile, then the reactant can reach the catalyst by way of evaporation into the gas phase, and subsequently by gas-solid mass transfer. The second route is by liquid-solid mass transfer. For the system studied, only the second route is possible. Even if the system is not liquid-solid mass transfer controlled, liquid must contact the catalyst in order for a non-volatile liquid phase reactant to reach the catalyst, otherwise reaction will not occur. Until now, the discussion has been mainly of external catalyst wetting but this is not the only wetting mechanism occurring. In the case of a porous catalyst, liquid in contact with the outer catalyst surface can be drawn into the catalyst pores by capillary forces. In fact it has been shown by several authors including Colombo et al. (1976) and Mills and Dudukovic (1981) that the interior of a porous catalyst is usually completely filled or wetted. distribution of active sites within the catalyst is homogeneous, then it is possible that the diffusion of reactants to the active sites will be the rate limiting step (i.e., the effectiveness factor is much less than one). This is particularly important for liquid-filled catalyst pores compared to gas-filled pores, since the diffusivity of reactants is of the order of 104 times less in liquids compared with gases (Gianetto and Silveston, 1986).

Several authors have quantified the external catalyst wetting factor (also known as wetting effectiveness or wetting factor) and have developed experimental techniques and theoretical models which, when used together, can provide numerical values. One of the first such techniques was developed by Colombo et al. (1976). It involved using an inorganic salt tracer injected into water flowing into the trickle-bed. The conductivity of the solution leaving the trickle-bed was measured over time. A partial differential equation adsorption model of the salt solution was developed and transformed from the time domain to the Laplace transform domain. Different moments were then calculated from the conductivity-

time data and compared with the moments from the model to provide correlations of wetting efficiency.

Mills and Dudukovic (1981) also used tracer methods to determine liquid-solid contacting. Their results were in agreement with Colombo et al. (1976). They found that internal catalyst wetting was complete (as stated earlier) and that the external catalyst wetting increased monotonically with liquid mass velocity up to complete coverage at the highest liquid velocities. The experiments were conducted in a 1.35 cm ID glass column and over the liquid flow rate range of 0.15 kg/(m² s) and 3.5 kg/(m² s). The bed with a porosity of 0.374, consisted of 20-28 mesh alumina pellets (average particle size of 0.0718 cm) which had an average pore diameter of 27 angstroms, while the pellet porosity itself was 0.495. The range of Re_L (Reynolds number of the liquid phase based on particle diameter was 0.33 to 7.91. From this study, two correlations were developed relating catalyst external wetting and liquid velocity as well as liquid physical properties given as

$$\eta_{CE} = \sqrt{\frac{(D_{EO})_{app}}{(D_{EO})_{LF}}} = 1.0 - exp \left(-1.35 Re_L^{0.333} Fr_L^{0.235} We_L^{-0.170} \left(\frac{a_t d_p}{\epsilon_R^2} \right)^{-0.0425} \right)$$
(2.26)

and

$$\eta_{CE} = \sqrt{\frac{(D_{EO})_{app}}{(D_{EO})_{LF}}} = tanh \left(0.664 \, Re_L^{0.333} \, Fr_L^{0.195} We_L^{-0.171} \left(\frac{a_t d_p}{\epsilon_B^2} \right)^{-0.0615} \right)$$
(2.27)

Several other authors have used similar techniques with variations in models to produce different correlations of wetting efficiency.

2.1.6 Axial Dispersion

The role of axial dispersion in trickle-bed reactors under cocurrent operation has been documented in the literature by several authors. In general, axial dispersion is not important in trickle-bed reactors if the reactions are first order in the gas phase reactant and zero order in the liquid phase reactant (Ramachandran, 1985). The degree of axial dispersion is expressed by the liquid phase Peclet number defined by

$$Pe'_{L} = \frac{u_{L}d_{p}}{D_{FL}} \tag{2.28}$$

Some correlations for predicting Pe'L are given in Table 2.4.

Correlation for Pe'L	Author(s)
$13 Re_L^{0.4} Ga_L^{-0.333}$	Furzer and Michell (1970)
$\left(\frac{Re_L}{\varepsilon_{LD}}\right)^{0.7} Ga_L^{-0.32}$	Michell and Furzer (1972)
$7.58 \times 10^{-3} Re_L^{0.703}$	Sater and Levenspiel (1966)
$Pe'_L = 0.034 Re_L^{0.5} 10^{0.003 Re_c}$	Hochman and Effron (1969)

Table 2.4 Correlations for predicting the liquid phase Peclet number under trickle flow conditions

Note that in the above table the liquid phase Reynolds (Re_L) and Galileo (Ga_L) numbers, and the gas phase Reynolds number (Re_G) are defined as:

$$Re_L = \frac{u_L d_p \rho_L}{\mu_L}$$
 (2.29) $Ga_L = \frac{d_p^3 g \rho_L^2}{\mu_L^2}$ (2.30) $Re_G = \frac{u_G d_p \rho_G}{\mu_G}$ (2.31)

By estimation of Pe'_L and subsequently D_{EL} one can then account for the axial dispersion effect by using the comprehensive trickle-bed model. However, the solution of the equations may not be possible analytically and may require

numerical solution. Under certain conditions, the effect of axial dispersion may be neglected. For an isothermal trickle-bed, Mears (1971) presented the following criterion as a guide for neglecting the effect of axial dispersion

$$\frac{L}{d_p} > \frac{20m}{Pe_L} \ln \frac{C_i}{C_o} \tag{2.32}$$

where m is the reaction order, L is the bed length, d_p is the particle diameter, C_i is the reactant concentration at the reactor inlet and C_o is the reactant concentration at the reactor outlet. If equation (2.32) is satisfied then plug flow can be assumed for the bed. Equation (2.32) can be expressed in terms of conversion, X by noting that

$$X = \frac{C_i - C_o}{C_i} \tag{2.33}$$

and by substitution into (2.32) gives

$$\frac{L}{d_p} > \frac{20m}{Pe_L} ln \frac{1}{1 - X} \quad . \tag{2.34}$$

Qualitatively, from equation (2.34) the conditions under which axial dispersion may be neglected include deep beds, high liquid velocities and low conversions. Figure 2.3 shows the conditions under which axial dispersion can be neglected. The horizontal line shown in the figure represents the ratio L/d_p . For the reactor system in this project, this quantity is 100. As can be seen, axial dispersion can become important at low liquid flow rates and high conversions.

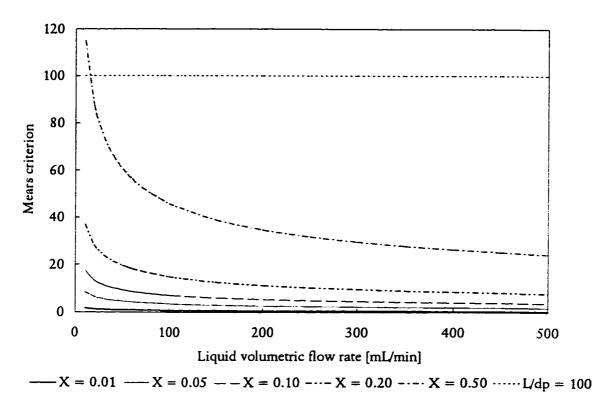


Figure 2.3 Mears Criterion for Neglecting Axial Dispersion as a Function of Conversion and Liquid Volumetric Flow rate for the Experimental Trickle-bed (L/d_p) is the ratio of catalyst bed length to catalyst particle diameter)

2.1.7 Trickle-bed Model Classifications

Trickle-bed models can be classified into two categories: those for steady operation and those for unsteady or dynamic operation. Actually the dynamic models also encompass the steady-operation models, which arise from simplifications to the dynamic models. Most widely covered in the literature are steady-state models, probably because interest of the industrial interest in the long-term operation of a trickle-bed at steady state. These steady trickle-bed models attempt to explain observed trickle-bed reactor performance by focusing on one or more features of trickle-bed behavior. The four types of models identified are pseudo-homogeneous, holdup, catalyst wetting and liquid irrigation models. The first three models are very similar and differ from each other, based on which physical parameters are included in the model. Actually the holdup and catalyst wetting

models are really just specialized cases of the pseudo-homogeneous model. The irrigation type models are much different since they try to model liquid flow through the trickle-bed and predict the liquid velocity distribution in the bed.

Pseudo-homogeneous models treat the entire trickle-bed as a single-phase homogeneous system. A mass balance and sometimes a heat balance are used but the momentum balance is ignored. Therefore the assumption is plug flow for both flowing phases. While this is the simplest of trickle-bed models, it is often very effective for modeling conversion as a function of liquid flow rate provided there is complete catalyst wetting in the bed.

Holdup based models attempt to account for trickle-bed reactor performance on the basis of dynamic and static liquid holdups usually obtained from experiment or correlation. As stated earlier, the holdup model is a pseudo-homogenous model which requires an estimate of liquid holdup. Again a mass balance and a heat balance (if large temperature effects are suspected) are used but a momentum balance is neglected. Liquid holdup is a parameter which basically describes how much liquid is in the bed. Therefore it should correlate with catalyst wetting and possibly mass transfer coefficients involving the liquid phase and it could be useful under conditions where liquid flow rate is such that catalyst wetting is incomplete. The liquid flow rate effect on conversion is then not limited to contact time in the catalyst bed as in the first model. Unfortunately when this model is applied, the liquid holdup is often assumed to be constant throughout the bed, through this assumption is probably not true.

Wetting-based models, like holdup models, are pseudo-homogeneous ones. In the place of liquid holdup, wetting models use an external wetting coefficient or parameter, in order to adjust the mass balance for the effects of incomplete catalyst wetting. This is particularly important if the reactant is in the liquid phase and is

non-volatile. Like the holdup based models, the wetting efficiency is obtained from experiment or correlations.

Irrigation type models are similar to wetting and holdup models in that they attempt to take into account liquid flow in the trickle-bed. This approach comes from the study of flow through porous media. Within this class there are two types of models, those which are diffusion based and those which are based on percolation theory. The latter attempt to determine individual flow patterns through the bed while the diffusional based models treat the bed as a pseudo-homogeneous media. Irrigation, while related to wetting, tries to take into account liquid maldistribution due various mechanisms including (but not limited to) liquid distribution upon introduction into the bed, liquid channeling through the bed, liquid wall flow, and bed packing characteristics. Thus, while holdup and wetting models take a macroscopic view of liquid flow through a trickle-bed, the irrigation models take a more microscopic view.

2.2 Periodic Operation

2.2.1 Background

The concept of periodic operation is not new. For over 30 years researchers have been conducting theoretical studies of reactor systems under periodic operation. Bailey's review (Bailey, 1973) of the subject provides an excellent starting point in describing the meaning of the term *periodic operation*. Periodic operation is the intentional manipulation of the control variable or variables of a process on a periodic basis with respect to time.

Bailey views periodic operation as consisting of four classes of processes: Process Life Cycles, Quasi-Steady Periodic Operation, Relaxed Steady-State Operation and Intermediate Periodic Operation. The criterion for classification is based on the relative magnitude of: 1) a parameter indicative of the natural response of the system or the characteristic response time of the system, τ_c and 2) a parameter

indicative of the forcing or periodic operation of the system, that is the cycle time, τ . A summary of the four classes of periodic operation is given in Table 2.5.

Periodic Operation Class	Relative magnitude of τ_c and τ
Process Life Cycles	τ _c <<< τ
Quasi-Steady Periodic Operation	τ _c << τ
Relaxed Steady-State Operation	$\tau_c >> \tau$
Intermediate Periodic Operation	$ au_{c} pprox au$

Table 2.5 Bailey's four classes of periodic operation

Process life cycles are the result of the long-term operation of a chemical process whose performance typically deteriorates with time and is then restored periodically. A good example of this is the operation of a catalytic reactor for which the activity of the catalyst decreases to the point that operation becomes uneconomical and is stopped. The catalyst is replaced with regenerated or fresh catalyst that has sufficient activity to resume economical operation of the reactor. In this case τ is huge in comparison to τ_c .

In quasi-steady periodic operation control variables are oscillated such that the period of oscillation is much larger than the characteristic response time of the system. As a result the measured variables effectively oscillate between two steady-state values. This is shown by Figure 2.4 where y_{qss} represents the average value of the variable y under periodic operation. Clearly y_{qss} is greater than y_{ss} .

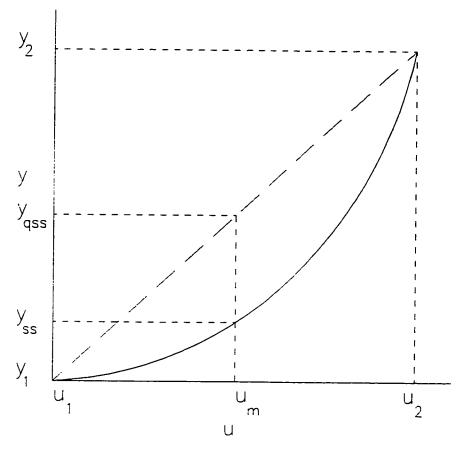


Figure 2.4 Output vs. input for a hypothetical process

Relaxed steady state is the opposite to quasi-steady operation. The manipulated variables of the process oscillate at a high rate relative to the characteristic response time of the system. The system under forced oscillation cannot respond to the rapid changes but instead reaches some time-invariant periodic state - the relaxed steady state. Intermediate periodic operation is, as the name implies, a mode of operation between the extremes of quasi-steady operation and relaxed steady-state periodic operation.

To compare steady and periodic operation two performance criteria come to mind, the first being performance based on some index of production; the second would be based on operational improvements. To measure the first criterion, one could look at reactant conversion, reactant consumption rates, and/or product formation rates either time-averaged or instantaneous. To compare operating modes on the

basis of throughput, the comparisons should be time-averaged because ultimately a reactor designer is interested in how much material can be passed through the reactor. From an operational improvement point of view comparison of the temperature distribution in the catalyst bed between the two operating modes could, as an example, be examined.

2.2.2 Reactor Studies

Many of the studies of periodic operation have been theoretical ones, focusing on the development of mathematical models of various reaction systems with subsequent analytical or numerical solution. The emphasis has been on lumped parameter systems such as CSTRs with various proposed reaction mechanisms for both heterogeneous and homogeneous reaction systems. A comprehensive compilation is given by Silveston (1994).

The types of systems which are of interest, are those for which periodic operation results in a desirable change in the average value of some process variable. Schädlich et al. (1983) provide a very useful classification of periodic control problems summarized in Table 2.6.

From Table 2.6 the only systems for which improvement is not possible is those in which both the system is linear in the state variables and control of the system is linear in the control variables. Most systems encountered in practice, either exhibit some nonlinearity or the control of such systems is nonlinear in the control variables. Therefore the opportunity for enhancement of the value of some desired state variables for many processes should exist.

System $\dot{y} = \frac{dy}{dt} = f(y, u)$	Linear Control $\frac{\partial f}{\partial u} = B$	Nonlinear Control $\frac{\partial f}{\partial u} = B(y, u)$
Linear System $\frac{\partial f}{\partial y} = A(u)$	$\Delta = 0$ no improvement possible	$\Delta \neq 0$ improvement possible
Nonlinear System $\frac{\partial f}{\partial y} = A(y, u)$	Δ≠0 improvement possible	$\Delta \neq 0$ improvement possible

Table 2.6 Classification of periodic operation control problems

One of the choices facing a process designer contemplating periodic operation is that of the state variable to attempt to improve. For example, one could choose to improve overall production rate, selectivity, or the temperature uniformity throughout the reactor (particularly important for exothermic reactions in distributed systems).

A decision must then be made as to what control variable(s) are to be oscillated. Once this decision is made, then the dynamic response of the system under study must be determined. This is usually accomplished by step-change experiments. In step-change experiments, the system is allowed to reach steady state and then a step change increase is made in a manipulated variable. The characteristic response of the desired state variables is then determined. The choice of which variables to manipulate could depend on several factors including:

1) which manipulated variable produces the most significant change in the desired state variables.

- 2) which manipulated variable produces the least undesirable changes in certain state variables.
- 3) which manipulated variable is easiest to change in a periodic manner.

Several schemes have been chosen in past studies for periodic operation. Two of the most common include feed flow rate cycling and feed concentration cycling. These two schemes have also been used for periodic operation of trickle bed reactors. In addition to these there is then the choice of which waveform to use for forced cycling. While there is a infinite choice of waveforms for periodic operation the most commonly used is square wave cycling. Figure 2.5 shows a typical square wave and the parameters which define it.

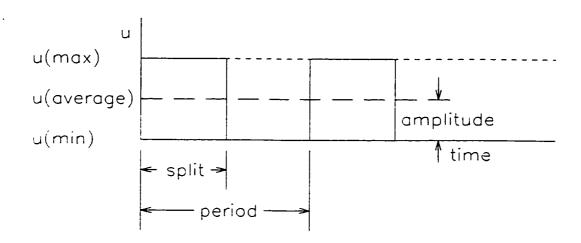


Figure 2.5 Typical square wave used in periodic operation

If the square wave of Figure 2.5 has $u_{min} = 0$, then on-off cycling results. The 3 parameters which define a cycle in on-off cycling are the period (the length of the cycle), the split (in this case the fraction of the cycle in which u is equal to u_{min}), and the amplitude (the maximum value of u during the cycle, in this case u_{max}).

Past theoretical studies of reactors have not included trickle-bed reactors per se; instead, continuous stirred tank reactors (CSTRs) and plug flow reactors (PFRs)

show that nonlinearity from any source within a system, can be responsible for the improvements seen in periodic operation. Some of these studies are summarized in Table 2.7. These studies may be used as a qualitative basis for new studies into the periodic operation of trickle bed reactors. It is only within the past ten years, however, that experimental studies into trickle-bed reactor performance under periodic operation have been carried out.

Researcher	Reactor/Reaction	Mode of Periodic	Results
	System	Operation	<u> </u>
Lannus and	tubular with axial	sinusoidal	improvement in
Kenshenbaum	dispersion and	variation in feed	conversion
(1970)	second-order	concentration	
	kinetics		
Bailey and	fixed-bed catalytic	bang-bang cycling	improvement in
Horn (1971)	reactor	of feed	conversion
		concentration	
Bailey et al.	CSTR	on-off heat flux	high frequency oscillations
(1971)		and concentration	are filtered by heat and
		in bulk phase	mass transfer resistances
Lee et al.	Isothermal CSTR	forced cycling of	improvement in
(1979)	with consecutive-	reactant feed	intermediate product yield
	competitive		
	reactions		
Thullie et al.	plug-flow with	feed	improvement in reaction
(1987)	two-step	concentration	rate and production rate
	adsorption-	forcing	•
	desorption model		

Table 2.7 Periodic operation reactor studies

2.2.3 Trickle-Bed Reactor Studies

The first published study of the periodic operation of a trickle-bed reactor was conducted by Haure et al. (1989), using the oxidation of sulfur dioxide over activated carbon. In this system, the manipulated variable was superficial liquid velocity and the dependent state variable of interest was the production rate of sulfuric acid. The steady-state results showed a highly nonlinear response of acid production rate with superficial liquid velocity (over a range of 0 to 7 mm/s

superficial liquid velocity). This nonlinear response was parabolic, with a minimum located at about 4 mm/s superficial liquid velocity. The periodic operation experiments, using on-off cycling, were conducted at 0.86 and 1.65 mm/s average superficial liquid velocity. The results showed that about a 20 percent increase in acid production rate for 0.86 mm/s average superficial liquid velocity and a 40 percent increase in acid production for 1.65 mm/s average superficial liquid velocity.

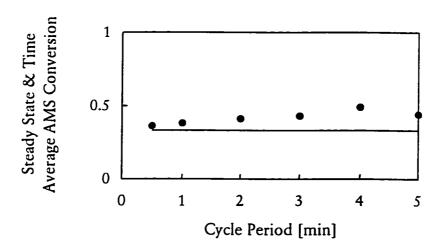
The choice of the superficial velocity as the manipulated variable for periodic operation was an appropriate one. The dependence of acid production rate on superficial liquid velocity was highly nonlinear and therefore, as was shown by experimentation, the time-average acid production rate could be higher under periodic operation than that under steady operation.

In sulfur dioxide oxidation in a trickle-bed reactor, both reactants are fed to the reactor in the gas phase. While it is necessary for water to be present to produce sulfuric acid, this addition of water is considered relatively fast in comparison to the oxidation step. Additionally, water is in a huge excess in comparison to both gas phase reactants. Intuitively it would seem that this process would be nonlinear in nature and hence an excellent candidate for improvement through application of periodic operation.

While the main focus of the Haure study was on-off liquid flow operation, experiments were also conducted where liquid flow was not completely interrupted. The experiments showed that an improvement in acid production was possible, although it was not as substantial as that observed for on-off liquid flow operation. Besides showing that periodic operation can improve acid production in the sulfur dioxide system, optimization of the periodic operation parameters is necessary (i.e., of both split and period length).

Another useful and interesting study is the hydrogenation of α -methylstyrene (AMS) under periodic operation in a trickle-bed reactor, conducted by Lange et al. (1995). The purpose of this study was to discover what conditions of periodic operation would improve the time-average conversion of AMS to cumene, relative to steady operation. In this study, symmetrical on-off cycling was used to vary the volumetric flow of AMS to the reactor. Experiments showed a maximum improvement in AMS conversion of about 50 percent over the same conversion under steady operation. The results are shown in Figure 2.6.

The time-average conversion shows interesting behavior with respect to cycle time. As the cycle time approaches 0, the time-average conversion approaches the steady-state value. This suggests that the relaxed steady state is the observed steady state under steady operation. If so, the best cycling strategy would be quasi-steady periodic operation with cycle period τ equal to about 4 minutes.



Periodic Operation ——Steady Operation

Figure 2.6 Comparison of steady state and time-average AMS conversion under periodic operation (Lange et al., 1995)

Both of these studies raise questions as to what mechanism is responsible for producing improved results under periodic operation. As stated previously, it is possible to produce improvements in desired process state variables under periodic operation if the process is nonlinear. In trickle bed reactors there may be many sources of nonlinear behavior. Both Haure's and Lange's studies imply a nonlinear relationship between conversion in a trickle bed reactor and superficial liquid velocity. However both systems are very different with respect to the feeds to each system. In Haure's system both oxidation reactants are relatively dilute and introduced to the reactor in the gas phase. In contrast, in Lange's system, one reactant is a pure gas (hydrogen) and the other is a pure liquid (AMS). Also, AMS can vaporize and react on dry catalyst surfaces. Clearly these differences will affect the behavior of each system.

The most recent experimental study of the periodic operation of a trickle-bed reactor in the literature is that of Castellari and Haure (1995). This study compared the hydrogenation of AMS to cumene under periodic and steady operation. This system is one with a gaseous reactant (hydrogen) mass transfer of which is a rate limiting step. Also since AMS is volatile it can exist in both gas and liquid phases. Compared to steady operation, improvement in cumene production rate was substantial. The explanation for this was twofold: during the liquid-off portion of the periodic operation cycles, gas-liquid mass transfer rates were increased and a substantial temperature rise was observed in the catalyst bed resulting in an increase in the reaction rate. The liquid phase reactant can vaporize rapidly enough to participate in reaction on dry catalyst pellets.

Haure et al. (1989) and Lange et al. (1995) suggest that enhanced mass transfer is one factor responsible for the improvements seen in time-average conversions for their respective systems. Intuitively this seems correct. However the question arises whether current models employing typical mass transfer coefficients found in the literature can be used to predict improvements in conversion as a result of

periodic operation. The parallel question also arises: could the nonlinearity observed in these systems be the result of some other phenomenon than mass transfer?

It would be desirable, given the parameters defining the trickle bed reactor, to be able to predict performance of the trickle bed reactor. Clearly, good mathematical models describing steady and periodic operation of trickle bed reactors are needed for this task. This seems essential not only for the design and possible scale-up of trickle bed reactors for industrial use but also for the development of control and optimization strategies.

2.3 Reaction System

Crotonaldehyde was chosen as the liquid phase reactant for this system for two reasons. First the hydrogenation occurs at mild conditions with several different catalysts. Secondly the hydrogenation of the double bond in the molecule has been suggested (Kenney and Sedriks, 1972) to be representative of the hydrogenation of double bonds in aliphatic compounds.

The possible reactions for the hydrogenation of crotonaldehyde significant to this study are

$$CH_{3}CH = CHCHO + H_{2} \xrightarrow{\text{catalyst}} CH_{3} (CH_{2})_{2} CHO \xrightarrow{\text{catalyst}} CH_{3} (CH_{2})_{2} CH_{2}OH$$
(2.35)

where CH₃CH=CHCHO is crotonaldehyde (2-buten-1-al), CH₃(CH₂)₂CHO is butyraldehyde (1-butanal) and CH₃(CH₂)₂CH₂OH is 1-butanol.

$$CH_3CH = CHCHO + H_2 \xrightarrow{\text{catalyst}} CH_3CH = CHCH_2OH$$

crotonaldehyde butenol (2.36)
2 - buten - 1 - al 2 - buten - 1 - ol

To study any reaction system, it is important that the reaction be thermodynamically feasible and that the reaction proceed at a practical rate. As listed in Appendix N, the crotonaldehyde hydrogenation to butyraldehyde is thermodynamically possible at 25°C.

Rylander (1967) reports that the hydrogenation of unhindered aliphatic α,β-unsaturated aldehydes usually results in selective hydrogenation of the carbon-carbon double bond. If the hydrogenation is carried out over Pd, the reaction stops after the formation of the saturated aldehyde (butyraldehyde). One exception is the hydrogenation over palladium-iron catalyst. The reaction with this catalyst forms the unsaturated alcohol. He also reports the hydrogenation of crotonaldehyde with Pt catalysts. The unsaturated alcohol could be formed provided the catalyst contained both iron and zinc as promoters and all metals were supported on either carbon or CaCO₃. Silver could also be substituted for zinc as a promoter. If the support was either alumina or BaSO₄, the product was butyraldehyde. These results are summarized in Table 2.8.

Catalyst	Catalyst	Atoms of metal	Solvent	Product
	Mass	per atom of Pt	(50 mL)	
5% Pt/C	2000	0.4 Fe 0.06 Zn	ethanol	2-buten-1-ol
5% Pt/CaCO ₃	1000	3.75 Fe 0.12 Zn	ethanol	2-buten-1-ol
5% Pt/C	2000	0.4 Fe 0.06 Ag	ethanol	2-buten-1-ol
5% Pt/BaSO ₄	2000	0.4 Fe 0.06 Zn	ethanol	butyraldehyde
5% Pt/Al ₂ SO ₃	2000	0.4 Fe 0.06 Zn	ethanol	butyraldehyde
10% Pt/C	1000	0.4 Fe 0.06 Zn	ethanol	2-buten-1-ol
30% Pt/C	300	0.4 Fe 0.06 Zn	ethanol	2-buten-1-ol

Table 2.8 Catalytic hydrogenation of crotonaldehyde, temperature: 25°C; pressure: 50 psig; iron was added as ferrous chloride, zinc as zinc acetate, and silver as silver nitrate (from Rylander, 1967).

Kenney and Sedriks (1972) found that the hydrogenation typically stops after the formation of butyraldehyde with Pd/Al₂O₃ catalyst. This is in agreement with Rylander. In their study, they determined a kinetic rate expression and its constant for the hydrogenation of crotonaldehyde in a slurry reactor. They found that the rate law was of the form

$$r_{\rm CRHO} = k \eta C_{\rm H}, \tag{2.37}$$

which is first order only in the liquid phase concentration of hydrogen. The result is not surprising given the fact that the liquid was pure crotonaldehyde and the solubility of hydrogen in the liquid phase is quite low. The rate constants over the range of temperatures studied are given in Table 2.9.

Temperature	Rate Constant [cm ³ /(h g Pd)]
90	$\frac{\left[\operatorname{cm}/\left(\operatorname{Hg}\operatorname{Pd}\right)\right]}{325\times10^4}$
51	133 × 10⁴
41	70 × 10⁴
31	56 × 10⁴

Table 2.9 Reaction rate constants for crotonaldehyde hydrogenation in a slurry reactor

2.4 Summary

The literature documents the use of periodic operation to improve trickle-bed reactor performance. These improvements are the result of enhanced mass transfer and thermal effects. The systems studied involved either concentration liquid reactant solutions (in some cases pure as in the case of α -methylstyrene hydrogenation) or gaseous reactants, with the liquid phase acting as a flushing medium.

This study will investigate the potential application of periodic operation to another type of system: one where the liquid phase reactant is dilute, a system such as hydrodesulphurization. The study will also attempt to discover the phenomena responsible for an improvement in performance, if one exists.

CHAPTER

THREE

EXPERIMENTAL WORK

3.1 Outline

The experimental work consisted of several components:

- 1. Steady and periodic operation experiments in a trickle-bed reactor
- 2. Hydrodynamic experiments to determine dynamic and static liquid holdups, and external catalyst wetting efficiency
- 3. Catalyst pore size experiments and bed porosity
- 4. Liquid sample analysis by gas chromatography

3.2 Trickle-Bed Reactor Steady And Periodic Operation Experiments

3.2.1 Experimental Equipment

A schematic of the trickle-bed reactor equipment is shown in Figure 3.1. Liquid feed was prepared in 200 L drums. Inside one of the drums was a heating coil capable of heating the liquid feed to about 50°C. The feed was pumped to a surge vessel (not shown) where it was then pumped by a Milton-Roy diaphragm pump to the bottom of the saturator. The saturator was a 1.5 m high column constructed from 316 SS 2" schedule 40 pipe filled with ¼" inch glass Raschig rings. Gas was metered to the saturator by a Unit Model 1100 mass flow controller. The function of the saturator was to saturate the liquid phase with the gas phase (and vice versa). The two phase mixture leaving the top of the saturator was fed into the top of an overhead tank, a 10 L stainless steel vessel. In the overhead tank, gas was separated and passed through the top of the overhead tank and was fed to the top of the trickle-bed reactor. The liquid was also fed to the top of the trickle-bed reactor using 3/8" SS tubing. Liquid level was maintained in the overhead tank by a level switch which opened a pneumatic valve, causing the periodic discharge of feed liquid back to the feed tank.

The trickle-bed reactor is shown in Figure 3.2. The reactor consisted of several sections. In the top section, gas and liquid were introduced to the reactor. The middle section was the catalyst bed that contains the catalyst and is shown in Figure 3.3. Liquid and gas exited from the bottom section. The reactor bed had 24 ports, 4 cm apart longitudinally and 120° apart radially, for the placement of thermocouples, pressure transducers, and sampling taps (Figure 3.4). At the boundary of each section was a distributor plate shown in Figure 3.5. The outlet section is shown in Figures 3.6 and 3.7.

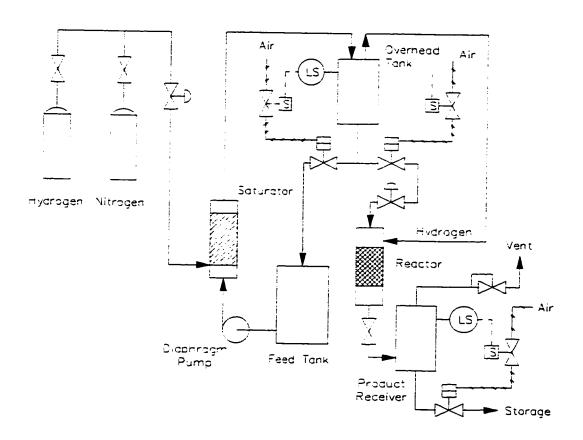


Figure 3.1 Experimental trickle-bed reactor process flow diagram

The liquid-gas mixture discharged from the bottom of the reactor was sent to a product receiver. The gas-liquid mixture was separated in the product receiver, with the gas being vented through a back-pressure regulator. Liquid level was maintained in the overhead tank by a level switch which opens a pneumatic valve, causing the periodic

discharge of product liquid from the receiver. Product liquid discharged from the receiver was collected for analysis.

The liquid flow rate to the trickle-bed reactor was set by a hand control valve. Three different Whitey valves sizes were used: 3/8", 1/4", and a micrometer valve. Since the level in the overhead tank is approximately constant, once the control valve was set, the liquid flow rate was set. The calculation of liquid flow through the reactor was made by collection and measurement of liquid product from the receiver over a set time interval. This usually coincided with the collection of receiver product for chemical analysis.

3.2.2 Experimental Procedure

In a typical experiment the reactor was flushed for between 1.5 and 2 hours with liquid feed flowing at between 150 and 200 mL/min while under a nitrogen purge of 1 SL/min. This was sufficient to obtain no traces of hydrogenation products in the liquid collected in the product receiver. After the liquid flush hydrogen flow of 1 SL/min was established to the reactor, the liquid flow rate was adjusted to the desired level, and periodic operation was initiated if desired.

Under steady and periodic operation liquid samples were collected at 2 to 3 intervals after 3 to 4 hours of hydrogenation had passed. This was sufficient for achieving steady state. Typically steady state was achieved between 1.5 and 3 hours. A sample of the feed was also taken from the overhead tank. The samples were analyzed using a gas chromatograph.

Three different sampling techniques were tested. One consisted of sampling a stream branching from the line leading to the product receiver, using a micrometer valve. The second was the use of a sample bomb placed in series with and between the reactor outlet and the product receiver. The most reliable sampling technique for both steady operation and periodic operation was the collection of an undivided sample from the

product receiver. The first technique is susceptible clogging by catalyst fines. The danger with this is that the fines act as a miniature plugflow reactor in series with the trickle-bed reactor. As a result additional crotonaldehyde conversion occurred giving falsified results. Therefore, this sampling technique was abandoned.

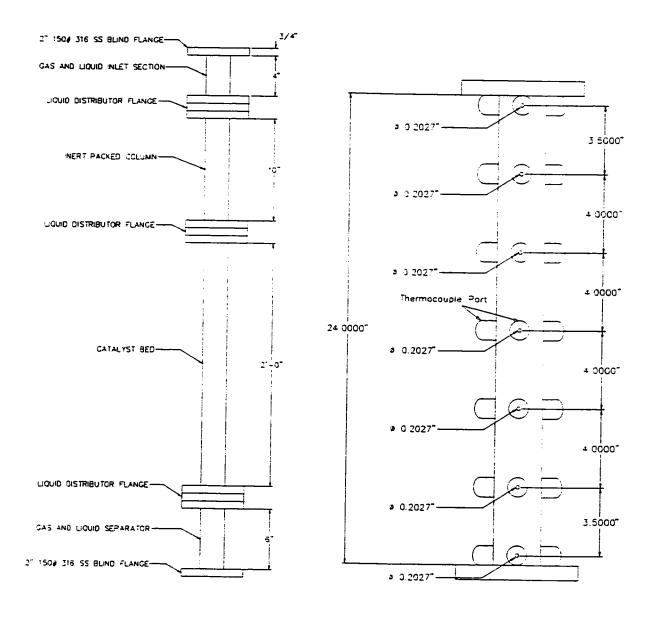


Figure 3.2 Trickle-bed reactor

Figure 3.3 Catalyst bed detail

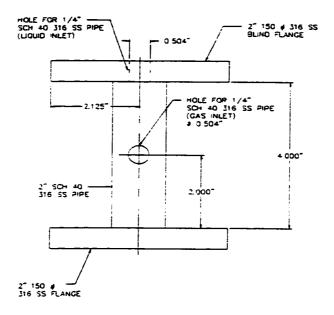


Figure 3.4 Inlet section

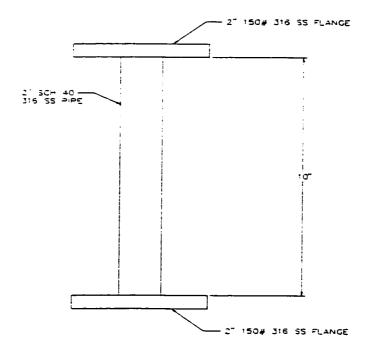


Figure 3.5 Prepacking section

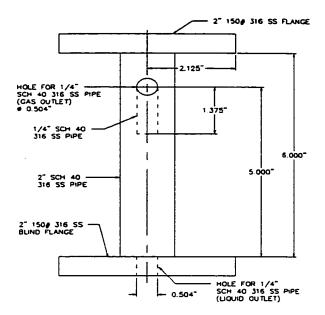


Figure 3.6 Outlet section

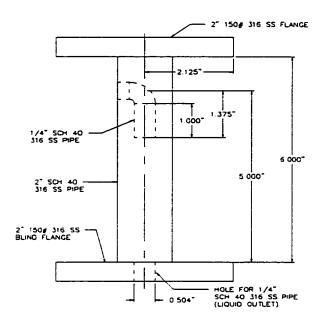


Figure 3.7 Outlet section rotated 90°

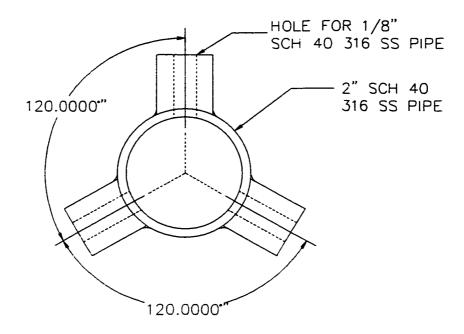


Figure 3.8 Catalyst bed cross-section

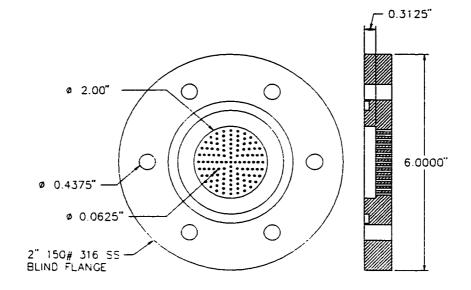


Figure 3.9 Distributor plate

The collection of an undivided sample from the product receiver was deemed the best sampling technique. The volume of product liquid collected in the product receiver was about 800 mL. To ensure that no additional reactant conversion was occurring a test was performed in which feed liquid was allows to sit in the product receiver for 6 hours with hydrogen present. The reactant conversions before and after the 6 hour time interval were compared; no conversion of reactant was observed in the product receiver.

The samples were collected and analyzed for 3 components: crotonaldehyde, butyraldehyde, and n-butanol. An HP Series II gas chromatograph (GC) installed with a J&W Scientific DB-Wax Megabore 0.53 mm ID capillary column and a flame ionization detector (FID). The FID signal was sent to a IBM compatible PC with an HP data acquisition board installed. HP ChemWindows software was used for all data acquisition, peak integration and report generation. A calibration curve for each component was made by preparing 4 samples with various masses of each component and the addition of 50 µL of acetone as an internal standard. Samples were collected from the reactor outlet and analyzed within 1 hour of collection. Each sample had an acetone internal standard added to it. 1 µL of the sample (containing the internal standard) was injected into the GC. At the start of the project duplicate injections were made into the GC. However it was quickly determined that the repeatability of the GC analysis was quite good, with a typical standard deviation of 0.5 to 1% of the mean of the injections being obtainable. From that point on only single injections were made of the samples collected.

To calculate the concentration of a given species in a sample, the response factors were determined for each component. These response factors were the slope of the calibration curves prepared for each species. The response factor is simply the ratio of mass of a component to the peak area of that component divided by the ratio of an internal standard to the peak area of the internal standard. The internal standard is used to compensate for the variation in the volume of liquid injected into the GC, since

this is the operation which is the least repeatable in the entire analysis procedure. By adding a fixed quantity of internal standard to each sample, and knowing the response factor it is then possible to calculate the concentration of each species in a given sample.

3.2.3 Planning Trickle-bed Experiments

From the literature review, several useful concepts were noted for planning the tricklebed reactor experiments. They include:

- a) The fundamental processes occurring in a trickle-bed reactor include mass transfer, both gas-liquid and liquid-solid, internal pore diffusion within the catalyst, and surface reaction. Any one or combination of the above-mentioned processes can control the overall rate of conversion of products to reactants.
- b) A quantitative description of trickle-bed reactors under steady operation under certain assumptions.
- c) Period length, split, and pulse amplitude can all affect conversion in a periodically operated trickle-bed reactor.

Preliminary experiments showed that conversion was affected by liquid flow rate but not gas flow rate. Two different catalysts were also tested. Of the two catalysts tested, the catalyst, consisting of 0.03 wt. % Pd/γ-Al₂O₃ spherical pellets of 4 to 6 mesh size, was chosen. The plan for steady operation experiments showing the various operating variables is listed in Table 3.1, while Table 3.2 shows the possible controlling mechanisms for the above experimental sets.

Experiment Set	1	2	3
Temperature [°C]	25	50	50
H ₂ pressure [atm]	11	11	1
H ₂ flow rate [L (STP)/min]	1	1	1
Liquid flow range [mL/min]	5 - 450	5 - 450	5 - 450

Table 3.1 Trickle-bed reactor experiment design

Experiment Set	1	2	3
Liquid flow rate 5 - 50 mL/min	liquid phase reactant mass transfer / surface reaction	liquid phase reactant mass transfer	gas phase reactant mass transfer
Liquid flow rate 50 - 450 mL/min	surface reaction	liquid phase reactant mass transfer / surface reaction	gas phase reactant mass transfer / surface reaction

Table 3.2 Matrix of liquid flow rates and experimental sets with anticipated controlling mechanism

The assumption based on preliminary experiments was that the Set 1 experiments will be surface reaction controlled. Quantitative evidence supporting this assumption are shown in Chapter 4. The experiments in Sets 2 and 3 were an attempt to move into control by mass transfer by increasing the temperature. The success of this attempt is discussed in Chapter 4.

Based on the behaviour of trickle-bed reactors under steady operation, an experimental plan was developed to test periodic operation under a wide range of conditions. A natural extension to the steady operation experiments would be selection of 3 sets with the same conditions as in Table 3.1, with the exception that Liquid flow range in the last line of Table 3.1 is a time-average value. Under the same operating conditions (with the exception of instantaneous liquid flow rates), a direct comparison of steady and periodic operation performance was made.

3.3 Hydrodynamic Experiments

The purpose of the hydrodynamic experiments was to determine parameters useful for understanding the behaviour of the trickle-bed reactor as well as for

^{*} Experiments undertaken by Stephanie Hackel as part of a Diplomarbeit

mathematical model development. These parameters included dynamic and static liquid holdups, and catalyst external wetting. The hydrodynamic experiments were also necessary to see if the system under study behaved as described in the literature. The dynamic and static liquid holdups were determined using the techniques described by Goto and Smith (1975a). These measurements were made using a clear plastic replica of the original trickle-bed reactor. A schematic diagram of the apparatus is shown in Figure 3.10.

Liquid holdup measurements were taken at room temperature and atmospheric pressure with helium as the gas phase and deionized water as the liquid phase. As shown by Larachi *et al.* (1990) at low gas velocities ($u_G \le 1$ cm/s), liquid holdup is independent of pressure and, as suggested by those investigators, the liquid holdup measurements made at atmospheric pressure can be assumed to occur at higher pressures. In this study, the gas phase maximum volumetric flow rate was 1 L (STP)/min which translates into a gas velocity of 0.833 cm/s at standard conditions. Since the data from these experiments were to be used for analysis of trickle-bed data at 1.1 MPa pressure, the Reynolds number of the gas phase, Re_G , was kept constant to maintain similar momentum transfer conditions between phases under the different pressure conditions.

The column used for the hydrodynamic experiments was clear acrylic with a 2.067 in. (5.25 cm) I.D. and about 24 in. (61 cm) in length. The column was filled with the catalyst used for trickle-bed experiments to a depth of about 12 in. (30 cm). The catalyst was supported in the column by a 20 mesh stainless steel screen. Gas and liquid were introduced separately into the column and the liquid distributor has the same hole distribution as that used in the trickle-bed reactor as shown in Figure 3.9.

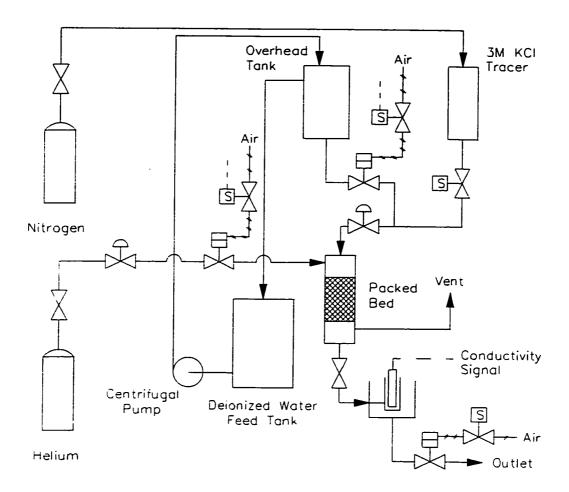


Figure 3.10 Hydrodynamic packed bed flow diagram (S = solenoid actuated valve)

For both liquid holdup and catalyst wetting experiments, deionized water from the feed tank was pumped to an overhead tank which overflowed back into the feed tank. This enabled a constant liquid height to be maintained in the overhead tank. The flow of liquid from the overhead tank was regulated by a rotameter. For the wetting experiments, a second smaller feed tank containing 3 mol/L KCl tracer, was pressurized with nitrogen. The pressure of nitrogen was great enough that the change in static head due to depletion of the tracer in the tank was negligible. The tracer was introduced into the liquid feed line far enough from the inlet to the packed bed so as to provide sufficient mixing of the tracer and the deionized water. The flow of tracer was metered by a hand-controlled valve. The liquid leaving the packed bed passed through a conductivity cell consisting of a conductivity probe inserted into a ½" PVC pipe.

The probe was connected to a conductivity meter and the signal was also sent to a data acquisition system. The conductivity was sampled by the data acquisition system every 2 seconds. This was considered more than satisfactory since the shortest runs were up to 3 hours in duration.

A typical experiment consisted of establishing a constant flow rate of deionized water and tracer to the packed bed; these flows were maintained for 1 to 3 hours. The purpose of these flows was to saturate the internal pores of the catalyst with liquid. A step-change was then made in tracer concentration by stopping its flow. The tracer concentration would then start to decrease monotonically with time. To generate the concentration response with time, several transformations of the data were required. Since the data directly measured was voltage from the conductivity meter, this signal was converted to conductivity by use of a calibration curve. Since conductivity is a function of temperature, the values were then corrected to a conductivity measured at 20°C. The conductivity vs. time curve was then integrated with respect to time to determine the zeroth and first moments. Theoretically, the conductivity should reach zero at infinite time. For practical purposes however, the experiment was concluded when the conductivity reached a value about 10⁻⁴ times the initial value. Since integration in required to determine the zeroth and first moments of the curve, the curve was extrapolated to zero by assuming an exponential tail from the point when the experiment ended to time infinity. The integration to determine a given moment consisted of two parts. The first was the numerical integration of the moment integrand using Simpson's rule and the second was the analytical integration of the exponential extension to the curve from the end time of the experiment to time infinity. The two contributions were then summed to give the required moment.

As a note, the one difficulty with a step-change experiment, is the tailing of the conductivity curve at very long times. This tailing effect can be magnified for the first moment compared to the zeroth moment due to the multiplication by time within the integrand for the first moment. In general moment techniques are useful and often

satisfactory, but Wakao et. al. (1982) point out that direct fitting of the model to the experimental data is usually superior to moment techniques. The advantage of moment techniques is that data processing is easier.

In addition to liquid holdups and external catalyst wetting, bed porosity and catalyst particle internal porosity were determined. The bed porosity was measured by weighing the bed dry and weighing it after filling the bed with liquid. This technique was similar to that of Goto and Smith (1975a). To calculate the bed porosity from these measurements the catalyst internal porosity was required and was determined by mercury penetrometry. Since mercury penetrometry cannot measure pore radii of less than 2 nm, BET analysis was used to determine the pore area and this was compared with the pore area as determined by mercury penetrometry.

Static and dynamic holdups were determined using the technique outlined by Goto and Smith (1975a). The procedure is used to establish constant liquid and gas flow through the bed. After steady state has been reached, liquid flow is stopped while maintaining constant gas flow. Liquid that drains from the bed is collected until no more liquid leaves the column. The residual liquid remaining in the bed is the total static liquid holdup which includes external and internal static liquid holdups. The total static liquid holdup is determined by weighing the bed and subtracting the dry weight of the bed from the total mass of the wet bed. To determine the external static liquid holdup, the internal liquid holdup is calculated based on the assumption of completely filled catalyst pores (Mills and Dudukovic, 1981; Colombo et al., 1976), which is widely accepted in the literature and the internal porosity as determined by mercury penetrometry. This internal liquid holdup is subtracted from the total static liquid holdup to give the external static liquid holdup. The cumulative sample collected provides the dynamic holdup. In addition to the cumulative sample, measurements of dynamic liquid holdup were made as a function of time to determine the response time of bed drainage.

CHAPTER FOUR

TRICKLE-BED REACTOR EXPERIMENTAL RESULTS

4.1 Outline

This chapter presents the results of two main sets of trickle-bed experiments: crotonaldehyde hydrogenation under steady-operation and under periodic operation. The steady operation results of Section 4.2 provide three pieces of information. The first is an estimate of the reaction rate law and kinetic parameters and demonstration that these estimates are reasonable. The second is the determination of which operating regimes occur under which operating conditions (for example mass transfer control versus reaction kinetic control. The third is the establishment of base case steady-operation experiments which are compared with periodic operation results of Section 4.3. The presentation of the results of Section 4.3 is followed by an interpretation of these results in Section 4.4.

4.2 Trickle-bed Reactor Steady Operation Experiments

4.2.1 Estimation of Kinetic Rate Law and Kinetic Parameters from Steady Operation Data at 1.1 MPa

To estimate kinetic data from a trickle-bed reactor several conditions must be fulfilled:

- 1. External mass transfer must not control the overall rate of reactant consumption.
- 2. Internal pore diffusion must not control the overall rate of reactant consumption.
- 3. External catalyst wetting should be complete.
- 4. Conversion of limiting reactant(s) should be as low as possible (less than 20%).
- 5. Significant temperature gradients should not exist within the reactor. The reaction should thus occur at a low temperature.

For the trickle-bed reactor under study, the best possible operating conditions for satisfying 1, 3, 4, and 5 are high liquid velocity. Under sufficiently high liquid

velocities, condition 1 can be fulfilled since external mass transfer coefficients increase with liquid velocity. External catalyst wetting increases with liquid velocity so at sufficient liquid velocity, condition 3 should be satisfied. As external catalyst wetting approaches unity, high liquid velocity should also prevent significant thermal gradients (condition 5). However, that though the hydrogenation of crotonaldehyde is exothermic, its concentration in the liquid phase is so dilute that even at high conversions, the temperature rise would be very small. Higher liquid velocity also means a lower residence time which will maintain low conversion, a necessary requirement for condition 4. Maintaining a low temperature (condition 5) ensures that the intrinsic reaction kinetics are the rate determining step in the hydrogenation of crotonaldehyde. Internal diffusion can be important but as stated by Satterfield (1991) the effectiveness factor can be considered close to unity for shell impregnated catalysts, that is, catalysts that have the active material deposited in a thin layer within the porous support of the catalyst near the outer surface of the particle much like a thin shell. The Pd/γ -Al₂O₃ catalyst used in this study is such a catalyst and therefore the effectiveness factor assumed to be unity.

From the trickle-bed steady operation experiments, at the two temperatures of operation, 25°C and 50°C, at 1.1 MPa hydrogen pressure and at the highest liquid velocities, the following steady-state observations were recorded.

Liquid Flow [mL/min]	Conversion	Rate [mol/min]	Temperature	Pressure [MPa]
475.4	0.00500	8.48×10^{-6}	25	1.1
447.3	0.22016	3.52×10^{-4}	50	1.1

Table 4.1 Trickle-bed reactor steady operation data for estimation of kinetic rate parameters

The rate constants were calculated assuming that the intrinsic reaction rate of crotonaldehyde hydrogenation was controlling and that the reaction rate law had first order dependence on liquid-phase crotonaldehyde concentration,

$$-r_{\rm CRHO} = k\eta C_{\rm CRHO} \tag{4.1}$$

and with $\eta \cong 1$ equation (4.1) becomes

$$-r_{\rm CRHO} = kC_{\rm CRHO} \tag{4.2}$$

This assumption is typical (Gates et. al., 1979) and was deemed valid at 1.1 MPa pressure since the concentration of hydrogen compared to crotonaldehyde in the liquid phase was calculated (Appendices A and B) to be in the ratio of over 2:1 as listed in Table 4.2.

	T [°C]		
P [atm]	25 50		
1	0.22 0.20		
11	2.42	2.24	

Table 4.2 Ratio of dissolved hydrogen and crotonaldehyde concentrations (mol H₂/mol crotonaldehyde)

At 1.1 MPa, if the crotonaldehyde conversion is about 20%, the hydrogen concentration in the liquid phase will drop less than 10% from its initial feed value. Therefore the assumption that the hydrogen concentration is constant is reasonable and equation (4.2) can be assumed to be independent of dissolved hydrogen concentration. Notice however that the opposite is true at 0.1 MPa hydrogen pressure where the ratio of hydrogen to crotonaldehyde in the liquid phase is about 1:5.

To estimate the rate constant of equation (4.2), two approaches were used. The first assumed that if the conversion of crotonaldehyde is sufficiently low, then the crotonaldehyde concentration is approximately constant across the length of the trickle-bed. This first approach approximates the behavior of the trickle-bed reactor with that of a CSTR and is treated in detail in Appendix E. The second approach

treats the trickle-bed as a plug-flow reactor with respect to the crotonaldehyde concentration and the reactor design equation is integrated over the entire trickle-bed length. The second approach is treated in detail in Appendix F. Common to both approaches is the use of correlations to estimate liquid-solid mass transfer coefficients. The analysis was adapted from the work of Sylvester (1975) and his treatment of the estimation of kinetic rate parameters from slurry and trickle-bed reactor data, as shown in Appendix D. From these two techniques, the kinetic rate constant was estimated for equation (4.2) as listed in Table 4.3.

Temperature [°C]	CSTR Estimate [s ⁻¹]	Integral Estimate [s-1]	Percent Difference
2.5	7.242×10^{-5}	7.250×10^{-5}	0.11
50	3.113×10^{-3}	3.530×10^{-3}	13.4

Table 4.3 Estimates of the kinetic rate constant of equation (4.2) from trickle-bed steady operation experimental data (1.1 MPa hydrogen pressure)

The agreement between the estimates at 25°C is very good and even at 50°C is reasonable, given the fairly high crotonaldehyde conversion of about 22%. Since the reaction rate constants are obtained from two different temperatures an estimate of the activation energy of the kinetic rate constant was made by using the Arrhenius expression. Estimates of the activation energy are given in Table 4.4.

Activation energy estimate technique	Activation energy [kJ/mol]
CSTR	120.50
Integral PFR	124.49
Percent Difference	3.3 %

Table 4.4 Estimates of the activation energy for the reaction rate constants of Table 4.3

As in the case of the reaction rate constants, the agreement between the two estimates of the activation energy is very good. Note that studies of crotonaldehyde

hydrogenation on Pd/γ - Al_2O_3 are present in the literature, the hydrogenation of dilute aqueous phase crotonaldehyde is not.

Given the calculations of the kinetic rate constant and the activation energy it is important to attempt to verify that the rate constant estimated is a measure of the reaction rate and not for example the rate of mass transfer. This means that the data used for the estimation of the reaction rate constant, were from experiments conducted in the kinetically controlled regime and not the mass transfer controlled regime. Further it would be useful to verify the assumption that the catalyst effectiveness factor is close to unity implying that internal diffusion effects can be ignored.

To verify that the rate constant is a measure of the intrinsic reaction rate constant, the resistance of each individual rate process (i.e. surface reaction and liquid-solid mass transfer) is determined. The largest resistance is then the rate determining or controlling step. The calculations are shown in Appendix G and the results of this analysis are shown in Figure 4.1. This figure shows how the relative magnitudes of the rate process resistances vary with liquid velocity. It is assumed that the external catalyst surface is wetted with liquid. As shown in the figure, the rate of crotonaldehyde hydrogenation at 25°C is exclusively controlled by the rate of surface reaction not only at high liquid velocities but over the entire range of liquid flow rates. This is correct assuming that the mass transfer coefficients are correct. At 50°C the rate controlling process the distribution of resistances changes but it is still dominated by kinetic control over the entire liquid velocity range although at the lowest liquid velocities liquid-solid mass transfer accounts for a maximum of about 30% of the overall resistance to the overall rate of crotonaldehyde consumption. demonstrates that estimating the reaction rate constant from steady-state experimental data at the highest liquid flow rates should not be in serious error.

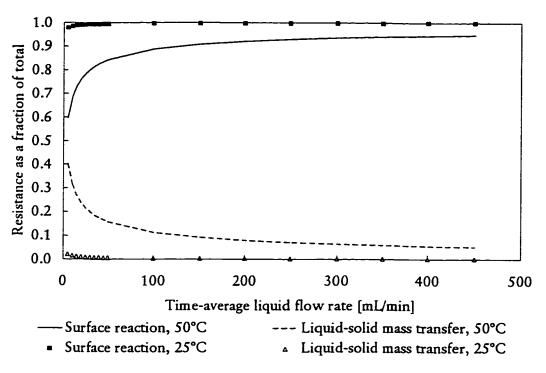


Figure 4.1 Contributing resistances to overall reaction rate as a function of liquid flow rate for steady operation experiments at 25 °C, 1.1 MPa and 50 °C, 1.1 MPa

The estimate of the activation energy of 124.49 kJ/mol suggests that the rate of crotonaldehyde hydrogenation is not controlled by internal diffusion within the catalyst since the apparent activation energy for strong diffusion control ranges typically between 8 and 24 kJ/mol (Fogler, 1986). Since this is also the range of external film diffusion control it too can be assumed to be absent.

A second approach can be used to verify calculated reaction rate constants for 25°C and 50°C and 1.1 MPa pressure, and the activation energy. Recall equation (2.17), a first order model developed assuming a first order dependence of reaction rate on crotonaldehyde concentration,

$$ln\frac{1}{1-X} = \frac{k_{v}(1-\varepsilon_{B})\eta f}{SV}$$
 (2.17)

If steady-state data at 25° C and 50° C and 1.1 MPa, at the highest liquid flow rates is fitted to equation (2.17), then f can be assumed close to unity, since catalyst external wetting becomes complete at large liquid flow rates. The effectiveness factor is also assumed to be unity since the catalyst particles are shell impregnated (Satterfield, 1992). Equation (2.17) then becomes

$$\ln\frac{1}{1-X} = \frac{k_{v}(1-\varepsilon_{B})}{SV} \tag{4.3}$$

Figures 4.2 and 4.3 show equation (4.3) fitted to the steady-state data at 25°C and 50°C and 1.1 MPa.

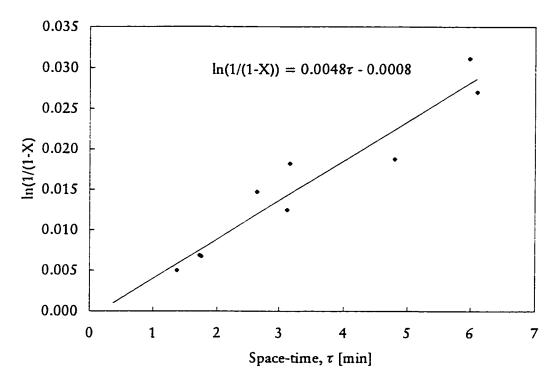


Figure 4.2 First order plot of steady-state data at high liquid flow rates (greater than 100 mL/min) for 25°C and 1.1 MPa

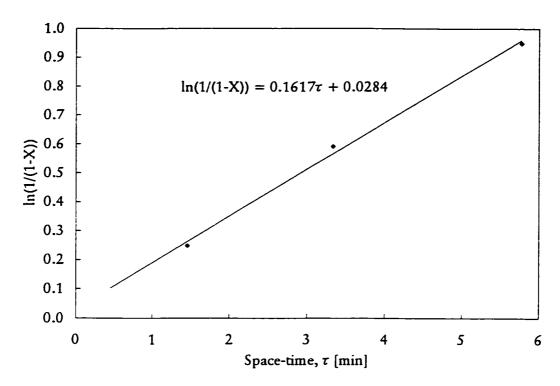


Figure 4.3 First order plot of steady-state data at high liquid flow rates (greater than 100 mL/min) for 50°C and 1.1 MPa

Table 4.5 lists the rate constants calculated from Figures 4.2 and 4.3 and compares them with the rate constants calculated previously.

Reaction rate constant estimate	25°C	Percent difference*	50°C	Percent difference*
First order rate law	8.000×10^{-5}		2.695×10^{-3}	·
CSTR	7.242×10^{-5}	9.5	3.113×10^{-3}	-15.5
Integral	7.250×10^{-5}	9.4	3.530×10^{-3}	-31.0

^{*} Percent difference compared to first order rate law

Table 4.5 Reaction rate constant estimates for steady operation at 25°C and 50°C and 1.1 MPa

The rate constants at 25°C are in better agreement with each other, than those at 50°C. One likely reason for this is that the estimate of the rate constant from the first order model is an apparent rate constant, which includes not only the reaction rate constant but also a liquid-solid mass transfer coefficient, as discussed in Appendix D. At 50°C

the difference between the magnitudes of the kinetic rate constant and the liquid-solid mass transfer coefficient is lower, thus contributing to a larger deviation between the kinetic rate constant and the apparent rate constant. A calculation, similar to that of Appendix E or F, can be performed to estimate the reaction rate constant, accounting for the liquid-solid mass transfer coefficient. However, the first order rate constant estimates, even without the correction, provide reasonable confirmation of the reaction rate constant values estimated in Appendices E and F. The other reason for the discrepancy could also be the estimate of the liquid-solid mass transfer coefficients, since this will depend on the correlation used.

With the first order rate constant estimates of Table 4.5, an activation energy can also be calculated. This estimate and the two previous estimates are listed in Table 4.6. The agreement between the various activation energy estimates is reasonable suggesting that the previous reaction rate constant estimates are sound.

Activation energy estimate data source	Activation energy value [kJ/mol]	Percent difference
First order rate law	112.69	
CSTR	120.50	-6.9
Integral	124.49	-10.5

^{*} Percent difference compared to first order rate law

Table 4.6 Activation energy estimates for steady operation at 1.1 MPa

4.2.2 Estimation of Kinetic Rate Law and Kinetic Parameters from Steady Operation Data at 0.1 MPa

Figure 4.4 shows steady-state crotonaldehyde conversions at the three different reaction conditions: 25°C, 1.1 MPa; 50°C, 1.1 MPa; 50°C, 0.1 MPa. From this figure, the effect of hydrogen pressure on conversion is apparent.

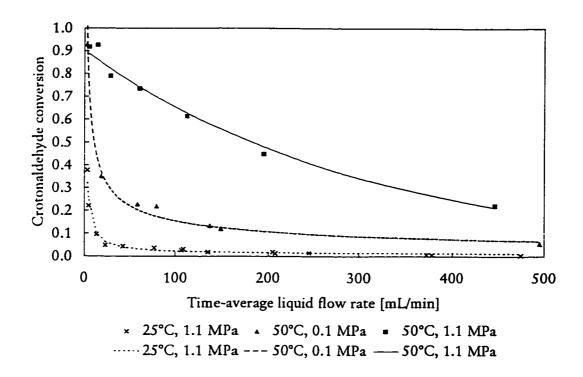


Figure 4.4 Steady-state crotonaldehyde conversion vs. liquid flow rate data for 25°C, 1.1 MPa, 50°C, 1.1 MPa, and 50°C, 0.1 MPa

If hydrogen mass transfer is the cause of the observed reduction, then the rate of hydrogenation, $r_{hydrogenation}$, will be proportional to the pressure of hydrogen divided by the sum of resistances to product formation

$$\tau_{hydrogenation} = \frac{P_{H_1}}{\sum \text{Resistances}}$$
 (4.4)

where

$$\sum \text{Resistances} = \frac{1}{k \eta C_{CRHO}} + \frac{1}{k_s a_s} + \frac{1}{k_L a_i}$$
 (4.5)

If mass transfer is important at 0.1 MPa, then \sum Resistances at 0.1 MPa will be greater than the \sum Resistances at 1.1 MPa and therefore

$$\left(\frac{r_{bydrogenation}}{P_{H_1}}\right)_{1.1 MPa} > \left(\frac{r_{bydrogenation}}{P_{H_2}}\right)_{0.1 MPa}$$
(4.6)

Since at high liquid flow rates (and low conversions) the hydrogenation rate is proportional to the conversion, then

$$\left(\frac{X}{P_{H_1}}\right)_{1.1\,MP_a} > \left(\frac{X}{P_{H_2}}\right)_{0.1\,MP_a}$$
 (4.7)

These ratios are calculated in Appendix F. The result is that the above inequality is not satisfied (the ratio on the left is about 1/3 of the ratio on the right). Therefore the reduction of hydrogen pressure from 1.1 MPa to 0.1 MPa does not result in a reduced gas-liquid mass transfer coefficient, such that it controls the rate hydrogenation instead of reaction kinetics. Rather, the reduction in the hydrogenation rate is most likely due to the reduced concentration of hydrogen in the liquid phase as described by Henry's law.

Using the high liquid flow rate steady state data at 50°C for both pressures it should be possible to determine a kinetic rate expression dependent upon hydrogen and crotonaldehyde concentrations. The kinetic expression derived in Appendix F, is

$$-r_{CRHO} = kC_{H_1}^{0.5}C_{CRHO} (4.8)$$

The kinetic rate constants are calculated in Appendix F and are listed in Table 4.7. Note that calculations of the rate constant at 50°C were done with 0.1 MPa and 1.1 MPa steady-state data, and as anticipated, their values are almost equal (about a 6% difference). Additionally, the activation energy is estimated at 122.2 kJ/mol, by using

the rate constants in Table 4.7. This estimate of the activation energy compares well with the estimates of activation energy for the kinetic rate law which was first order in crotonaldehyde concentration only.

Conditions	Rate constant [(L/mol) ^{1/2} min ⁻¹]
25°C, 1.1 MPa	0.063
50°C, 1.1 MPa	2.95
50°C, 0.1 MPa	2.78

Table 4.7 Kinetic rate constants for equation (4.8)

The kinetic rate law, equation (4.2), can be treated as a special case of equation (4.8), where the concentration of hydrogen is assumed constant in the liquid phase. This is possible if the conversion of hydrogen is low, thus insuring no significant reduction in hydrogen pressure and a relatively constant gas-liquid mass transfer gradient. In Appendix B the ratio of hydrogen mole flow (at 1 L/min STP) to crotonaldehyde mole flow (at a maximum value of 450 mL/min) was calculated to be approximately 28:1. Therefore, if conversion of crotonaldehyde were 100 percent at the maximum liquid flow rate, the conversion of hydrogen could only reach a maximum of about 4 percent. In reality the maximum crotonaldehyde conversion observed was about 20 percent at 450 mL/min, so the hydrogen conversion would be less 1 percent. Provided pressure drop is not significant, as was also observed in the experiments of this study, hydrogen pressure across the bed should be relatively constant. Therefore the hydrogen concentration (now assumed constant along the bed length for a given hydrogen pressure) can be incorporated into the kinetic rate constant, resulting in equation (4.2). The implication of this is that the kinetic rate constant is a function of hydrogen pressure.

The kinetic rate constant for 50°C and 0.1 MPa assuming a first order dependence of the kinetic rate law on crotonaldehyde concentration can estimated by the techniques used in the previous section. The utility of such an estimate is that it can then be used

for a resistance analysis, similar to that of Figure 4.1. The simplest way of estimating the kinetic constant is by linear regression of high liquid flow rate steady-state data (liquid flow rates exceeding 100 mL/min) with the first order model, equation (4.3). While it may not be the most accurate, its results are of acceptable accuracy as seen previously. Figure 4.5 shows the resulting linear regression.

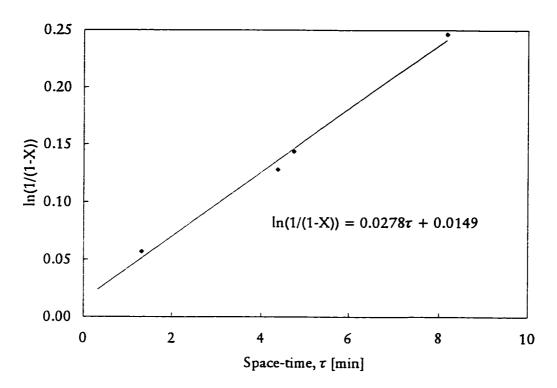


Figure 4.5 First order plot of steady-state data at high liquid flow rates (greater than 100 mL/min) for 50°C and 0.1 MPa

From Figure 4.5, $k_{0.1 \text{ MPa}, 50^{\circ}\text{C}} = 4.63 \times 10^{-4} \text{ s}^{-1}$ and is used to generate Figure 4.6 which shows the contributing resistances impeding the overall rate of reaction. The results of Figure 4.6 are not surprising. The kinetic rate constant $k_{0.1 \text{ MPa}, 50^{\circ}\text{C}}$ is between the values for 50°C and 1.1 MPa and 25°C and 1.1 MPa combined with the results of Figure 4.1, one could predict that reaction kinetics would control the overall rate of reaction.

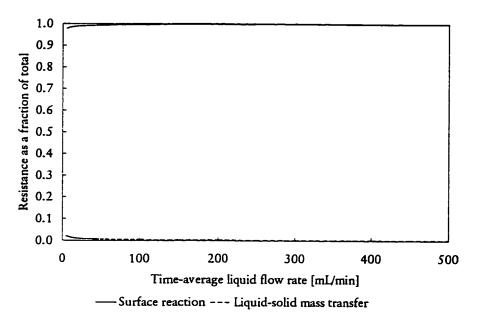


Figure 4.6 Contributing resistances to overall reaction rate as a function of liquid flow rate for steady operation experiments at 50 °C, 0.1 MPa

The calculation of resistances to the overall reaction rate is dependent upon the estimation of the liquid-solid mass transfer coefficient. For the calculations of these resistances, the correlation of Goto and Smith (1975a) was used. However, many liquid-solid mass transfer correlations exist in the literature as summarized by Gianetto and Silveston (1986). From the large selection of correlations, the Goto-Smith correlation was chosen for several reasons. First, liquid and gas flow rate ranges of the correlation encompassed the gas flow rate and most of the liquid flow rate range used in this study, as summarized in Table 4.8. It was the best of the choices available for this criterion.

	Liquid flow	Gas flow rate
	rate range	range
	$[kg/(m^2 s)]$	$[kg/(m^2 s)]$
Goto-Smith correlation	0.48 to 5	0 to 0.009
This study	0.04 to 3.8	7.4×10^{-4}

Table 4.8 Fluid flow ranges for Goto-Smith liquid solid mass transfer coefficient correlation

Second, the liquid used was water and the gas oxygen which has a solubility in water comparable to hydrogen (Perry and Green, 1984). Finally the particle sizes used in the Goto-Smith study were comparable to those used in this study. Taking these criteria into account, it was the best choice of the liquid-solid mass transfer correlations available. Despite these reasons, however, the system used for the development of the Goto-Smith correlation is not identical to the system studied here and large deviations between the mass transfer coefficient predicted by the Goto-Smith correlation and those present in this system are possible. It may also be that the Goto-Smith correlation is not the best for this system but rather another correlation. With this in mind, it would be useful to estimate how sensitive the resistance analysis is to the estimate of the liquid-solid mass transfer coefficient.

It has been established in Figures 4.1 and 4.6 that the rate of hydrogenation is controlled by reaction kinetics. To test the effect of the liquid-solid mass transfer coefficient value on the resistance analysis, resistance analysis are repeated, assuming liquid-solid mass transfer coefficients ½ and 2 times the values predicted by the Goto-Smith correlation. The results shown in, Figures 4.7 and 4.8 confirm that the hydrogenation rate is controlled by reaction kinetics, certainly over the entire liquid flow rate range at 25°C, and for most of the liquid rate range at 50°C, with the exception being at the lowest liquid flow rates at 50°C. The calculation was not repeated for 50°C and 0.1 MPa since it was shown earlier that the resistance curves for these conditions lie between those of 25°C, 1.1 MPa, and 50°C, 1.1 MPa.

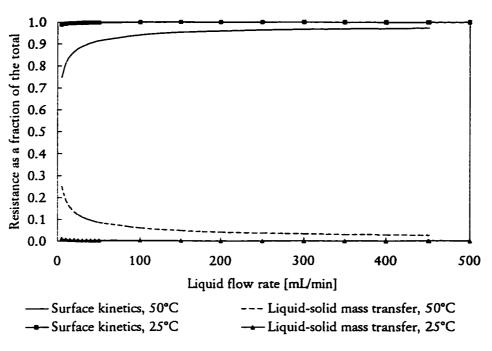


Figure 4.7 Contributing resistances to overall reaction rate as a function of liquid flow rate for steady operation at 25°C and 50 °C, 1.1 MPa, assuming a liquid-solid mass transfer coefficient twice that predicted by the Goto-Smith correlation

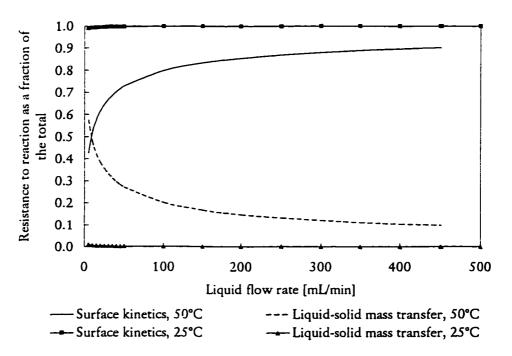


Figure 4.8 Contributing resistances to overall reaction rate as a function of liquid flow rate for steady operation at 25°C and 50 °C, 1.1 MPa, assuming a liquid-solid mass transfer coefficient half that predicted by the Goto-Smith correlation

4.3 Comparison of Steady and Periodic Operation

4.3.1 Comparison of Steady and Periodic Operation Data at 25°C and 1.1 MPa

In Figure 4.9, crotonaldehyde conversion is plotted against time-average liquid flow rate under steady operation conditions. Steady operation implies that the liquid flow rate is temporally constant and varies only insignificantly around some average value (due to random fluctuations). Therefore the time-average liquid flow rate into the reactor can be considered the *instantaneous* flow rate into the reactor. As seen in the figure, high liquid flow rates result in low conversions with the converse true at low liquid flow rates. This suggests a relationship between conversion and residence time of the flowing liquid. As suggested in Chapter 2 a pseudo-homogeneous model can be used which assumes that the trickle-bed is a single-phase reactor. Therefore equation (2.12) can be used to describe the relationship between conversion and liquid velocity (or space velocity)

$$ln\frac{1}{1-X} = \frac{k_{\nu}(1-\epsilon_B)\eta L}{u_I} = \frac{k'_{\nu}\eta}{SV}$$
 (2.12)

provided the gas phase reactant is in excess compared to the liquid phase reactant, which implies that the gas phase reactant concentration is relatively constant over the length of the catalyst bed.

Note that if the effectiveness factor approaches unity, then the constant k'_{v} is the reaction rate constant if the system described by the model is reaction limited. If the system is mass-transfer limited, then k'_{v} represents a measure of the mass transfer resistance. One such analysis was shown in Figure 4.1. Also the effect of external catalyst wetting cannot be overlooked either since it too is strongly dependent on liquid velocity, and it will influence the value of k'_{v} observed, particularly in the low liquid flow rate regions.

Figure 4.10 provides a plot of equation (2.12) over the entire liquid flow rate range. This liquid range from 0 to 450 mL/min is quite large and by examining Figure 4.10 it becomes evident that the regression line over the entire liquid flow rate range is not necessarily the best straight line at the very low time-average space times. This becomes more evident if the data for just the low time-average space times is plotted with the line of same slope from Figure 4.10, as shown in Figure 4.11. The line from Figure 4.10 has a slope which is lower than that for the data of Figure 4.11. This is possible, since over such a wide liquid flow rate range, the effect of liquid flow rate on the apparent rate constant could appear due to reduced mass transfer or poor catalyst external wetting at the lower liquid flow rates. This suggests that the data for the entire flow rate range be broken into separate sections and treated separately. This is done in Figures 4.12 and 4.13.

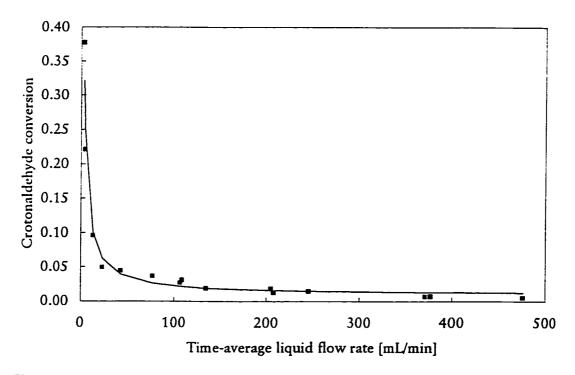


Figure 4.9 Crotonaldehyde conversion vs. liquid flow rate under steady operation, 25 °C, 1.1 MPa, liquid flow rate range: 0 to 450 mL/min

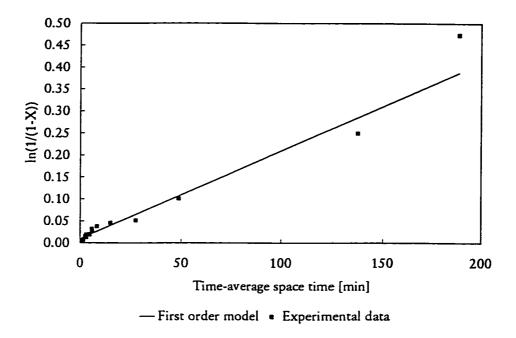


Figure 4.10 First order rate law plot for steady operation, 25 °C, 1.1 MPa, liquid flow rate range: 0 - 450 mL/min

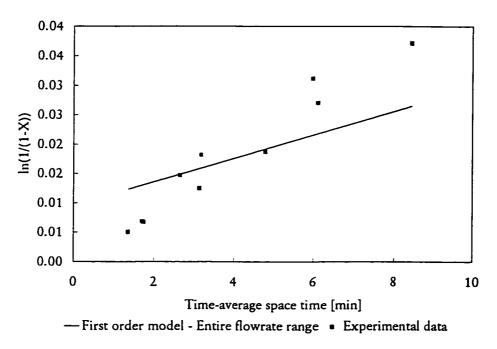


Figure 4.11 First order rate law plot for steady operation, 25 °C, 1.1 MPa Comparison of experimental data, liquid flow rate range: 50 - 450 mL/min with first order model fitted over entire flow rate range (5 - 450 mL/min)

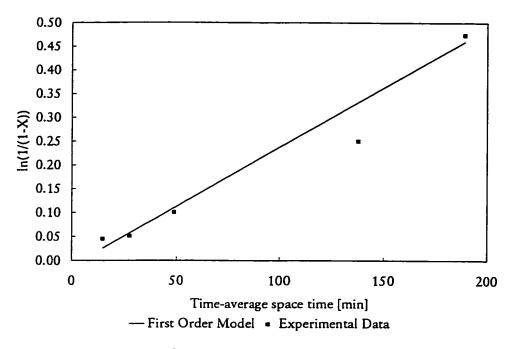


Figure 4.12 Steady operation first order plug flow model 25 °C, 1.1 MPa, liquid flow rate range: 0 - 50 mL/min

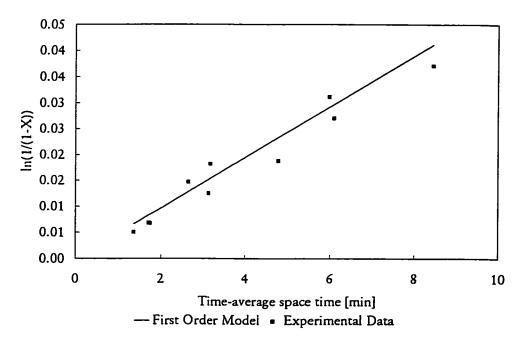


Figure 4.13 Steady operation first order plug flow model, 25°C, 1.1 MPa, liquid flow rate range: 50 - 450 mL/min

From the data in Figures 4.12 and 4.13, an apparent rate constant can be determined from the straight line fitted through the data. A summary of this analysis is shown in Table 4.9.

Liquid Flow rate Range [mL/min]	Apparent <i>k</i> [s ⁻¹]	R ² of regression
0 to 50	0.002499	0.94
50 to 450	0.004880	0.94

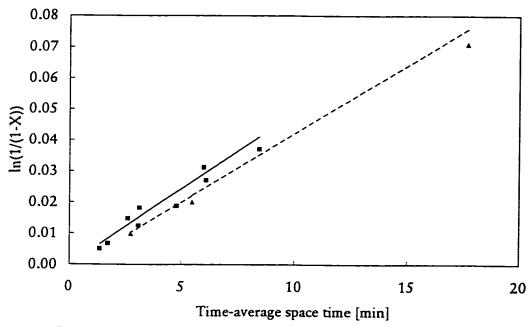
Table 4.9 Apparent rate constants for steady operation at 25°C and 1.1 MPa

The apparent k for the higher liquid flow rate region is about twice that of the lower liquid flow rate region. As shown previously, mass transfer is not the rate determining step in the region above 50 mL/min. This suggests that the bed is well wetted in this region since the apparent k shows no change with liquid flow rate. However the value of k in the higher liquid flow rate region does not remain constant as the liquid flow rate drops below 50 mL/min. While the effect of mass transfer on the overall rate of crotonaldehyde consumption is an increasing factor (as high a about 30% of the overall resistance to crotonaldehyde consumption at a liquid flow rate of 5 mL/min), it is not the dominant one. However in this low liquid flow rate region, poorer external catalyst wetting should become a factor.

To compare steady and periodic operation results with each other at 25°C, the basis of comparison was the calculation of a time-average apparent k as a function of the liquid flow rate. As before, experiments for periodic operation were conducted over a wide range of liquid flow rates so the results were broken into two regions. Given the limitations of experimental equipment, not all choices of independent variables are possible in a desired flow range. For example while it is possible to have steady operation data for a liquid flow rate of 450 mL/min, to accomplish the same time-average liquid flow rate with a split of 0.1 would require the instantaneous liquid flow

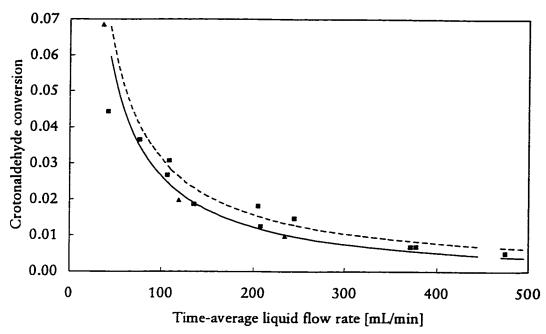
rate to be 10 times the steady operation value or 4.5 L/min, a condition not possible with this equipment.

Figure 4.14 shows this comparison between steady operation and periodic operation for a 5 minute period and 0.5 split over the 50 to 450 mL/min range in the form of a first order plot. Figure 4.15 shows the same data as Figure 4.14 but plotted as conversion against liquid flow rate. Figure 4.14 shows that the slope of the first order plot for periodic operation is virtually the same as for steady operation suggesting that for this liquid flow range and these conditions there is no difference in performance.



- Steady Operation Experimental Data Steady Operation First Order Model
- ▲ Periodic Operation Experimental Data --- Periodic Operation First Order Model

Figure 4.14 Steady and periodic operation (5 min period, 0.5 split) first order rate law plot, 25 °C, 1.1 MPa, liquid flow rate range: 50 - 500 mL/min



- Steady Operation Experimental Data --- Steady Operation First Order Model
- Periodic Operation Experimental Data Periodic Operation First Order Model

Figure 4.15 Steady and periodic operation (5 min period, 0.5 split) crotonaldehyde conversion vs. liquid flow rate, 25 °C, 1.1 MPa

Figure 4.16 shows a comparison to that in Figure 4.14 but with a 5 min period and a 0.1 split. Note that the time-average liquid flow rate range is from 0 to 50 mL/min. In this figure the slope of the periodic operation first order model is greater than slope of the steady operation first order model. This suggests that the apparent rate constant under periodic operation is greater than that for steady operation and that periodic operation results in a performance improvement compared to steady operation in this low liquid flow rate region. The rationale for this is that in the low liquid flow rate region under steady operation, external catalyst wetting becomes much poorer as shown by the Mills and Dudukovic correlation (1981). At the same time-average liquid flow rate under periodic operation, a higher liquid flow rate is required during the liquid-on portion of the cycle since the liquid is on for only a fraction of the time. The higher liquid flow rate results in a higher effective wetting of the external catalyst surface. Once liquid flow has stopped, the static liquid holdup remaining should be well distributed.

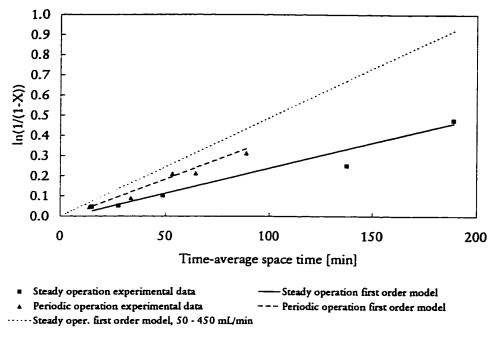


Figure 4.16 Steady and periodic operation (5 min period, 0.1 split) first order rate law plot, 25 °C, 1.1 MPa, liquid flow rate range: 0 - 50 mL/min

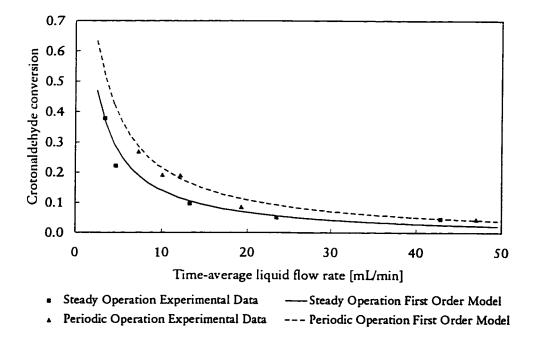


Figure 4.17 Steady and periodic operation (5 min period, 0.1 split), 25 °C, 1.1 MPa, Conversion vs. Liquid flow rate

In comparing Figures 4.14 and 4.16 it is evident that on the comparison of split, the higher splits are not as effective as the lower splits. The reason for this observation is twofold. First of all, a lower split will yield a lower time-average liquid flow rate. Since, when liquid flowed, it did so at about 450 mL/min, thus for a 0.1 split the timeaverage liquid flow rate is calculated to be about 45 mL/min. Therefore the periodic operation experiments with a 0.1 split were compared with steady operation data of the lowest liquid flow rates which are expected to have the poorest external catalyst wetting and therefore poor utilization of the catalyst. For the 0.5 split experiments the periodic operation is compared with steady operation results which are in the higher liquid flow rate region where external catalyst wetting is superior and its utilization is likewise improved. Secondly for a particular time-average flow rate, the wetting occurring during liquid flow under periodic operation is superior at lower splits since the magnitude of the liquid flow rate must increase as split decreases. For the 0.1 split experiments, the instantaneous liquid flow rate is 10 times that required to give the same time-average liquid flow rate under steady operation, while for the 0.5 split experiments the instantaneous liquid flow rate required to give the same time-average liquid flow rate under steady operation conditions is only twice that of the instantaneous liquid flow rate under steady operation. This means that the effective wetting should, at least for the duration of the liquid flow, tend to be better at the smaller splits for the same time-average liquid flow rate. This is shown by comparison of the wetting occurring with liquid flow under periodic operation as compared to steady operation in Figure 4.18.

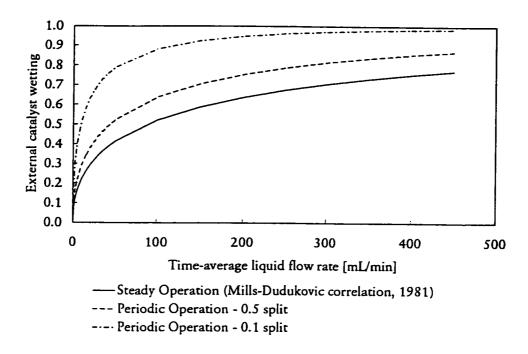


Figure 4.18 Comparison of catalyst external wetting under steady and periodic operation as a function of time-average liquid flow rate

The steady operation catalyst external wetting of Figure 4.18 is the Mills-Dudukovic correlation. To generate the 0.1 split catalyst external wetting curve consider how a single point on the curve is calculated. First select a time-average liquid flow rate, for example 45 mL/min. The liquid pulse flow rate is then 450 mL/min (1/0.1×45 mL/min). Next calculate the catalyst external wetting using the Mills-Dudukovic correlation for 450 mL/min. This value is then the catalyst external wetting for a time-average liquid flow rate of 45 mL/min under periodic operation employing a 0.1 split. A similar procedure is used for calculation of catalyst external wetting for 0.5 split periodic operation. The assumption required for these calculations, is that catalyst external wetting under periodic operation remains at the level achieved while liquid is flowing. The curves of Figure 4.19 are the ratio of each periodic operation curve (i.e. 0.1 and 0.5 splits) to the steady operation curve (i.e. the Mills-Dudukovic correlation). From Figures 4.18 and 4.19, it is clear that the difference between wetting effectiveness under periodic operation as compared to steady operation is most pronounced with lower splits and in the low liquid flow rate region.

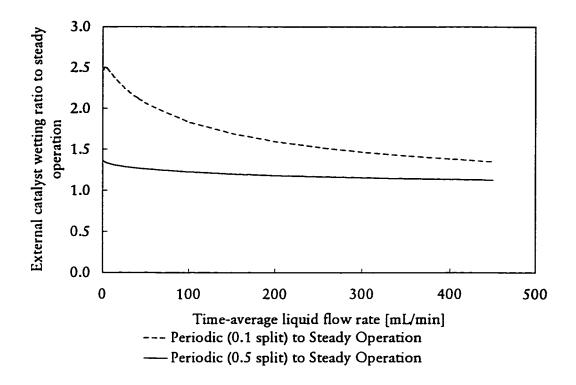
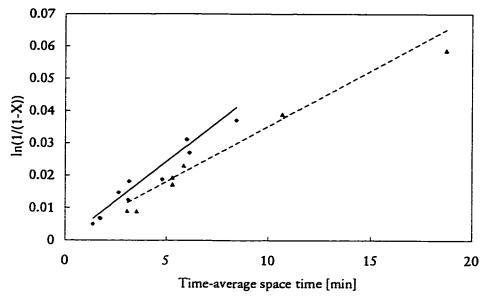


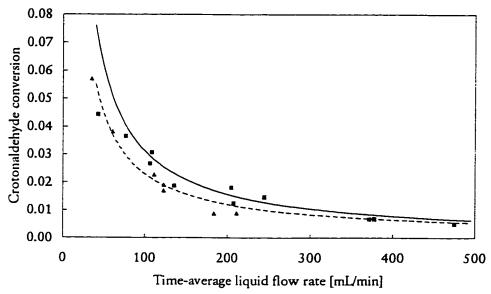
Figure 4.19 Ratio of external catalyst wetting under periodic operation (5 minute period) to that under steady operation as a function of time-average liquid flow rate

Experiments were conducted with the same splits, 0.1 and 0.5 but with a period of 20 minutes. Figure 4.20 is a first order plot of periodic operation (0.5 split) data compared with steady operation and Figure 4.21 is a plot of crotonaldehyde conversion against liquid flow rate. The liquid flow rate range is 50 to 450 mL/min. Using the previous analysis Figure 4.20 shows that the apparent rate constant is smaller for periodic operation and therefore periodic operation is inferior to steady operation. As discussed previously periodic operation is not expected to be superior to steady operation in this region. However the difference between the steady and periodic operation is greater for the 20 minute period than it is for the 5 minute period. This suggests that the longer periods are not advantageous to better performance. Leaving investigation of the cause of this until later in this section, it does suggest that at the very least an optimum value for split exists.



- Steady Operation Experimental Data ---- Steady Operation First Order Model
- A Periodic Operation Experimental Datal --- Periodic Operation First Order Model

Figure 4.20 Steady and periodic operation (20 min period, 0.5 split), first order rate law plot, 25 °C, 1.1 MPa, liquid flow rate range: 50 - 450 mL/min



- Steady Operation Experimental Data ——Steady Operation First Order Model
- Periodic Operation Experimental Data --- Periodic Operation First Order Model

Figure 4.21 Steady and periodic operation (20 min period, 0.5 split), 25 °C, 1.1 MPa, Conversion vs. Liquid flow rate

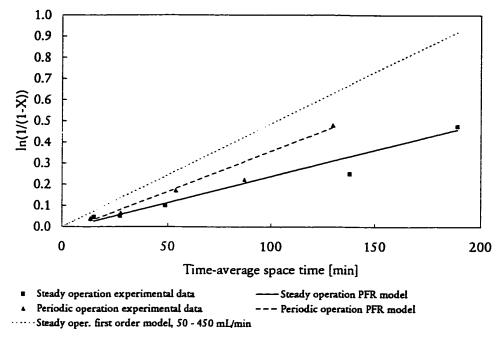
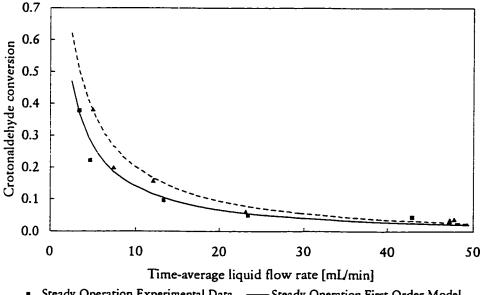


Figure 4.22 Steady and periodic operation (20 min period, 0.1 split), first order rate law plot, 25 °C, 1.1 MPa, liquid flow rate range: 0 - 50 mL/min



Steady Operation Experimental Data — Steady Operation First Order Model
 Periodic Operation Experimental Data --- Periodic Operation First Order Model

Figure 4.23 Steady and periodic operation (20 min period, 0.1 split), 25 °C, 1.1 MPa, Conversion vs. liquid flow rate

Figures 4.22 and 4.23 show the comparison of periodic operation with a 20 minutes period and a 0.1 split and steady operation. In contrast to Figure 4.20, Figure 4.22

shows that periodic operation has a greater apparent rate constant as compared to steady operation. This is consistent with the periodic operation results of Figure 4.16 where the period was 5 minutes and the split was 0.1. A summary of the results for the apparent rate constants is listed in Table 4.10.

	Apparent k [s ⁻¹]		Ratio to Steady Operation	
Trickle-bed Operation	Liquid Flow [mL/min]		Liquid Flow [mL/min]	
	0 to 50	50 to 450	0 to 50	50 to 450
Steady	0.00249	0.00487	1.00	1.00
Periodic (split, period)				
0.1, 5 min	0.00391		1.57	
0.5, 5 min		0.00440		0.90
0.1, 20 min	0.00383		1.54	
0.5, 20 min		0.00342		0.70

Table 4.10 Comparison of Apparent Rate Constants for Steady and Periodic Operation at 25°C and 1.1 MPa

From Table 4.9 for the low liquid flow rate range, the apparent rate constant for periodic operation is about 55% higher than the corresponding steady operation apparent rate constant. However for the high liquid flow rate range, the apparent rate constant for periodic operation is from 10 to 30% lower compared to steady operation.

To this point the comparison has been on a time-average liquid flow rate basis meaning that periodic operation data have been compared to steady operation data, taking into account that the liquid is not always flowing into the reactor - hence a time-average liquid flow rate is calculated (this also applies to time-average space-time). However it would be desirable to compare periodic operation with steady operation at the full range of liquid flow rates. One approach would be the calculation of a rate of throughput, i.e. the amount of material treated. In Figure 4.21 such a comparison is made by taking the first order model obtained for each liquid flow rate region and then calculating a rate of product formation. Mathematically this is

$$-r_{\text{CRHO,V}} = C_{\text{CRHO,0}} X \nu_L \tag{4.1}$$

with the term $-r_{\text{CRHO,V}}$ being the rate of consumption of crotonaldehyde [mol/min]. Another approach would be to use the data of Table 4.10 to extrapolate values of conversion at different liquid flow rates. This approach is similar to comparing the apparent rate constants in Table 4.10. Ultimately the goal is to establish the best possible operating conditions globally. The comparison is made, in Table 4.11, to the best steady operation apparent k value.

	Apparent k Liquid Flow [mL/min]		Ratio to Steady Operation Liquid Flow [mL/min]	
Trickle-bed Operation				
	0 to 50	0 to 450	0 to 50	0 to 450
Steady	0.00487*	0.00487*	1.00	1.00
Periodic (split, period)]		
0.1, 5 min	0.00391		0.81	
0.5, 5 min		0.00440		0.90
0.1, 20 min	0.00383		0.79	
0.5, 20 min		0.00342		0.70

^{*} Highest steady operation apparent k value, 50 to 450 mL/min range

Table 4.11 Comparison of Apparent Rate Constants for Steady and Periodic Operation at 25°C and 1.1 MPa, based on the highest apparent k value observed

While it is true that under certain liquid flow rate ranges periodic operation is better than steady operation within the same liquid flow rate range as shown in Figure 4.13, it is clear from Figure 4.14 that periodic operation does not provide the highest apparent rate constant over all possible liquid flow rate ranges. This raises the question: under what circumstances is periodic operation a suitable alternative to steady operation? While the answer to this question will be left to later in this chapter one comment will be made: for some of the most industrially significant reactions conducted in trickle-bed reactors periodic operation could be a viable operating alternative. Finally one other comment: while the higher liquid flow rates give higher conversions they do so at the price of reactor size and, as will be shown later, typical

trickle-bed reactor are not operated at such low space times for practical reasons. Therefore while it is true that the best steady operation mode is better than the best periodic operation mode examined in this study, for all intents and purposes it is not practical.

4.3.2 Comparison of Steady and Periodic Operation Data at 50°C and 1.1 MPa

Increasing the temperature at which a chemical reaction occurs increases the reaction rate as described by the Arrhenius expression. In section 4.1.1 this expression was used to calculate the reaction rate constant for the crotonaldehyde hydrogenation at 50°C. The reaction rate constant at 50°C was approximately 43 times its value at 25°C. However, as shown in Figure 4.1, the rate of crotonaldehyde consumption at 50°C is still dominated by surface reaction in the high liquid flow rate range. This crotonaldehyde consumption rate falls in the low liquid flow rate range as liquid-solid mass transfer resistance becomes a substantial part of the overall resistance to product formation. Thus a major difference between the experiments at 25°C and 50°C is that liquid flow rate can influence the trickle-bed behavior in two ways, especially at low liquid flow rates: The first is external catalyst wetting and the second is the liquid-solid mass transfer rate. By contrast the liquid flow rate affects trickle-bed reaction rates at 25°C through external catalyst wetting since liquid-solid mass transfer resistance was minimal compared to surface reaction.

Figure 4.24 shows crotonaldehyde conversion as a function of liquid flow rate for 50°C and 1.1 MPa for steady operation. Notice the shape of the curve is similar to Figure 4.2 for 25°C with the only difference being the magnitude of the conversion.

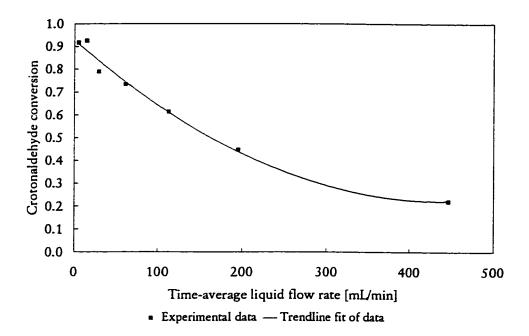


Figure 4.24 Steady operation crotonaldehyde conversion vs. liquid flow rate, 50°C, 1.1 MPa

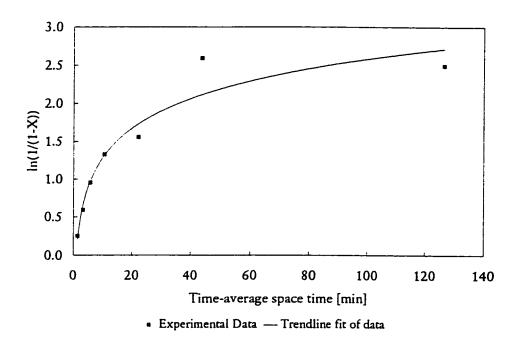


Figure 4.25 Steady operation first order plot, 50°C, 1.1 MPa

Conversions at 50°C are typically 3 to 4 times greater for a given liquid flow rate compared to the 25°C data. Figure 4.25 is a first order plot for the data of Figure

4.24. On Figure 4.25 a best fit curve using a logarithmic expression was used. The equation itself is not so important as is the shape of the curve. Clearly the slope is not constant with liquid flow rate, once again suggesting that the liquid flow rate effects the apparent rate constant. The use of the first order plot for this data is probably not advised, especially for the data at the very high space-times. This can be seen from Figure 4.25 where a straight line drawn through the points at the four highest space-times would not pass through the origin, as such a first order model should. Therefore, the comparison between steady and periodic operation data will be made using plots of conversion against time-average liquid flow rate. For the figures showing plots of crotonaldehyde conversion vs. time-average liquid flow rate, the trendlines plotted are best fit curves of the data.

Figure 4.26 shows a plot of conversion against time-average liquid flow rate for steady operation and periodic operation with a 0.1 split and 5 minute period. The results clearly show that periodic operation is inferior to steady operation under these conditions. The difference is greatest between the two operating modes at the higher liquid flow rates. However as liquid flow rate is reduced, the difference decreases and it appears that the two curves approach each other. This is consistent with previous results (i.e., at 25°C and 1.1 MPa). If steady operation is better than periodic operation at higher liquid flow rates, then as the liquid flow rate is reduced, external catalyst wetting will eventually deteriorate. As shown previously at the lower liquid flow rates periodic operation improves conversion, probably by increasing bed utilization. Thus, periodic operation should be able at least to equal steady operation in performance at low liquid flow rates. Figure 4.26 however shows that it does not surpass steady state operation. The reason for this will be discussed later in this chapter. External catalyst wetting is suggested as the reason why steady and periodic operation approach each other in conversion at low liquid flow rates. However since the temperature is now 50°C the overall rate of product formation is not controlled entirely by surface reaction resistance, since liquid-solid mass transfer becomes more important especially at very low liquid flow rates as shown in Figure 4.1.

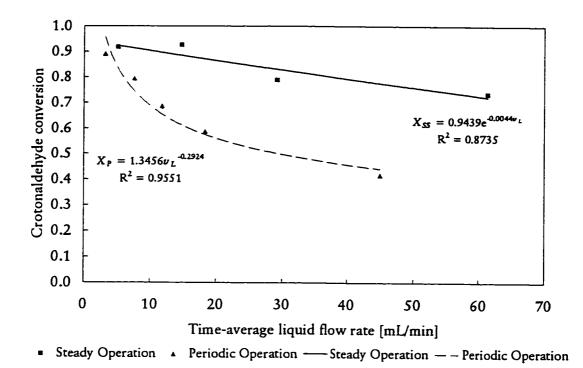


Figure 4.26 Steady and periodic operation 5 min period, 0.1 split Crotonaldehyde conversion vs. Liquid flow rate, 50°C, 1.1 MPa

Figure 4.27 plots conversion against time-average liquid flow rate for steady operation and periodic operation with a 0.5 split and 5 minute period. The difference in performance between steady and periodic operation becomes constant at the higher liquid flow rates since wetting is assumed to become complete at higher liquid flow rates. At low flow rates, conversion for periodic operation overtakes steady state conversion.

Figure 4.28 shows the comparison between steady and periodic operation for 0.1 split and a 20 minute period. Once again, the conversion for periodic operation seems to approach that for steady operation at the lowest liquid flow rates. As liquid flow rate is increased, conversion under periodic operation falls substantially below that under steady operation. The large difference between steady state and periodic operation for

the 20 minute period is probably due to the depletion of crotonaldehyde during the liquid-off portion of the cycle.

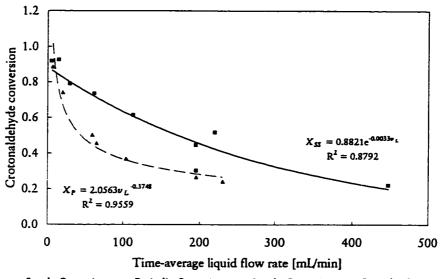


Figure 4.27 Steady and periodic operation 5 min period, 0.5 split Crotonaldehyde conversion vs. liquid flow rate, 50°C, 1.1 MPa

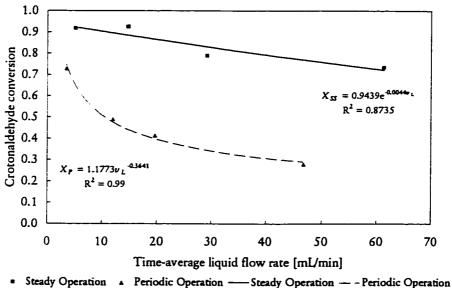
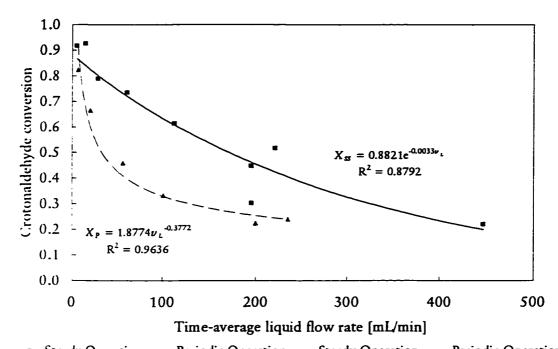


Figure 4.28 Steady and periodic operation 20 min period, 0.1 split Crotonaldehyde conversion vs. liquid flow rate, 50°C, 1.1 MPa



■ Steady Operation → Periodic Operation ——Steady Operation ——Periodic Operation

Figure 4.29 Steady and periodic operation 20 min period, 0.5 split crotonaldehyde conversion vs. liquid flow rate, 50°C, 1.1 MPa

Figure 4.29 shows the comparison for steady and periodic operation for 0.5 split and a 20 minute period. Again the difference between steady and periodic operation remains relatively constant at the higher liquid flow rates. However, at lower liquid flow rates, periodic operation matches steady state performance. The reason for this is the shorter duration between recharging the bed.

Figures 4.30 and 4.31 are a summary of the last four figures in that it shows the ratio of periodic and steady operation crotonaldehyde conversions using the trendline functions shown in the previous figures. These trendline curves are used to calculate the conversion ratios of Figures 4.30 and 4.31. As an example, for the 5 min period curve of Figure 4.30, the conversions are calculated over the range of 0 to 50 mL/min using the trendlines from Figure 4.26 ($X_P = 1.3456v_L^{-0.2924}$ for 5 minute period, 0.1

split periodic operation where X_P is crotonaldehyde conversion under periodic operation and v_L is time-average liquid volumetric flow rate) and Figure 4.24 ($X_{SS} = 0.9439e^{-0.0044v_L}$ for steady state, where X_{SS} is steady-state conversion). The conversion ratios are calculated and plotted in Figure 4.30 and 4.31 are X_P/X_{SS} .

In Figure 4.30 for both period lengths periodic and steady operation conversions approach each other as the liquid flow rate, decreases. Periodic operation using a 20 minute period is poorer than periodic operation with a 5 minute period. As discussed earlier, this is probably due to a depletion of crotonaldehyde, which occurs during the longer cycle periods. In Figure 4.31 periodic operation is again inferior to steady operation over the entire liquid flow but as liquid flow rate increases and approaches 450 mL/min, periodic operation conversion approaches steady operation conversion. As seen before, periodic operation using a 5 minute period is better than with the 20 minute period, again probably due to depletion crotonaldehyde during the longer, 20 minute period.

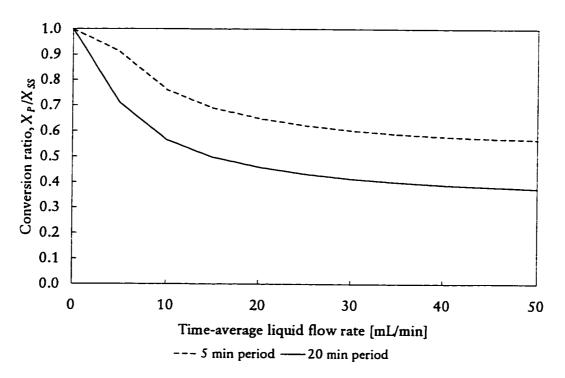


Figure 4.30 Conversion ratios for periodic to steady operation, 0.1 split, 0 - 50 mL/min, 50°C, 1.1 MPa

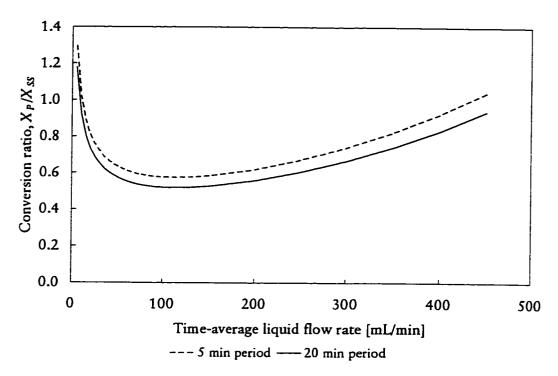


Figure 4.31 Conversion ratios for periodic to steady operation, 0.5 split, 0 - 450 mL/min, 50°C, 1.1 MPa

4.3.3 Comparison of Steady and Periodic Operation at 50°C and 0.1 MPa

The final set of trickle-bed reactor experiments were those performed at 50° C and 0.1 MPa hydrogen pressure. The objective here was to see the effect of reducing the amount of hydrogen available in the liquid phase as a consequence of Henry's law. Recall from Table 4.2 that the mole ratio of hydrogen to crotonaldehyde in the liquid phase is approximately 1:5. Therefore the situation has changed from one in which hydrogen is in excess to one where crotonaldehyde is now in excess in the liquid phase. Note that the amount of hydrogen being supplied in the gas phase is still quite large compared to crotonaldehyde and is constant for all experiments at 1 L (STP)/min. This translates to a molar flow rate of 44.6×10^{-3} mol/min. So the interesting situation arises: the amount of hydrogen supplied to the reactor is quite high as molar flow rate compared to crotonaldehyde (at the highest liquid flow rate of 450 mL/min, the flow rate of crotonaldehyde is 1.606×10^{-3} mol/min). This means that the moles of

hydrogen being supplied to the reactor are at least 27 times greater than the moles of crotonaldehyde supplied. This number increases as the liquid flow rate decreases. Thus, there is never starvation of hydrogen in the gas phase. However the concentration of hydrogen in the liquid phase is much lower (about 11 times lower than at 1.1 MPa) because of Henry's law. As shown earlier in this chapter, the hydrogenation rate at all but the lowest liquid flow rates, is controlled by reaction kinetics, under these conditions.

Figure 4.32 shows conversion against liquid flow rate for steady operation at 50°C, 0.1 MPa and 50°C, 1.1 MPa. As expected the conversion at most flow rates is lower than the conversion under steady operation at 1.1 MPa hydrogen pressure. This is also shown by taking a ratio of the conversions (based on models) for 0.1 and 1.1 MPa, in Figure 4.33.

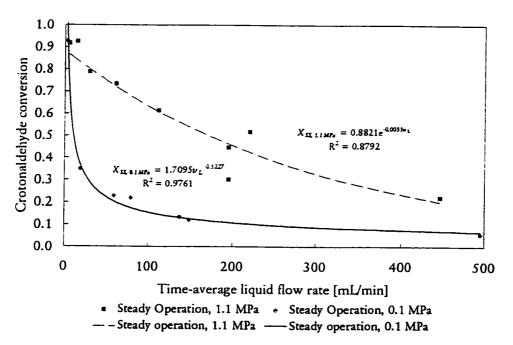


Figure 4.32 Steady operation crotonaldehyde conversion vs. liquid flow rate, 50°C, 0.1 MPa and 50°C, 1.1 MPa

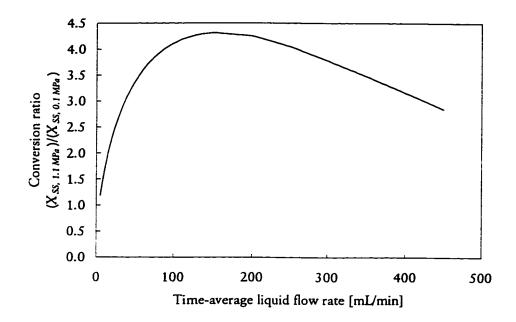


Figure 4.33 Conversion ratio ($X_{SS, 1.1 \text{ MPa}}/X_{SS, 0.1 \text{ MPa}}$) for steady operation at 50°C, 1.1 MPa and 50°C, 0.1 MPa

Figure 4.34 shows steady operation compared with periodic operation (0.1 split and 5 minute period) while Figure 4.35 shows the comparison of steady operation with 0.5 split and 5 minute period periodic operation. In both figures periodic operation gives lower conversion than steady operation especially at the higher liquid flow rates. As liquid flow rate is reduced; however, the steady and periodic operation curves approach each other and in Figure 4.34 they appear to cross each other at approximately 50 mL/min. Although the difference between both curves is small, it appears that periodic operation outperforms steady operation as the time-average liquid flow rate is decreased. Interestingly, this contrasts with the results of the previous set of experiments (25°C and 1.1 MPa hydrogen pressure), where the smaller split (0.1) produced conversion greater than steady operation. This observation may be explained by considering two factors. First the trend observed is that with lower liquid flow rates for both figures, time-average periodic operation conversion approaches and equals or exceeds steady operation. This suggests that external catalyst wetting is a factor or possibly gas-liquid mass transfer. However, if this is the case, then one would argue that a lower split should produce the highest conversion, the

reason being that a lower split means a higher flush amplitude (instantaneous flow rate) which should result in better catalyst wetting since this hydrodynamic parameter is strongly dependent on liquid flow rate. This is not observed but it does not rule out the possibility that external catalyst wetting and/or gas-liquid mass transfer are not important. Rather it suggests that the period length itself has an optimum value. The reason this optimum value exists is possibly due to the faster rate of crotonaldehyde consumption at 50°C and 0.1 MPa hydrogen pressure, as compared with the rate at 25°C and 1.1 MPa (where a lower split gave higher conversion). Consider Figure 4.36 and Figure 4.37 below showing the periodic operation conversions at 25°C and 1.1 MPa hydrogen pressure for 0.1 and 0.5 splits at 5 minute periods. As can be seen, the conversions at 50°C and 0.1 MPa (50°C and 1.1 MPa not shown but conversions are higher than those at 50°C, 0.1 MPa) are much higher than those at 25°C and 1.1 MPa hydrogen pressure which means that the rate of crotonaldehyde consumption is higher for the experiments at 50°C. That the rate of crotonaldehyde consumption is much greater in periodic operation, suggests that liquid phase reactant is being depleted during the portion of the cycle when liquid flow is stopped. The consequence would be that the additional benefit attained by using a lower split and hence a higher liquid flush rate is offset by the depletion of liquid phase reactant so that it becomes the limiting reactant. This result is consistent with the experimental data at 50°C and 1.1 MPa where the highest conversions and hence highest crotonaldehyde consumption rates were achieved. At 50C and 1.1 MPa, periodic operation was poorer with 0.1 split and 0.5 split again most likely due to a depletion of the liquid phase reactant during the liquid-off portion of the cycle. The reason why the effect is not as severe at 50°C and 0.1 MPa is simply that the rate of crotonaldehyde consumption is not great compared to 50°C and 1.1 MPa.

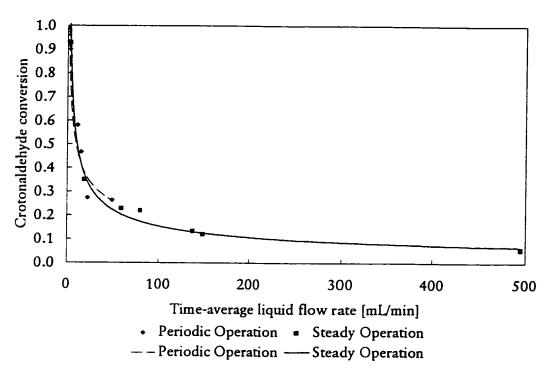


Figure 4.34 Steady and periodic operation (5 min period, 0.1 split) crotonaldehyde conversion vs. liquid flow rate, 50°C, 0.1 MPa

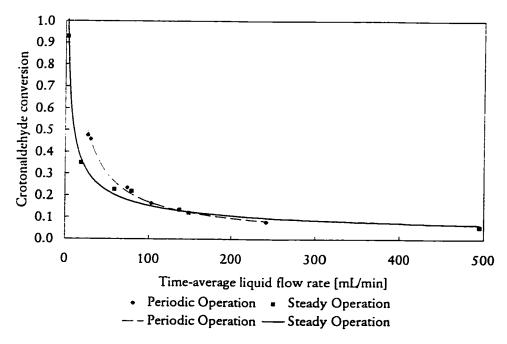
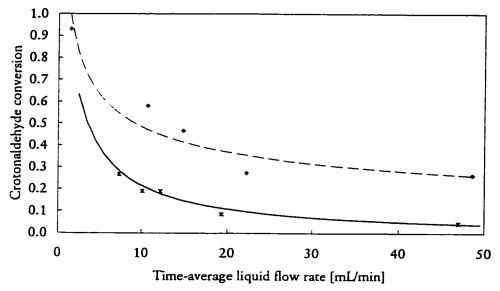
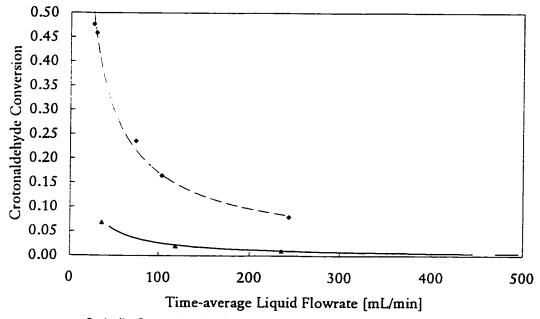


Figure 4.35 Steady and periodic operation (5 min period, 0.5 split) crotonaldehyde conversion vs. liquid flow rate, 50°C, 0.1 MPa



- Periodic Operation 25°C, 1.1 MPa Periodic Operation, 25°C, 1.1 MPa
- Periodic Operation, 50°C, 0.1 MPa - Periodic Operation, 50°C, 0.1 MPa

Figure 4.36 Comparison of periodic operation at 25°C and 50°C, 1.1 MPa for a 5 min period and 0.1 split



- ▲ Periodic Operation, 25°C, 1.1 MPa ——Periodic Operation, 25°C, 1.1 MPa
- Periodic Operation, 50°C, 0.1 MPa Periodic Operation, 50°C, 0.1 MPa

Figure 4.37 Comparison of periodic operation at 25°C, 1.1 MPa and periodic operation at 50°C, 0.1 MPa for a 5 min period and 0.5 split

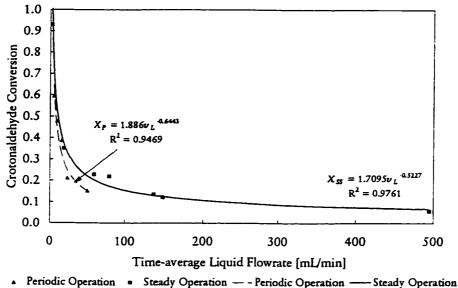


Figure 4.38 Steady and periodic operation (20 min period, 0.1 split) crotonaldehyde conversion vs. liquid flow rate, 50°C, 0.1 MPa

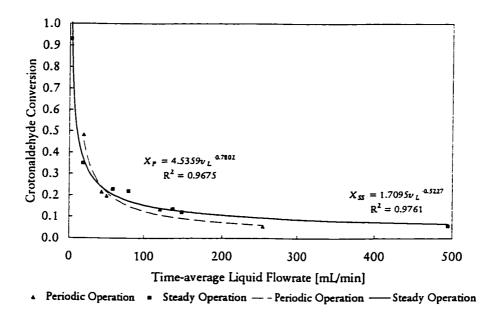


Figure 4.39 Steady and periodic operation (20 min period, 0.5 split) crotonaldehyde conversion vs. liquid flow rate, 50°C, 0.1 MPa

Figure 4.38 shows steady operation compared with periodic operation (0.5 split and 20 minute period) while Figure 4.39 shows the comparison of steady operation with periodic operation (0.1 split and 20 minute period). The results of Figures 4.38 and 4.39 show again that 0.5 split periodic operation is superior to 0.1 split periodic operation because the bed is starved of crotonaldehyde at the shorter split (0.1). Interestingly the 0.5 split periodic operation conversion is slightly lower than steady operation and the 0.1 split periodic operation conversion is much lower than periodic operation. This suggests that an optimum period also exists. The reason for this can be explained again on the basis of depletion of liquid phase reactant. During the no-liquid-flow portion of a period, no crotonaldehyde is being supplied. The longer this portion of the period, the more unproductive.

4.4 Explaining Observed Periodic Operation Behavior

For the system studied, the experimental results show periodic operation is superior to steady operation at 25°C, 1.1 MPa and at 50°C, 0.1 MPa for some select conditions. Figure 4.1 showed that liquid-solid mass transfer is likely not a significant contributing factor to reduced reactor performance at 25°C since the crotonaldehyde consumption is virtually controlled by surface reaction. Thus by elimination at 25°C, any liquid flow rate effects are likely only catalyst external wetting effects. However, at 50°C and 0.1 MPa, this may not be strictly true at very low liquid flow rates, since mass transfer resistance is significant.

Thus, periodic operation can exceed steady operation in performance, if the reaction system is surface reaction controlled and if the system must be operating in such a way that under steady liquid flow, catalyst external wetting is poor or liquid-solid mass transfer resistance is limiting. The mechanism for non-uniform catalyst wetting is complex and can result not only from low liquid flow rates but also liquid maldistribution, that results possibly from uneven distribution of liquid at the entrance to the reactor.

In a trickle-bed under steady liquid flow, the reaction is limited to regions in which the liquid phase reactant and the catalyst are in contact. If the same quantity of liquid is spread over a larger surface of catalyst, then two things happen: first more catalyst surface is involved in the reaction and second the liquid film covering the catalyst will be thinner resulting in reduced mass transfer resistance. The second phenomenon will be of benefit to the reaction rate only if the system is not surface reaction controlled.

Consider the mechanism by which periodic operation functions. Liquid flows for a fraction of a cycle. For some particular choice of time-average liquid flow rate v_L to be obtained the amplitude (A) of the liquid flow pulse must vary as the reciprocal of the split (s) i.e. $v_L = A \cdot s$. If the split (the fraction of period in which liquid flows) is quite small, the amplitude (i.e. of the liquid flow rate) must therefore be very large. Because of the tendency of a large flow rate to spread across the diameter of the column, "flooding" the bed locally with liquid, there will be a tendency for large flows to distribute liquid widely and thus to cause complete wetting of the catalytic packing. The result is more effective external catalyst wetting. The liquid flow is then stopped while gas flow is maintained. Any dynamic liquid holdup drains from the bed relatively quickly and whatever liquid remains is the static liquid holdup. This static liquid holdup has two components: that which is internal to the particles and that which is external. The external liquid holdup, being stationary, contains reactant and acts as a reservoir. As reactant in the liquid holdup is consumed, it must then move to the catalyst by diffusion. If the static liquid holdup is spread over a larger external catalyst surface area, then the film thickness of this static liquid holdup is smaller, which should enhance the diffusion rate. Regardless of whether a larger fraction of the catalyst external surface area is covered, more liquid phase reactant should be able to reach the surface of the catalyst for reaction. In addition to liquid-solid mass transfer, gas penetration to the liquid surface should be increased also.

Note that this may only be a benefit if the system is reaction controlled. If it is not, then periodic operation be a detriment since the additional gain of increased catalyst surface area would be lost, since diffusion would now be the limiting step (i.e. diffusive mass transfer). If this is the case, then the system is better operated under steady state where at least mass transfer is by a convective process, as mass transfer with flow always exceeds static diffusion transfer.

Alternatively, diffusion through a thin film could exceed convective mass transfer through a thicker one. Therefore, if the reaction rate is mass transfer (gas-liquid or liquid solid) controlled, an improvement may be possible, thus excluding reaction control as a necessary condition.

At 50°C and 1.1 MPa, periodic operation gave the poorest performance, while at 50°C and 0.1 MPa periodic operation was about as effective as steady operation. The reason for this is most likely that crotonaldehyde was being depleted during the portion of the cycle without liquid flow. This supported by two observations. First the rate of reaction at 50°C, 1.1 MPa was much greater than at 50°C, 0.1 MPa, resulting in much quicker depletion of crotonaldehyde. Second longer periods and lower splits produced poorer performance since the duration without liquid flow is longer than for shorter periods and higher splits.

One final observation concerns the very low time-average liquid flow rate results where the periodic operation results are almost the same as the steady operation results. In this case as lower liquid flow rates are approached, the liquid-solid mass transfer resistance increases and the catalyst external wetting is uneven.

CHAPTER

FIVE

HYDRODYNAMIC EXPERIMENTS

5.1 Objective

The objective of the hydrodynamic experiments was twofold. First it was to quantify the hydrodynamic parameters of the trickle-bed reactor. These include static holdups and dynamic holdup, and the catalyst external wetting factor. The second was to observe the time response of the dynamic liquid holdup in the trickle-bed.

5.2 Liquid Holdup

The hydrodynamic experiments as mentioned in Chapter 3, were conducted in a clear plastic column identical to that used for trickle-bed experiments. The total static holdup was determined to be 0.463 and this consisted of an internal static holdup of 0.430 and external static holdup of 0.033. Thus, most of the liquid in the reactor when there is no liquid flowing is held in the catalyst pores. This measurement is supported by the high porosity of the catalyst, 0.6853, as measured by mercury penetrometry. Note that the holdups are ratios of liquid volume to total reactor volume as opposed to liquid volume to void space volume.

Experiments were conducted to determine the variation of external static and dynamic liquid holdups with gas flow rate and liquid flow rate. Figure 5.1 shows the total static and external static liquid holdups as functions of gas velocity. The static holdup should be independent of liquid velocity but might be dependent on gas velocity. Since in the literature it was found that external static holdup was dependent upon the Eötvös number, which does not include any dependence on gas flow rate, it is expected that the effect should be small. As seen in Figure 5.1 the effect is negligible.

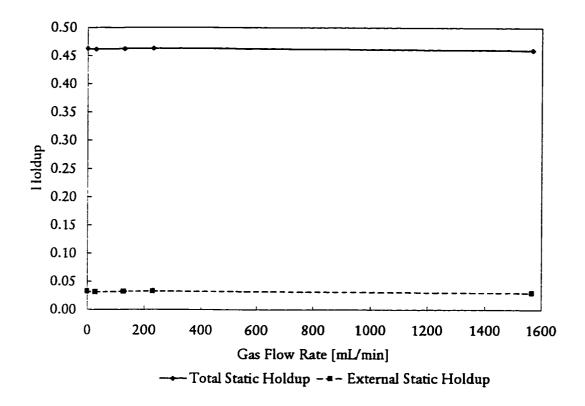


Figure 5.1 Total static liquid holdup and external static liquid holdup as a function of gas flow rate

The dynamic liquid holdup was measured at the same time as the static liquid holdup. Not only was the dynamic liquid holdup measured, but the time response of liquid drainage from the bed was determined also. Figure 5.2 shows the time response of liquid drainage from the bed for a liquid flow rate 480.6 mL/min with different gas flow rates.

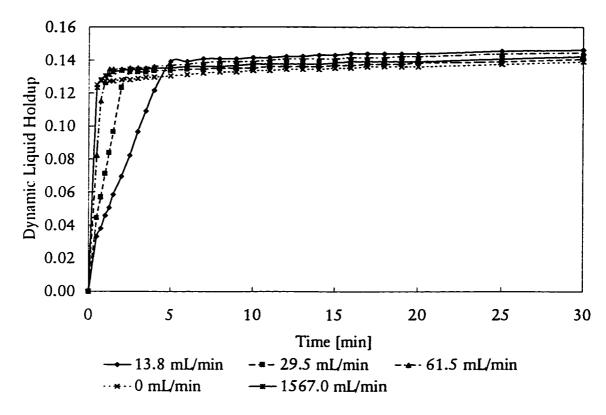


Figure 5.2 Time response of dynamic liquid holdup drainage from the catalyst bed as a function of gas flow rate

Figure 5.2 shows the expected effect of gas flow rate on drainage times. Higher gas flow rates result in a faster drainage times as a result of higher momentum transfer from the gas phase to the liquid phase. Interesting however is the small dependence of dynamic holdup on the gas flow rate. This supports the observation of the independence of external static liquid holdup on gas flow rate, as shown in Figure 5.1. If the total external liquid holdup is a weak function of gas flow rate and total external static liquid holdup is also a weak function of gas flow rate, then dynamic liquid holdup must also be weakly dependent on gas flow rate.

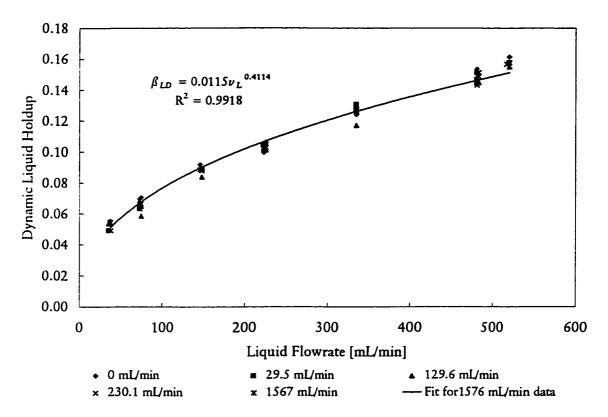


Figure 5.3 Dynamic liquid holdup as a function of liquid and gas flow rate

Figure 5.3 shows the dependence of the dynamic liquid holdup on liquid flow rate and gas flow rate. It shows the dynamic liquid holdup is a weak function of gas flow rate. However, dynamic liquid holdup is strongly dependent on liquid flow rate, a result consistent with the literature. Note that the curve in Figure 5.3 is fit to the data collected at 1576 mL/min gas flow rate. The strong dependence of dynamic liquid holdup on liquid flow rate should not be surprising since in the limit as liquid flow rate were to be increased indefinitely the catalyst bed would eventually flood and most of the void space would be occupied by liquid.

5.3 Catalyst External Wetting

The tracer experiments were conducted in the same apparatus as the liquid holdup experiments and from the data the external catalyst wetting was determined, which is shown as a function of liquid flow rate in Figure 5.4.

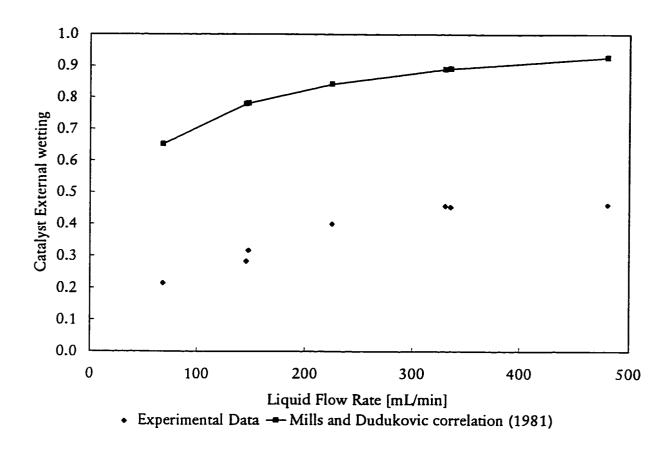


Figure 5.4 Catalyst external wetting efficiency as a function of liquid flow rate

From the figure there is an obvious discrepancy between the experimental data and the published correlation of Mills and Dudukovic (1981). The experimental data is useful in one respect however, and that is that the trend parallels the Mills-Dudukovic correlation suggesting that the trend is correctly predicted if not the absolute magnitude of the catalyst external wetting. Figure 5.5 is virtually the same as Figure 5.4 except that the data have been shifted upwards by adding a constant value to each point. This was done to demonstrate that the flow rate at which the slope of the curve is zero should correspond with complete wetting. To determine the constant to add to the experimental data, a second order polynomial fit of the data was made; the flow rate at which this polynomial's slope was zero, was determined. Physically this is the point where wetting does not change with increasing velocity (i.e. complete wetting).

This value was calculated to be 420.2 mL/min. This flow rate was then used to calculate the wetting value for the experimental data (0.4698). Since this should correspond to complete wetting (f=1), the difference was the constant (1 - 0.4698) = 0.5302. If this value is added to the experimental data, it produces the shifted data in Figure 5.5.

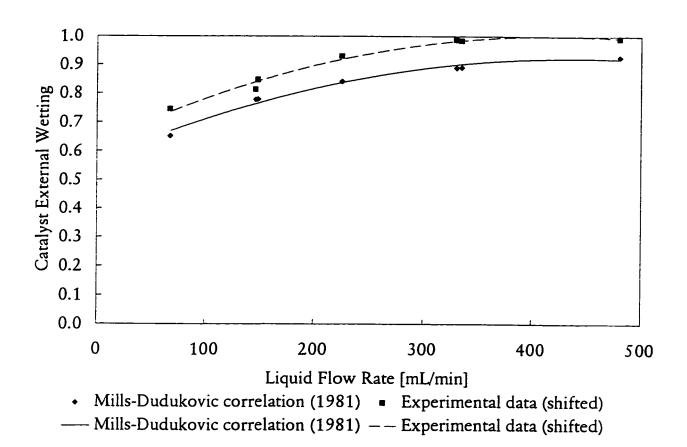


Figure 5.5 Catalyst external wetting as a function of liquid flow rate with experimental data shifted

As shown by Figure 5.5 the trends are very similar, suggesting that the experimental work in principle, establishes the correct relative relationship between catalyst external wetting and liquid flow rate. For the purposes of this study, however, absolute magnitudes of catalyst external wetting are calculated using the Mills-Dudukovic

correlation. This is certainly necessary at the very low liquid flow rates (i.e., below about 50 mL/min) where experimental data were not obtained.

CHAPTER

SIX

APPLICATION OF PERIODIC OPERATION TO TRICKLE-BED REACTORS

6.1 The Case for Periodic Operation of Trickle-Bed Reactors

In Chapter 4, the question was asked: under what circumstances is periodic operation a suitable alternative to steady operation? At this point the reactor design engineer might argue that if the trickle-bed reactor is operating in the reaction controlled regime then the obvious answer to improving reactor performance is to raise the temperature. However the problem with this strategy is that the increase in temperature may bring about reduced selectivity. This is especially critical for fine chemical production in which the products must be of high purity. This would be an important consideration for the hydrogenation of dextrose to sorbitol. The other commonly experienced problem with increased temperature is reduced catalyst lifetime (see for example Shah 1979, hydrodesulfurization study). Another condition for deciding to use periodic operation is whether the liquid flow rate in the reactor will cause non-uniform catalyst external wetting. As seen from the steady operation data, this occurs at liquid phase space times greater than about 10 min. On the other hand, from a practical standpoint it is important to realize that it is not always practical to operate at the lowest space times (highest space velocities) because conversion per pass through the reactor is just too low even though it has been observed that the best performance (in terms of actual throughput) can be achieved at the highest liquid flow rates. From the steady operation data shown for 25°C and 1.1 MPa hydrogen pressure, the ratio of the conversion at 50 mL/min compared to 450 mL/min is about 10:1.

To make a case for the use of periodic operation in trickle-bed operation, it is probably useful to examine some industrially important processes. For example, hydrodesulphurization is a very important unit operation in petroleum refining. Hydrodesulphurization is a good system to examine with respect to this study because

it also has non-volatile reactants in dilute quantities in the liquid phase. Table 6.1 shows typical operating conditions and Table 6.2 shows how the LHSVs (liquid hourly space velocities) in Table 6.1 convert to space times. Table 6.2 also shows the liquid flow rates used for the experiments. From Table 6.2 it is clear that LHSVs achieved in the experimental reactor would correspond to liquid flow rates where poor external catalyst wetting would occur. In fact the external catalyst wetting would be expected be poorer in the full scale industrial reactor, compared to the experimental reactor used in this study since it is often difficult to achieve good liquid distribution in very large diameter industrial trickle-bed reactors.

	Feedstock	
Processing conditions	Light petroleum (distillates)	Heavy petroleum (feedstocks)
Temperature (°C)	300 to 400	340 to 425
Pressure (atm)	35 to 70	55 to 170
LHSV (vol. feed/ vol. catalyst/h)	2 to 10	0.2 to 1
H ₂ recycle rate (std ft³/bbls)	300 to 2000	2000 to 10000
Catalyst life (years)	≈ 10	0.5 to 1

Table 6.1 Typical hydrodesulphurization operating conditions (Gianetto and Silveston, 1986)

	Feedstock	
	Light petroleum (distillates)	Heavy petroleum (feedstocks)
LHSV (vol. feed/ vol. catalyst/h)	2 to 10	0.2 to 1
Space time (min)	120 to 6	300 to 60
Liquid Flow rate (mL/min)	5 to 100	2 to 10

Table 6.2 Hydrodesulphurization LHSVs converted to equivalent space times and liquid flow rates for the reactor used in this study

6.2 Experimental Investigation of a Potential Application

A set of experiments were conducted using a subset of typical industrial operating conditions. Additionally, the bulk liquid phase was changed from water to a light

petroleum distillate, comparable to naphtha in its physical properties. Most importantly, however, the experiments conducted were different in one other important aspect: the periodic operation used was not on-off but rather cycling between high and low liquid flow rates. This operation scheme is different than that presented in Chapter 4 and from an industrial point of view may be the most appealing since it would appear to deviate less from conventional trickle-bed operation than on-off cycling. Crotonaldehyde was used as the liquid phase reactant. The catalyst used was the same as that used for the aqueous experiments.

Preliminary experiments were conducted to determine operating conditions for the steady and periodic operation experiments at conversions between 20 and 80 percent. Three variables to be manipulated in the preliminary experiments were - crotonaldehyde concentration, catalyst bed length and temperature. Initially experiments were run in a 60 cm bed, at 25°C and a crotonaldehyde concentration of 2000 ppm by weight. At 25°C it was hoped that the reaction would occur under the kinetically controlled regime. Also, 2000 ppm crotonaldehyde concentrations were convenient to analyze accurately. Thus, the only remaining variable to be determined was bed depth. At the lowest liquid flow (0.7 kg/(m² s) which is about 120 mL/min) in the 60 cm catalyst bed length, a conversion of about 95% was observed under steady state operation. This was deemed too high to represent industrial operation so the decision was made to halve the catalyst bed length to 30 cm. For this bed a steady-state experiment at 0.7 kg/(m² s) produced a conversion of about 55%. Therefore it was decided to carry out steady-state experiments in the 30 cm catalyst bed.

Steady-state experimental data are tabulated in Appendix K and plotted in Figures 6.1 to 6.7. Figure 6.1 shows the nonlinear decrease of crotonaldehyde conversion with increasing liquid flow. A more interesting graph is Figure 6.2 which shows the expression $\ln(1/1-X)$ (where X is conversion) plotted versus space time. The significance of this plot is that according to theory, a straight line through the origin at (0,0) indicates that the reaction is first order in the concentration of the liquid phase

species. It appears that a straight line does pass through the experimental data points, but does not go through the origin (0,0). Data for a change in G/L (ratio of gas to liquid volumetric flow rate) are included. Thus, the kinetics are dependent on the crotonaldehyde concentration. Since there is little effect of G/L ratio on the conversion results, this would suggest that the conversion of hydrogen is quite low. Figure 6.1 and Figure 6.2 also show that there is no significant effect of gas-liquid ratio on the crotonaldehyde conversion over the liquid flow range studied.

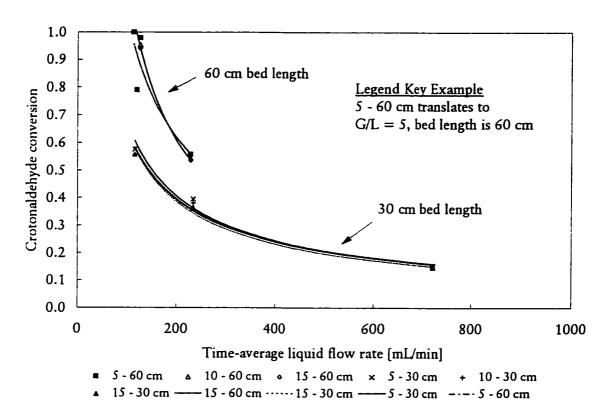


Figure 6.1 Crotonaldehyde conversion as a function of liquid flow rate, gas flow rate and bed depth

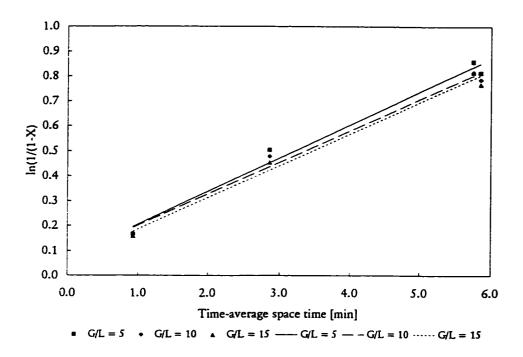


Figure 6.2 First order plot of steady operation data at different gas/liquid ratios

The periodic operation experimental data are also tabulated in Appendix K. Figure 6.3 shows the effect of cycle period (expressed as time-average liquid loading) on the time-average conversion of crotonaldehyde. Because the high flow (4.2 kg/(m² s), which is about 720 mL/min duration) was constant, the longer cycle period appears as the lowest time-average liquid loading. The longest cycle period was 10 min. The high liquid loading duration was 30 s. On the same graph are plotted the steady-state results. Note that the periodic operation results have been corrected for a loss of catalyst activity shown in Appendix K. These corrected data are plotted in Figure 6.3 and all subsequent graphs. Figure 6.3 shows that the periodic operation data points lie almost over top of the curve of steady-state data. With respect to crotonaldehyde conversion, periodic operation appears to be no different from steady-state operation. Figure 6.4 shows the effect of flush duration (expressed as time-average liquid flow) on the time-average conversion of crotonaldehyde. Steady-state data are also plotted on this graph. Here too, periodic operation data points almost coincide with the steady-state data except at a gas-liquid ratio of 5 (volume at STP/volume liquid) where the

periodic operation points are significantly lower than the curve of steady operation data. An explanation for this is not obvious. It should be noted that there was a low conversion point in Figure 6.1 at G/L=5 (volumetric flow ratio).

Finally, the periodic operation conversion results were compared to what are known as the quasi-steady state conversion results. Quasi-steady state conversion is a hypothetical limit calculated from weighting the steady state conversions at the low liquid flow (0.7 kg/(m² s) and at high liquid flow (4.2 kg/(m² s)) for a given cycle period and flush duration. These results are listed in Appendix K and plotted in Figure 6.5, and Figure 6.6 as time-average conversion versus time-average liquid loading. The periodic operation data points lie almost on the quasi-steady operation curve. The significance of this is that it shows that the system under study is in fact behaving as a quasi-steady state system. Thus, after a change in liquid flow, the trickle bed reactor adapts almost instantaneously to the new steady-state. This means that the quasi-steady state curve may be used to predict the performance enhancement due to periodic operation. Since the quasi-steady state curve lies on or slightly below the steady state curve, it would appear that periodic operation should have little beneficial effect on conversion under the conditions of this study.

These results suggest that the catalyst is fully wetted and the liquid is well distributed over the catalyst in the trickle bed reactor under the lowest liquid loading used in the study. With good distribution, one would expect coverage of the catalyst with liquid to be relatively uniform. For the liquid loadings used in this study, therefore, periodic operation should provide little if any improvement in crotonaldehyde conversion.

The objective of the study was to test if periodic switching of liquid flow improves crotonaldehyde conversion over steady state. Our study assumed but did not test, that catalyst coverage with liquid is incomplete at loadings of 0.7 kg/(m² s). It seems this assumption was not justified for the 60 cm bed, perhaps because of the attention paid

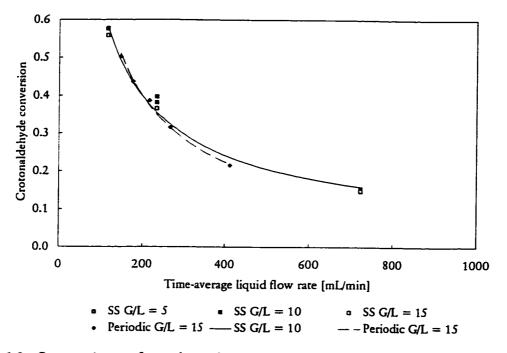


Figure 6.3 Comparison of steady and periodic operation crotonaldehyde conversion - effect of cycle period

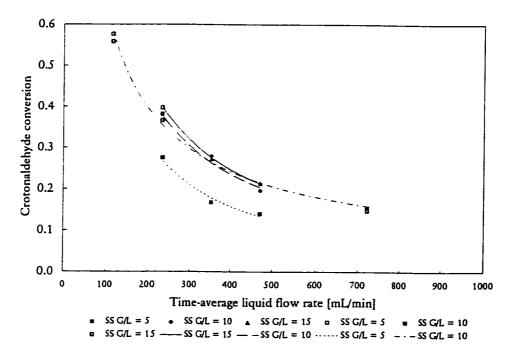


Figure 6.4 Comparison of steady and periodic operation crotonaldehyde conversion - effect of flush duration

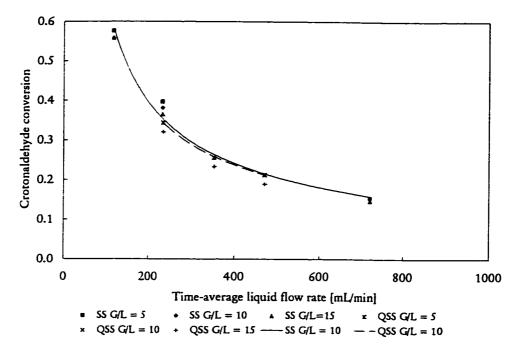


Figure 6.5 Comparison of quasi-steady and steady crotonaldehyde conversion

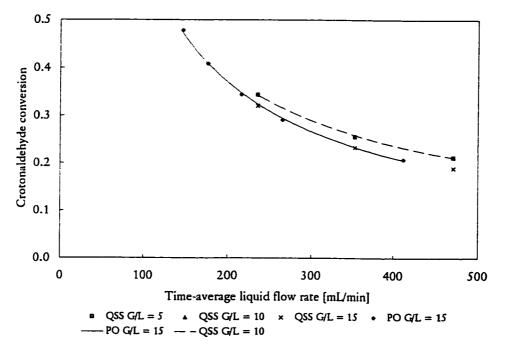


Figure 6.6 Comparison of quasi-steady and periodic operation crotonaldehyde conversion - effect of cycle period

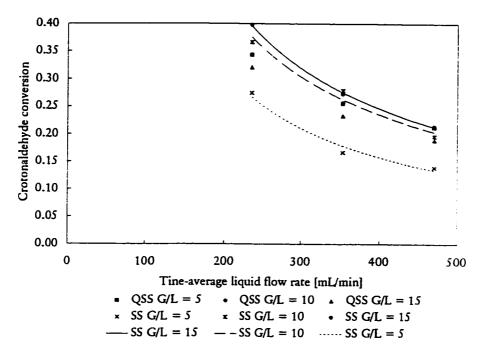


Figure 6.7 Comparison of Quasi-Steady and Periodic Operation Crotonaldehyde Conversion - Effect of Flush Duration

to good liquid distribution and shortening bed depth to 30 cm. Of course, liquid maldistribution is more likely in large industrial trickle bed reactors than in small bench scale reactors. A logical continuation of our study would be a reduction of the liquid flow to a level where catalyst coverage with liquid is incomplete. Another alternative would be intentional flow maldistribution by manipulating the distribution of liquid to the top of the reactor bed.

The experimental results can be viewed in another way: periodic switching of liquid flow to high rate did <u>not</u> decrease the time-average crotonaldehyde conversion except for some unexplained outlier points at G/L = 5. Periodic flooding offers a means of quenching developing hot spots. Thus, using periodic switching between high and low liquid loading permits operating at lower than design loadings without incurring hot spot problems.

CHAPTER

SEVEN

MODELING

7.1 Outline

This chapter presents computer simulations of mathematical models of trickle-bed reactor operation. The models are dynamic, that is, they include the time-dependent terms. Steady or time-invariant simulation are also examined and compared with steady and periodic operating data. Two models are considered. The first utilizes the external catalyst wetting factor and is compared with the experimental results for steady operation. The second model is a modification of the first adapted for periodic operation. Note that the comparisons are with experimental data for 25°C, 1.1 MPa, 50°C, 1.1 MPa and 50°C, 0.1 MPa.

7.2 Trickle-bed reactor models

7.2.1 Steady-operation trickle-bed models

Chapter 2 introduced a general trickle-bed reactor model under steady state conditions. It included mass balances for all components in all phases, a heat balance, and used a pressure drop correlation in the momentum balance. The model described in this chapter was modified by several simplifying assumptions which reduce the number of equations to be solved. First, the model considered only the liquid phase reactant as rate limiting; consequently, only the mass balance for the liquid phase reactant crotonaldehyde was included. Since thermal effects were small because the liquid phase reactant was dilute, an energy balance was ignored. The momentum balance was also ignored. The other key feature of this model is an accumulation term within the transient mass balance, a necessary condition for any dynamic simulation.

The models were evaluated by comparison with the experimental data presented in Chapter 4. Specifically, the experimental time-average conversion was compared with

time-average results from the simulations. Two models were presented for steady operation and were designated Steady-operation Model A and Model B.

7.2.2 Steady-operation model A

Model A considers the liquid surrounding the outside of the particle as consisting of two parts: a flowing portion (dynamic holdup) and a stagnant film (static holdup). The movement of liquid to the stagnant film is described by liquid-solid mass transfer. When liquid is flowing the assumption is that complete contact between the flowing liquid and the static liquid is maintained and the only liquid in contact with the catalyst is the static liquid. Incomplete wetting appears between the static liquid and the catalyst surface, when present.

The steady-operation model is given by one partial differential equation and a series of ordinary differential equation. The partial differential equation is the mass balance on crotonaldehyde in the flowing liquid phase and the ordinary differential equation is the mass balance on the crotonaldehyde in the stagnant liquid at the catalyst external surface. The second mass balance is not a partial differential equation since it is assumed that the stagnant liquid phase inside the porous catalyst has no velocity component in the longitudinal direction. The first mass balance, equation (7.1), is for the flowing liquid phase

$$\frac{\partial C_L}{\partial t} = -u_L \frac{\partial C_L}{\partial z} - k_s a_s (C_L - C_s)$$
 (7.1)

with initial and boundary conditions given by

$$C_L(t,0) = C_{L0}$$

 $C_L(0,z) = C_{L0}$ (7.2)

The second mass balance is for the stagnant liquid phase

$$\frac{dC_s}{dt} = -kfC_s + k_s a_s (C_L - C_s) \tag{7.3}$$

which has the initial condition

$$C_{s}(0,z) = C_{L0} (7.4)$$

These initial and boundary conditions of the two mass balances specify that the bed is initially saturated with liquid feed before the hydrogen is fed to the reactor to allow reaction to start. This procedure was used for all steady and periodic operation experiments. The solution of equations (7.1) through (7.4) at very long times, is the steady-state solution.

The physical situation at the particle level, of the model of equations (7.1) through (7.4) is shown in Figure 7.1. Figure 7.1 shows the contact of liquid with the catalyst particle is incomplete. In equation (7.1) the incomplete wetting is accounted for by multiplication of the reaction kinetic term by the catalyst external wetting factor. Notice the film surrounding the particle (large dashed lines) is considered to be the thin shell around the outside of the particle and this film penetrates slightly into the catalyst particle.

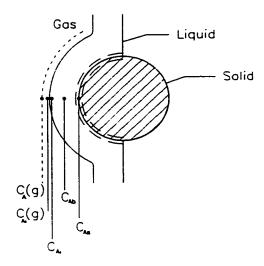


Figure 7.1 Gas-liquid-solid contact at the particle level for Model A

7.2.3 Steady-operation model B

Model B is almost identical with the exception of how the catalyst external wetting is incorporated into the model. Instead of multiplication of the kinetic rate term by the wetting factor, the liquid-solid mass transfer term is multiplied by that parameter. The rationale for this is that the only way liquid-solid mass transfer can only occur is with catalyst surface that is wetted. The model equations to be solved then become

$$\frac{\partial C_L}{\partial t} = -u_L \frac{\partial C_L}{\partial z} - k_s a_s f(C_L - C_s)$$
 (7.5)

$$\frac{dC_s}{dt} = -kC_s + k_s a_s f(C_L - C_s) \tag{7.6}$$

while keeping the same initial and boundary conditions given by equations (7.2) and (7.4).

$$C_L(t,0) = C_{L0}$$

 $C_L(0,z) = C_{L0}$ (7.3)

$$C_s(0,z) = C_{L0} (7.4)$$

Figure 7.2 depicts the liquid-solid contact.

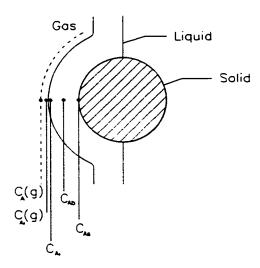


Figure 7.2 Gas-liquid-solid contact at the particle level for Model B

7.2.4 Trickle-bed reactor model parameters

The liquid solid mass transfer coefficient was estimated by the correlation of Goto and Smith (1975a) as follows:

$$k_S a = D_L \alpha_S \left(\frac{G_L}{\mu_L}\right)^{n_S} \left(\frac{\mu_L}{\rho_L D_L}\right)^{\frac{1}{3}}$$
(7.7)

The external catalyst wetting efficiency was estimated by the correlation of Mills and Duduukovic (1981) as:

$$f = \sqrt{\frac{(D_{EO})_{app}}{(D_{EO})_{LF}}} = 1.0 - \exp\left(-1.35 \operatorname{Re}_{L}^{0.333} Fr_{L}^{0.235} We_{L}^{-0.170} \left(\frac{a_{i} d_{p}}{\varepsilon_{B}^{2}}\right)^{-0.0425}\right)$$
(7.8)

Other parameters and physical properties are listed in Appendix C.

7.2.5 Periodic operation trickle-bed models

The periodic operation models are similar to the dynamic models proposed. They have essentially two mass balances of exactly the same form as the steady operation model. However the models must accommodate the variation in liquid flow rate with time. Assumptions are also necessary regarding how catalyst external wetting and total liquid holdup behave during periodic operation.

A suitable reference point for a periodic operation model would be the steady operation model. Under steady operation, i.e., constant liquid flow, the catalyst external wetting and the instantaneous liquid-solid mass transfer coefficient parameters are assumed to remain constant throughout the bed (spatial assumption) and with time (temporal assumption). The spatial assumption will be retained for periodic operation but the temporal cannot since both of the above mentioned parameters are functions of liquid velocity which is varying with time.

During periodic operation, the trickle-bed reactor moves between two states: a irrigated state and a non-irrigated state. It would be reasonable to assume that the operation of the trickle-bed during irrigation is similar to that of a trickle-bed reactor under steady-operation. Therefore it would be reasonable to consider applying the steady-operation model to the periodically operated reactor only under irrigation. The difference between the steady and periodic operation models will then lie in how the non-irrigated portion of a cycle is modeled. To develop this, it is necessary to visualize what is occurring over a complete on-off irrigation cycle. The catalyst is shell impregnated so most of the internal liquid holdup is not in contact with the catalyst.

When liquid is flowing it is assumed that there is no difference between continuous and periodic operation as stated above. Dynamic holdup and drainage-time measurements, show that the bulk of the dynamic holdup drained very quickly, often in less than 10 seconds. This is agrees with an observation by Hasokowati et al. (1995). For modeling purposes, the first assumption will be that the dynamic liquid

holdup drains instantaneously from the bed leaving behind holdup external to the particles and within the particles, the static holdup. This static holdup can store crotonaldehyde for further reaction on the catalyst surface. It will also be assumed that the crotonaldehyde in this external static holdup reaches the catalyst external surface by diffusion and not convective mass transfer, since the liquid flow has been stopped. To model the diffusion process will require an assumption regarding how the external static holdup is distributed over the catalyst external surface. To address this, the catalyst external wetting must be examined. The holdup in the particles will also be assumed to diffuse outward from the particle pores. However, the material diffusing through the particle may not be as great as that diffusing from the outside of the particle since diffusivity will be reduced due to tortuosity within the particle. This is despite the fact that Figure 5.1 showed the majority of the static holdup is held inside the catalyst particles, not externally. As a first approximation only the external static liquid holdup will be considered.

Prior to irrigation's being stopped, the catalyst external wetting has a certain value which is assumed to be uniform throughout the trickle-bed. It will be assumed that the catalyst external wetting will retain the same value after irrigation has ceased. This may be an optimistic assumption. The alternative would be to assume that the catalyst external wetting goes to zero, the scenario predicted by the Mills and Dudukovic correlation which is not realistic. Most likely, reality exists in an as yet-unknown region, somewhere between these two extremes. The assumption that the catalyst external wetting remains at the value it at was prior to liquid flow stoppage is a simple starting point for a model which can be later modified when more information becomes available. From these assumptions, an expression for diffusion mass transfer from the external static liquid holdup can be developed.

As for steady operation, two models will be described for periodic operation, the difference between them being how the external catalyst wetting factor is incorporated

into the respective models. These models are designated Periodic Operation Model A and B.

7.2.6 Periodic operation models A and B

Periodic model A is analogous to steady operation model A. First, in the two mass balances, the liquid-solid mass transfer coefficient will be replaced by a parameter $k_s a_{s,eff}$.

$$\frac{\partial C_L}{\partial t} = -u_L \frac{\partial C_L}{\partial z} - f k_s a_{s,eff} (C_L - C_s)$$
 (7.9)

$$\frac{dC_s}{dt} = -kC_s + fk_s a_{s,eff} \left(C_L - C_s \right) \tag{7.10}$$

These two equations model the trickle-bed during non-irrigation. The parameter $k_s a_{s,eff}$ is calculated by

$$k_{s}a_{s,eff} = \frac{Da_{t}}{\delta} \tag{7.11}$$

where D is the diffusion coefficient of crotonaldehyde in water, a_t is the total catalyst external surface area per volume of bed, which, for a bed of spheres, is given by

$$a_t = \frac{6(1 - \varepsilon_B)}{d_p} \tag{7.12}$$

and δ is the path length for diffusion. To calculate $k_s a_{s,eff}$, δ must be estimated. This is taken as the external liquid holdup volume divided by the catalyst external surface area

$$\delta = \frac{V_{LSE}}{A_{CE}} = \frac{V_{TBR}\beta_{LSE}}{V_{TBR}a_t} = \frac{\beta_{LSE}}{a_t}$$
 (7.13)

 V_{LSE} is the external static holdup volume, β_{LSE} is the external static liquid holdup, A_{CE} is the catalyst external surface area and V_{TBR} is the total reactor volume. Goto and Smith (1975a) outline the above method for the estimation of $k_s a_{s,eff}$, however they also warn that the value calculated will be low for a trickle-bed operating with liquid flow. Since this is being used for no-liquid flow, it is a reasonable first estimate of $k_s a_{s,eff}$. Notice that it is assumed that the external holdup covers the entire catalyst external surface since the catalyst external wetting factor is taken into account in the second mass balance within the mass transfer term. From the above expressions, the value of $k_s a_{s,eff}$ was calculated for 25 °C and 50 °C, by using equations (7.11) through (7.13) in the simulation code.

Periodic operation model B is analogous to steady operation model B, with the catalyst external wetting factor multiplied by the kinetic reaction term instead of the liquid-solid mass transfer term. The equations are

$$\frac{\partial C_L}{\partial t} = -u_L \frac{\partial C_L}{\partial z} - k_s a_{s,eff} f(C_L - C_s)$$
 (7.14)

$$\frac{dC_s}{dt} = -kC_s + k_s a_{s,eff} f(C_L - C_s)$$
(7.15)

7.2.7 Trickle-bed Reactor System Classification

In Chapter 2, Table 2.6 showed criteria, used to determine if periodic operation can improve performance compared to steady operation. From Table 2.6, periodic operation cannot result in an improvement if the system is linear and the control scheme is also linear. Assuming that steady operation model A reasonably describes the functional dependency on state $(C_L \text{ and } C_S)$ and the controlled variable (u_L) , the

analysis can be done. The analysis given in Appendix R shows that the system in nonlinear in the state variables and nonlinear in the controlled variable. Therefore periodic operation may produce an improvement in reactor performance.

7.2.8 Numerical solution of trickle-bed models

The above set of equations was solved using a program named gPROMS developed at Imperial College. The program can solve systems of differential-algebraic-equations (DAEs) and allows the user to specify the types of approximations for partial derivatives. Very often spatial partial derivatives are approximated by finite differences. In finite differences the spatial domain is divided into grid points and the spatial derivatives are approximated at these grid points by formulae which use surrounding grid points. For example a first order (referring to accuracy of the approximation) forward difference formula would approximate a first derivative as

$$\frac{\partial C}{\partial z} \cong \frac{C(z + \Delta z, t) - C(z, t)}{\Delta z} \tag{7.16}$$

and a first order backward difference formula would approximate a first derivative as

$$\frac{\partial C}{\partial z} = \frac{C(z, t) - C(z - \Delta z, t)}{\Delta z} \tag{7.17}$$

Equation (7.9) is a first-order hyperbolic equation and the convective term usually requires special treatment. The order of the approximation derives from the fact that these formulae are truncations of Taylor series' from which they are derived where all terms exceeding first-order are eliminated. Higher order approximations are possible and can be found in texts by Schiesser (1991) and Silebi and Schiesser (1992).

However for a hyperbolic partial differential equation, a special treatment of the partial derivative term is required (Schiesser, 1991; Silebi and Schiesser, 1992). This

treatment is known as upwind differencing. The reason for this lies with the partial derivative which is the convective term of the equation. This term represents a moving front of some property, in this case concentration, which travels longitudinally. When the front moves through any longitudinal point, the concentration undergoes an instantaneous increase in value. Essentially the rate of change of the concentration is infinite. The problem is how to approximate this sudden increase in concentration. A first-order forward difference could be used

$$\frac{\partial C}{\partial z}\Big|_{z} \cong \frac{C(z + \Delta z, t) - C(z, t)}{\Delta z}$$
 (7.18)

When a first-order forward difference is used the result is an excessive overshoot and oscillation in the value of concentration as the discontinuity passes through the point of interest (Schiesser, 1991; Silebi and Schiesser, 1992). To control this, another approach is necessary. On a physical basis, the argument is to use points upwind of the point being traversed so as to drive the slope of the concentration to as high a value as possible without excessive overshoot and oscillation. Mathematically this is given by

$$\frac{\partial C}{\partial z}\bigg|_{z} = \frac{C(z,t) - C(z - \Delta z,t)}{\Delta z} \tag{7.19}$$

This approximation is not the best solution for two reasons. First, it is only first-order accurate and, second, it results in a phenomenon known as numerical diffusion. The term "first-order accurate" refers to the accuracy of the partial derivative approximation. The approximations for partial derivatives are derived from Taylor series expansions. A partial derivative approximation which is first-order accurate is one which retains the term linear in Δz only, dropping all higher order terms. Therefore the approximation is $O(\Delta z)$ i.e. of order Δz or first-order in Δz . Numerical diffusion is the reduction of the slope of the front from its infinite value. The solution takes on the appearance of a front produced by a hyperbolic partial differential equation which has a diffusion term, that is a second-order term of the form

$$D\frac{\partial^2 C}{\partial z^2} \tag{7.20}$$

This type of term will tend to reduce the slope or sharpness of the front. Since no such term is present in a first-order hyperbolic PDE, the term "numerical dissipation" is applied. A further discussion of this phenomenon is given by Press et al. (1990).

As mentioned previously the second disadvantage of the upwind difference formula chosen is that it is only "first-order accurate". As the order of the upwind approximation is increased, the amount of numerical diffusion is reduced, however, at the cost of undershoots and overshoots in the solution. However as suggested by Silebi and Schiesser (1992), it is usually better to use a higher order upwind approximation. For both steady and periodic operation simulations, a second-order upwind difference was used.

The approximation of the spatial derivative is important in determining the accuracy of the solution. Also important, however, is the discretization of the spatial dimension under simulation, i.e., how many grid points are sufficient to produce given degree of accuracy. This aspect of the numerical solution of differential equations is usually treated with test equations which have analytical solutions. These exercises are useful in that they do show that typically increasing the number of grid points in a given spatial (or temporal) dimension will reduce the error between the simulated results and the analytical solution. Unfortunately most systems of equations for many problems do not have analytical solutions, and hence the need for numerical solution techniques. To test whether the chosen number of discretization points is adequate is usually an exercise in successively increasing the number of grid points until a certain accuracy tolerance is achieved. This has been suggested by Schneider (1996) for use with finite elements and is equally applicable to finite differences. Several steady operation simulations were started with 10 grid points in the longitudinal direction and these

simulations were repeated with 20 and 30 grid points. The time-average crotonaldehyde conversion from the simulations showed very little change (less than 1%) amongst the three grid values. Since the simulations ran relatively quickly, 30 grid points were used for the remaining steady and periodic operation simulations.

7.3 Simulation results

7.3.1 Steady operation simulation results at 25°C and 1.1 MPa

The simulations results presented are time-average crotonaldehyde conversions for 25 °C and 1.1 MPa and these are compared with the experimental data for these conditions. The *gPROMS* code for a sample steady operation simulation is listed in Appendix O. The *gPROMS* code for a sample periodic operation simulation is also listed in Appendix O.

Figures 7.3 and 7.4 show steady operation models A and B compared with the experimental data at 25 °C and 1.1 MPa, after all transients have vanished. Generally the models predicts the trend well over the entire liquid flow rate range. The poorest agreement between the model and the experimental data is at very low liquid flow rates where the model estimates of crotonaldehyde conversion are significantly lower than the experimental observations. The models appear to be identical for the conditions simulated.

As discussed earlier, the basis for explaining the improvement in crotonaldehyde conversion was that catalyst external wetting was poorest at the lowest liquid flow rates. As a test of this idea simulations were run assuming complete catalyst external wetting by setting f equal to 1. Figures 7.3 and 7.4 show the results of the simulations compared with the experimental data and this reveals two interesting things. First the assumption that complete wetting is occurring at high liquid flow rates is reasonable as shown by the agreement between the model and experimental data at liquid flow rates above 200 mL/min. Second the assumption that wetting is variable at the lower liquid flow rates is also reasonable since below 200 mL/min liquid flow rate, the model

assuming complete catalyst external wetting consistently overestimates crotonaldehyde conversion. Also this overestimation increases with decreasing liquid flow rate which is consistent with the rationale that lower liquid flow rates result in poorer catalyst external wetting.

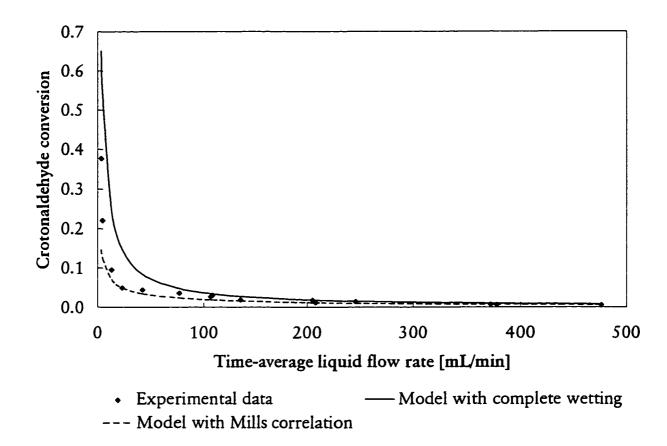


Figure 7.3 Steady operation Model A assuming variable catalyst external wetting with experimental data (Mills-Dudukovic wetting correlation used) and complete catalyst wetting (f = 1)

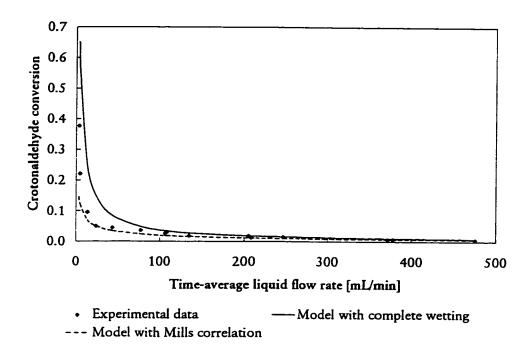
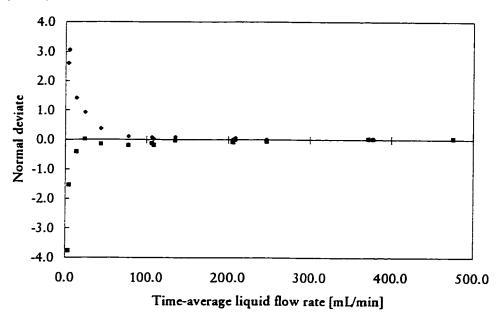
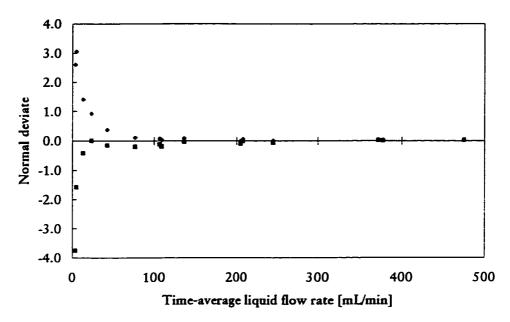


Figure 7.4 Steady operation Model B assuming variable catalyst external wetting with experimental data (Mills-Dudukovic wetting correlation used) and complete catalyst wetting (f = 1)



• Model with complete wetting • Model with Mills correlation

Figure 7.5 Steady Model A normal deviate for complete and variable wetting



• Model with complete wetting • Model with Mills correlation

Figure 7.6 Steady Model B normal deviate for complete and variable wetting

The normal deviates associated with each model are shown in Figures 7.5 and 7.6. The normal deviate is the difference between the experimental data and the model prediction (i.e. residual) divided by the standard deviation of these residuals (Draper and Smith, 1981). Noticeable is the increase in the magnitude of the normal deviate for the complete catalyst wetting model with the decrease in liquid flow rate whereas for the variable catalyst wetting model the percentage error is consistently lower.

Finally, Figures 7.7 and 7.8 show the variation of crotonaldehyde concentration in the bulk liquid phase and at the catalyst surface as a function of position and liquid flow rate. They correctly show the decrease of liquid phase crotonaldehyde concentration with axial position, and a larger rate of crotonaldehyde concentration decrease with a decrease in liquid flow rate.

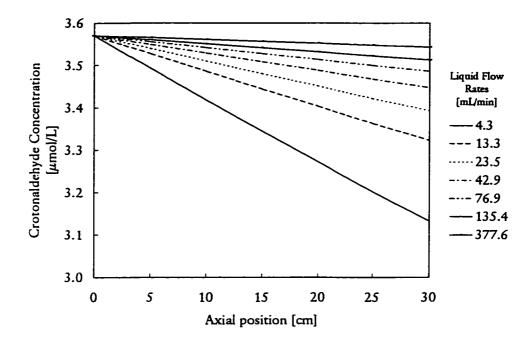


Figure 7.7 Bulk liquid phase crotonaldehyde concentrations as predicted by simulation Model A under steady operation at 25°C and 1.1 MPa

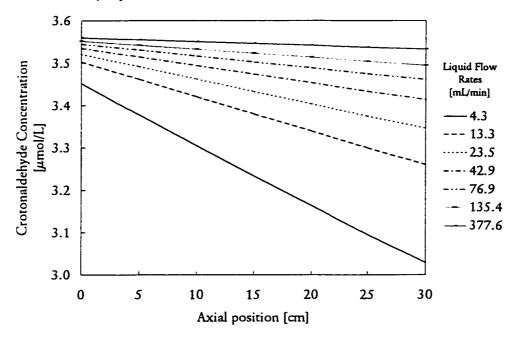


Figure 7.8 Crotonaldehyde concentrations at the catalyst outer surface as predicted by simulation Model A under steady operation at 25°C and 1.1 MPa

7.3.2 Periodic operation simulation results at 25°C and 1.1 MPa

Four sets of periodic operation experiments consisted of combinations of 5 and 20 minute periods and 0.1 and 0.5 splits. These same conditions were simulated using the models described in section 7.2.6 and are compared with the experimental data and with the steady operation simulations.

Figure 7.9 shows the simulation results for 0.1 split and a 5-minute period. As the figure shows, periodic operation models A and B predict the trend of crotonaldehyde conversion with liquid flow rate shown by the experimental data. Model B however is consistently higher than Model A. What is also interesting is that both periodic operation models predict a significantly higher time-average crotonaldehyde conversion compared with the steady operation model.

Figure 7.10 is similar to Figure 7.9 except that the split is changed from 0.1 to 0.5 at a constant period length of 5 minutes. Again, periodic models A and B correctly predict the trend of the experimental data and also predict that the time-average crotonaldehyde conversion is higher than that for steady operation. Also, the models correctly predict that the difference between periodic and steady operation should decrease as liquid flow rate is increased. This is an expected result since under steady-operation conditions, as higher liquid flow rates are approached, catalyst external wetting becomes complete. Since it is assumed that catalyst external wetting accounts for the observed difference between steady and periodic operation at low liquid flow rates this difference between the operating modes should thus diminish at

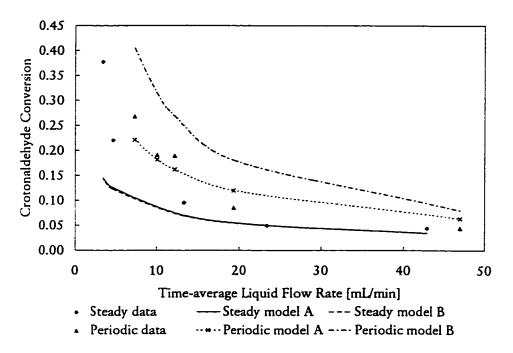


Figure 7.9 Comparison of periodic and steady operation model with experimental data at 25°C and 1.1 MPa; periodic operation parameters: 0.1 split 5 minute period

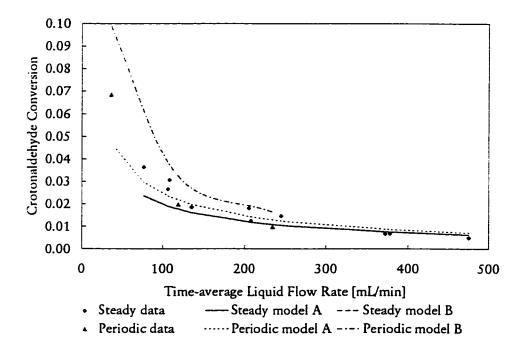


Figure 7.10 Comparison of periodic and steady operation model with experimental data at 25 °C and 1.1 MPa; periodic operation parameters: 0.5 split 5 minute period

the higher liquid flow rates. Again, the results predicted by model B exceed those of model A.

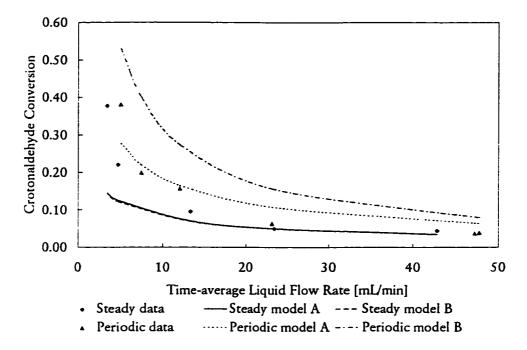


Figure 7.11 Comparison of periodic and steady operation model with experimental data at 25 °C and 1.1 MPa; periodic operation parameters: 0.1 split 20 minute period

Figure 7.11 shows simulation results for periodic operation for a 0.1 split but now for an increased period of 20 minutes. Once again, the periodic operation model correctly predicts the trend of the experimental data although it underestimates the conversion at the lowest liquid flow rate and overestimates it at the highest liquid flow rates. Compared with the steady operation model, the periodic operation model does predict that the crotonaldehyde conversion should be higher under periodic operation.

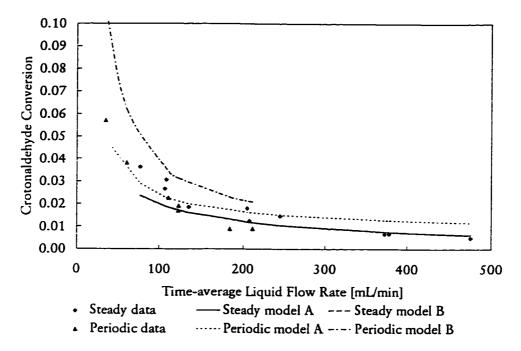


Figure 7.12 Comparison of periodic and steady operation model with experimental data at 25 °C and 1.1 MPa; periodic operation parameters: 0.5 split 20 minute period

Finally Figure 7.12 shows the simulation results for periodic operation with a 0.5 split and a 20 minute period. The results are similar to those for periodic operation with a 0.5 split and 5 minute period. The time-average crotonaldehyde conversion is better than steady conversion but not by a great amount. Periodic model A in this instance seems to conform to the data well except at the lowest liquid flow rate where it tends to underestimate the time-average conversion. Periodic model B tends to overestimate the data compared to periodic model A.

In summary, the periodic operation models consisted of two mass balances: one for the flowing liquid phase, and the other for the liquid at the catalyst external surface. Two assumptions were incorporated into the model: first, dynamic liquid holdup drained instantaneously from the bed, and second, the degree of catalyst wetting at the start of the non-flow portion of the period was the same as that under liquid flow conditions. Model A incorporated the catalyst external wetting in the kinetic reaction term while model B included this parameter in the liquid-solid mass transfer term.

7.3.3 Steady operation simulation results at 50 °C and 1.1 MPa

Figures 7.13 and 7.14 show steady operation models A and B compared with the experimental data at 50°C and 1.1 MPa, after all transients have vanished. Generally model A predicts the trend well over the entire liquid flow rate range. The poorest agreement between model A and the experimental data is at very low liquid flow rates where the model estimates of crotonaldehyde conversion are significantly lower than the experimental observations. Interesting with model A is the overprediction of the experimental data if complete wetting is assumed. Unlike the results for 25°C and 1.1 MPa, the models are not identical. Periodic model A reproduces the data much better than model B, with B once again predicting higher conversions as compared to model A. Figures 7.15 and 7.16 are normal deviate plots for periodic models A and B.

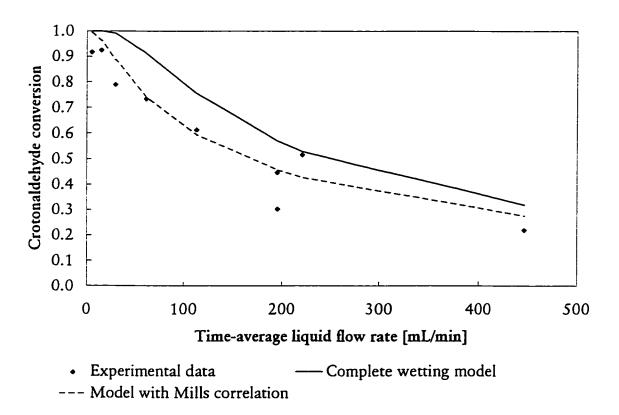


Figure 7.13 Steady operation Model A assuming variable catalyst external wetting with experimental data (Mills-Dudukovic wetting correlation used) and complete catalyst wetting (f = 1)

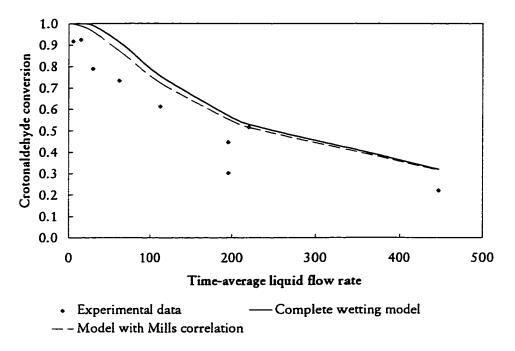
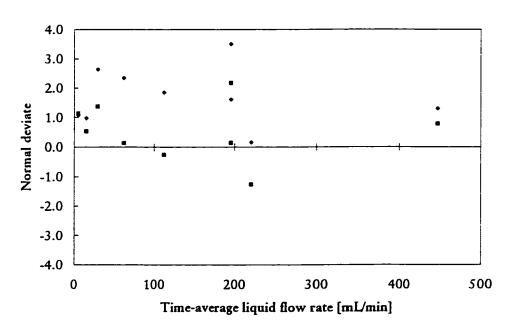
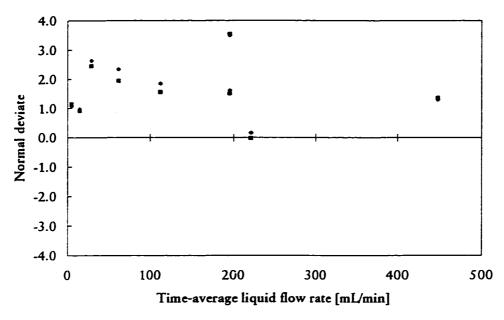


Figure 7.14 Steady operation Model B assuming variable catalyst external wetting with experimental data (Mills-Dudukovic wetting correlation used) and complete catalyst wetting (f = 1)



• Model with complete wetting • Model with Mills-Dudukovic correlation

Figure 7.15 Steady Model A normal deviate for complete and variable wetting



• Model with complete wetting • Model with Mills-Dudukovic correlation

Figure 7.16 Steady Model B normal deviate for complete and variable wetting

The normal deviates of these figures reiterate the fact shown in Figures 7.13 and 7.14 - steady model A with the Mills correlation deviates least from the experimental data. Also the assumption of complete wetting across the entire liquid flow rate range consistently overestimates conversion.

7.3.4 Periodic operation simulation results at 50°C and 1.1 MPa

Figures 7.17 through 7.20 show the periodic operation simulation results for both models A and B. The figures show several facts. The periodic operation models do not predict the lower conversion compared to steady operation and the deviations are quite large. This may suggest that the models are not taking into account the depletion of crotonaldehyde during the portion of the cycle without liquid flow. This is supported by the observation that the largest deviations occur with the 0.1 split data. This is consistent with the fact that the highest amount of crotonaldehyde depletion will occur at the lower split since a longer "dry" interval exists. Interestingly, the

periodic models predict that periodic operation should be superior to steady operation under the experimental conditions.

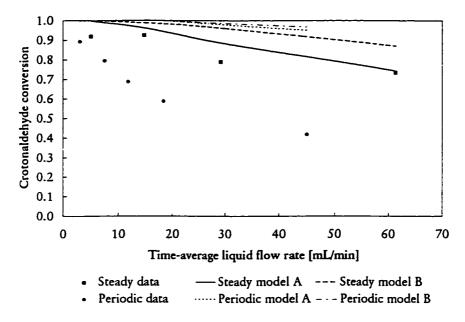


Figure 7.17 Comparison of periodic and steady operation model with experimental data at 50°C and 1.1 MPa; periodic operation parameters: 0.1 split 5 minute period

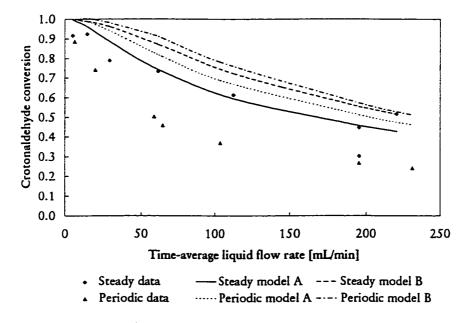


Figure 7.18 Comparison of periodic and steady operation model with experimental data at 50°C and 1.1 MPa; periodic operation parameters: 0.5 split 5 minute period

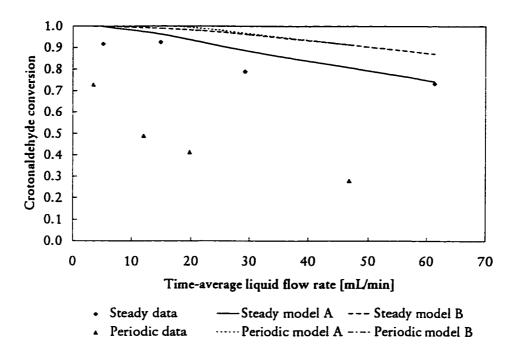


Figure 7.19 Comparison of periodic and steady operation model with experimental data at 50°C and 1.1 MPa; periodic operation parameters: 0.1 split 20 minute period

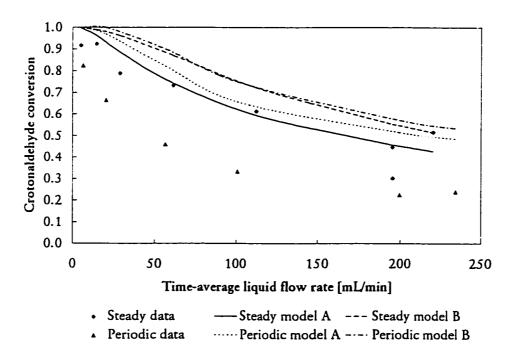


Figure 7.20 Comparison of periodic and steady operation model with experimental data at 50°C and 1.1 MPa; periodic operation parameters: 0.5 split 20 minute period

7.3.5 Steady and periodic operation simulation results at 50°C and 0.1 MPa

Figures 7.21 and 7.22 compare steady models A and B at 50°C and 0.1 MPa. Figure 7.21 shows that for model A the complete wetting model is in better agreement with the experimental data. In Figure 7.22 the two models are in very close agreement with each other and the data. Figures 7.23 through 7.26 show the periodic operation simulation results for both models. Both periodic operation models show close agreement with each other and both periodic models predict the 0.5 split tolerably well. However, they predict the 0.1 split data quite poorly. This suggests that, when the split is small, the models do not account for the way the residual liquid reacts and drains during the relatively lengthy part of the cycle in which liquid is stopped. The deviation is not as severe though as for the 50°C, 1.1 MPa data.

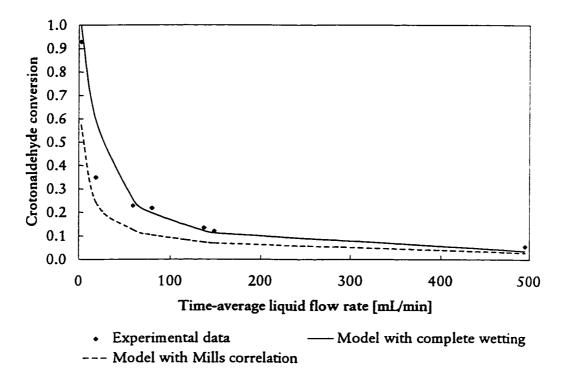


Figure 7.21 Steady operation Model A assuming variable catalyst external wetting with experimental data (Mills-Dudukovic wetting correlation used) and complete catalyst wetting (f = 1)

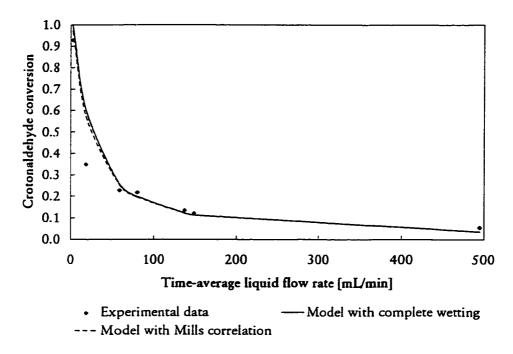


Figure 7.22 Steady operation Model B assuming variable catalyst external wetting with experimental data (Mills-Dudukovic wetting correlation used) and complete catalyst wetting (f = 1)

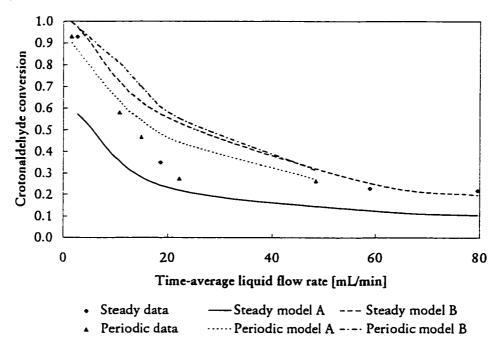


Figure 7.23 Comparison of periodic and steady operation model with experimental data at 50°C and 0.1 MPa; periodic operation parameters: 0.1 split 5 minute period

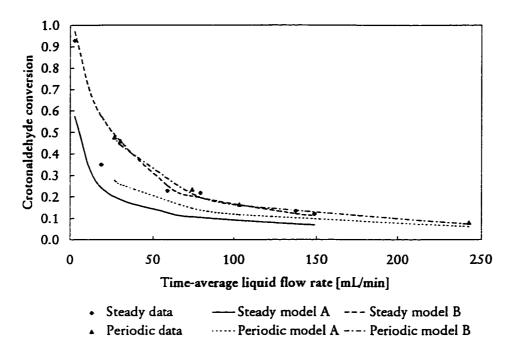


Figure 7.24 Comparison of periodic and steady operation model with experimental data at 50°C and 0.1 MPa; periodic operation parameters: 0.5 split 5 minute period

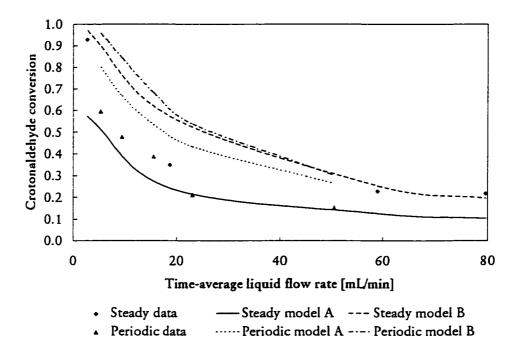


Figure 7.25 Comparison of periodic and steady operation model with experimental data at 50°C and 0.1 MPa; periodic operation parameters: 0.1 split 20 minute period

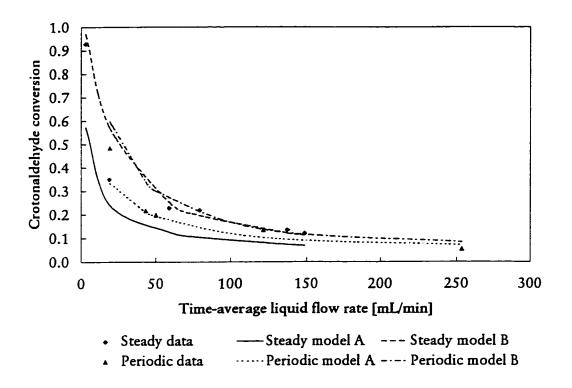


Figure 7.26 Comparison of periodic and steady operation model with experimental data at 50°C and 0.1 MPa; periodic operation parameters: 0.5 split 20 minute period

7.4 Summary of simulation results

From the results presented, several observations of steady and periodic operation simulation results can be made.

- 1. The models for periodic operation consistently predict higher time-average crotonaldehyde conversions than the steady operation model at comparable reactant flows.
- 2. The periodic operation models predict that a lower split produces a higher improvement in conversion than a higher split. The reason for this is the more intense bed flushing as a results of a higher amplitude pulse required to maintain a given time-average flow rate.

3. As liquid flow rate is increased, prediction from both periodic and steady operation models converge. This is consistent with the assumption that for both modes of operation at the higher liquid flow rates, the bed is approaching complete wetting.

- 4. Periodic model A appears to more closely reproduce the data more often than model B.
- 5. The periodic models appeared to predict the data at 25°C, 1.1 MPa and 50°C, 0.1 MPa well, while they were not as successful at predicting the experimental data at 50°C, 1.1 MPa. The worst predictions at the higher temperatures were for the lower split (0.1) suggesting that the models were weak at predicting the depletion of the liquid phase reactant during the portion of the cycle without liquid flow.

CHAPTER

EIGHT

CONCLUSIONS AND RECOMMENDATIONS

8.1 Conclusions

For the system studied, the hydrogenation of crotonaldehyde in water, the following conclusions were drawn:

- 1. Periodic operation, implemented as on-off liquid flow, can improve conversion in a trickle-bed reactor with a non-volatile liquid phase reactant. The improvement is possible if catalyst external wetting is incomplete under steady operation (i.e. constant liquid flow) conditions. This conclusion satisfies research objectives 1, 2 and 3.
- 2. Periodic operation does not improve conversion under all conditions of temperature, pressure and time-average liquid flow rate. Thus optimum values of the on-off periodic operation parameters, period and split, exist. However the optimum values, for a set of operating conditions, do not guarantee that periodic operation will improve conversion compared with steady-state conversion. This conclusion satisfies research objectives 1, 2 and 3.
- 3. The rate of hydrogenation, in the system studied, is controlled by reaction kinetics. The rate of hydrogenation is dependent upon hydrogen pressure, but changes in hydrogen pressure do not affect gas-liquid mass transfer, which appears to be controlled by the surface kinetics only.
- 4. Catalyst external wetting is a monotonic function of liquid flow rate, up to complete wetting.
- 5. The steady-state model presented predicts the experimentally observed trends in conversion, as a function of liquid flow rate. The periodic operation model predicts

the experimentally observed trends in conversion, but tend to overestimate timeaverage conversion at high liquid flow rates. This conclusion satisfies research objective 3.

6. Periodic operation can be applied where catalyst external wetting is incomplete. This conclusion satisfies research objective 4.

8.2 Recommendations

- 1. In the literature is has been suggested that periodic operation can improve conversion if the reaction rate is mass transfer controlled. This system should be adapted to move reaction rate control from reaction kinetics to liquid-solid and/or gasliquid mass transfer control. This may be accomplished by increasing the metal loading of Pd on the catalyst. Further temperature increases are not recommended since this will result in excessive liquid vaporization.
- 2. Catalyst external wetting experiments could be improved by adopting a pulse injection of tracer as opposed to the step change, which has the inherent problem of "tailing". Analysis of the data using the model equations directly, as opposed to transformation of the model to the Laplace domain, may also improve the estimation of catalyst external wetting.
- 3. The periodic operation model overestimated time-average conversion significantly at the higher liquid flow rates. The assumption that catalyst external wetting remains at the same value throughout the entire cycle period may be the reason. Realistically wetting is probably between the two extremes of unchanged wetting and zero wetting. A model incorporating this variation in wetting over the cycle period may be able to better predict the time-average conversion at higher liquid flow rates.

APPENDIX

A

Crotonaldehyde Feed Concentration and Mole Flow Rates

Sample Calculation

Example: Feed has 250 ppmw crotonaldehyde (CRHO). Find mole fraction CRHO

Molecular weights CRHO = 70.0868 g/mol

H₂O = 18.0156 g/mol

Assumptions: Feed is essentially H_2O . Therefore 1×10^6 g of feed is approximately 1×10^6 g H_2O .

Mole fraction CRHO is:

$$\frac{250 \cdot g \cdot CRHO}{10^6 \cdot g \cdot water} \cdot \frac{1 \cdot mol \cdot CRHO}{70.0868 \cdot g \cdot CRHO} \cdot \frac{18.0156 \cdot g \cdot water}{mol \cdot water} = 6.426 \cdot 10^{-5} \cdot \frac{mol \cdot CRHO}{mol \cdot water}$$

CRHO in	CRHO	CRHO
feed	mole	mole
[ppmw]	fraction	conc
		[mol/mL]
0	0	0
50	1.29×10 ⁻⁵	7.14×10 ⁻⁷
100	2.57×10 ⁻⁵	1.43×10 ⁻⁶
150	3.86×10 ⁻⁵	2.14×10 ⁻⁶
200	5.14×10 ⁻⁵	2.86×10 ⁻⁶
250	6.43×10 ⁻⁵	3.57×10 ⁻⁶
300	7.71×10 ⁻⁵	4.28×10 ⁻⁶
350	9.00×10 ⁻⁵	5.00×10 ⁻⁶
400	1.03×10 ⁻⁴	5.71×10 ⁻⁶
450	1.16×10 ⁻⁴	6.43×10 ⁻⁶
500	1.29×10 ⁻⁴	7.14×10 ⁻⁶

APPENDIX

B

Hydrogen Feed Concentration and Mole Flow Rates

Henry's Law Constants for hydrogen in water (Perry and Green, 1984)

T	Н
[°C]	[atm/mol
	frac solute]
20	6.83×10^4
25	7.07×10^4
30	7.29×10^{4}
45	7.60×10^4
50	7.65×10^4
60	7.65×10^4

Hydrogen mole fraction in liquid phase

Sample calculation for mole fraction of hydrogen in water at 25°C and 1.1 MPa

$$P = Hx \Rightarrow x = \frac{P}{H}$$

$$x = 11 \cdot \text{atm} \cdot \left[\frac{\text{(mol_frac)}}{7.07 \cdot 10^4 \cdot \text{atm}} \right]$$

$$x = 1.556 \cdot 10^{-4} \cdot \text{mol_frac}$$

The table below is completed for the various temperature pressure combinations

	T [°C]		
P [MPa]	25	50	
0.1	1.41×10^{-5}	1.31×10^{-5}	
1.1	1.56×10^{-4}	1.44×10^{-4}	

Hydrogen concentration in the liquid phase

Since the solution is mostly water, assume the concentration is 55.5560 mol/L

APPENDIX B 152

$$C_{H_{2},LIQ} = C_{TOTAL,LIQ} x_{H_{2}}$$

$$C_{Liq} = 55.5560 \cdot \frac{\text{mol}}{\text{L}} \cdot 1.556 \cdot 10^{-4} \cdot \frac{1 \cdot \text{L}}{1000 \cdot \text{mL}}$$

$$C_{Liq} = 8.645 \cdot 10^{-6} \cdot \frac{\text{mol}}{\text{mI}}$$

The table below lists hydrogen concentrations in the liquid phase [mol/mL]

	T [°C]		
P [MPa]	2.5	50	
0.1	7.86×10^{-7}	7.26×10^{-7}	
1.1	8.64×10^{-6}	7.99×10^{-6}	

Comparison between hydrogen and crotonaldehyde liquid feed concentrations

Crotonaldehyde liquid feed concentration at 250 ppm is 3.57×10⁻⁶ mol/mL

Ratio of crotonaldehyde concentration to hydrogen concentration in the feed

	T [°C]	
P [MPa]	25	50
0.1	0.220106	0.203418
1.1	2.421167	2.237601

Calculation of flowrates

An interesting situation arises when the hydrogen pressure is dropped since the concentration of hydrogen in the liquid phase is limited by Henry's Law even though the amount of hydrogen flowing into the reactor is much greater than the amount of crotonaldehyde.

For hydrogen assuming the ideal gas law applies

$$F_{H_1} = C_{H_1,Gas} v_{H_1,Gas} = \frac{P v_{H_1,Gas}}{RT}$$

APPENDIX B 153

$$F_{H} = 1 \cdot \text{atm} \cdot \frac{101.325 \cdot \text{kPa}}{\text{atm}} \cdot \frac{1 \cdot \text{L}}{\text{min}} \cdot \frac{\text{mol} \cdot \text{K}}{8.314 \cdot \text{L} \cdot \text{kPa}} \cdot \frac{1}{273.15 \cdot \text{K}}$$

$$F_{H} = 0.045 \cdot \frac{\text{mol}}{\text{min}}$$

For crotonaldehyde at the highest flowrate of about 450 mL/min

$$F_{CRHO} = C_{CRHO,Liq} v_{Liq}$$

$$F_{CRHO} = 3.57 \cdot 10^{-6} \cdot \frac{\text{mol}}{\text{mL}} \cdot 450 \cdot \frac{\text{mL}}{\text{min}}$$

$$F_{CRHO} = 1.607 \cdot 10^{-3} \cdot \frac{\text{mol}}{\text{min}}$$

The ratio of hydrogen to crotonaldehyde flowing to the reactor is then about 28:1. This means that regardless of the conversion of crotonaldehyde achieved, hydrogen in the gas phase will never be depleted. However, the concentration of hydrogen in the liquid phase is controlled by Henry's Law and therefore the effective concentration of hydrogen in the liquid phase will be affected significantly by hydrogen pressure.

APPENDIX

 \mathbf{C}

Fluids and Catalyst Properties

Hydrogen

Property	25°C	50°C	Reference
Henry's law constant	52.024	51.935	(Perry and Green, 1984)
Diffusivity in water	4.80×10^{-9}	8.48×10^{-9}	(see Appendix J)

Water

Property	25°C	50°C	Reference
Density [kg/m³]	997.1	988.1	(Streeter and Wylie, 1981)
Dynamic viscosity [cP]	0.894	0.549	(Streeter and Wylie, 1981)
Surface tension [N/m]	7.26×10^{-2}	6.82×10^{-2}	(Streeter and Wylie, 1981)
Vapour pressure [kPa]	3.2	12.4	(Streeter and Wylie, 1981)

Crotonaldehyde

Property	25°C	50°C	Reference
Diffusivity in water [m²/s]	1.14×10^{-9}	2.02×10^{-9}	(see Appendix J)
Vapour pressure [kPa]	4.104	13.835	(Daubert, 1989)

Butyraldehyde

Property	25°C	50°C	Reference
Vapour pressure [kPa]	0.739	2.114	(Daubert, 1989)

Catalyst and trickle-bed properties

Catalyst support	γ-Al ₂ O ₃
Pd loading	0.03 wt. %
Shape	spherical
Particle diameter	3.36 - 4.76 mm
Bulk density	1.0943 g/cm ³
Skeletal density	3.4775 g/cm ³
Internal porosity	0.62
Bed length	30 cm
Bed diameter	5.25 cm
Bed porosity	0.372

Three-phase Catalytic Reactor Overall Resistance Derivation

At steady state, the rates of all mass transfer processes and surface reaction are equal. For mass transfer through the gas phase, the rate R_o is given by

$$R_o = k_G a_G \frac{(C_G - C_{iG})}{m} \tag{D.1}$$

The mass transfer coefficient is $k_G a_G$ [s⁻¹], C_G [mol/cm³] is the bulk gas phase concentration, C_{iG} [mol/cm³], is the gas concentration at the gas phase boundary, and m is the catalyst mass per volume of reactor [g/cm³]. For mass transfer across the gasliquid interface, the rate R_o is given by

$$R_o = k_L a_G \frac{(C_{iL} - C_L)}{m} \tag{D.2}$$

The mass transfer coefficient is $k_L a_G$ [s⁻¹], C_L [mol/cm³] is the bulk liquid phase concentration, C_{iL} [mol/cm³], is the liquid concentration at the gas-liquid interface, and m is the catalyst mass per volume of reactor [g/cm³]. For mass transfer across the liquid-solid (catalyst) interface, the rate R_o is given by

$$R_o = k_C a_C \frac{(C_L - C_S)}{m} \tag{D.3}$$

The mass transfer coefficient is $k_C a_C$ [s⁻¹], C_L [mol/cm³] is the bulk liquid phase concentration, C_S [mol/cm³], is the liquid concentration at the solid surface, and m is the catalyst mass per volume of reactor [g/cm³]. For surface reaction, the rate R_o is given by

$$R_o = \frac{k\eta C_S}{\rho_P} \tag{D.4}$$

The intrinsic reaction rate constant is k [s⁻¹], the particle effectiveness factor is η , C_s [mol/cm³], is the liquid concentration at the solid surface, and ρ_P [g/cm³] is the catalyst particle skeletal density. Equations (D.1) through (D.4) can be rearranged as

$$\frac{R_o m}{k_G a_G} = (C_G - C_{iG}) \tag{D.5}$$

$$\frac{R_0 m}{k_L a_G} = (C_{iL} - C_L) \tag{D.6}$$

$$\frac{R_o m}{k_C a_C} = (C_L - C_S) \tag{D.7}$$

$$\frac{R_o \rho_P}{k \eta} = C_S \tag{D.8}$$

The next step is to add equations (D.4) through (D.8). Before proceeding, an expression relating the gas phase concentration at the gas-liquid interface, C_{iC} to the liquid phase concentration at the gas-liquid interface, C_{iL} , is required. This expression is Henry's Law

$$C_{iG} = H^{\bullet}C_{iI} \tag{D.9}$$

Equation (D.5) now becomes

$$\frac{R_{o}m}{k_{G}a_{G}} = (C_{G} - H^{*}C_{iL}) = H^{*}\left(\frac{C_{G}}{H^{*}} - C_{iL}\right)$$

$$\frac{R_{o}m}{k_{C}a_{C}H^{*}} = \frac{C_{G}}{H^{*}} - C_{iL}$$
(D.10)

By adding equations (D.6) through (D.8) and (D.10), the result is

$$R_o \left\{ \frac{m}{a_G} \left(\frac{1}{H^* k_G} + \frac{1}{k_L} \right) + \left(\frac{m}{k_c a_c} + \frac{\rho_P}{k \eta} \right) \right\} = \frac{C_G}{H^*}$$
 (D.11)

which can be written as

$$R_o = \frac{K_{o,G}C_G}{H^*} \tag{D.12}$$

where

$$\frac{1}{K_{o,G}} = \frac{m}{a_G} \left(\frac{1}{k_G} + \frac{1}{k_L} \right) + \left(\frac{m}{k_c a_c} + \frac{\rho_P}{k \eta} \right)$$
 (D.13)

The quantity $K_{0,G}$ represents an overall rate constant [s⁻¹] encompassing all mass transfer coefficients and the surface reaction rate constant. In the case of equation (D.13) it is assumed the reactant is in the gas phase. For the case of a non-volatile liquid phase reactant with a high gas-liquid interfacial area, the term containing k_G and k_L is not required. Therefore, equation (D.13) simplifies to

$$\frac{1}{K_{o,L}} = \frac{m}{k_c a_c} + \frac{\rho_P}{k\eta} \tag{D.14}$$

Note that equation (D.12) would then have the analogous form for the liquid phase of

$$R_o = K_{o,L}C_L \tag{D.15}$$

The quantity $K_{o,L}$ can then be used in a reactor design model under steady operation such as a CSTR model or an integral reactor type model, such as a PFR model.

Steady Operation CSTR Model Equation Using the Overall Rate Constant

It is not necessarily true that a trickle-bed reactor is a fully backmixed reactor such as a CSTR. However the implicit assumption in the CSTR design equation is the uniformity of concentration throughout the reactor's domain. If the conversion of a reactant is low, a trickle-bed reactor can approach this assumption of uniform concentration for that particular reactant and the CSTR model can be applied without significant error. The CSTR design equation is simply

$$(-R_o)m_{cat} = F_o X \tag{D.16}$$

where $-R_o$ is the rate of disappearance of a reactant [mol/min], F_o is the flowrate of the reactant into the reactor [mol/min], and X is the conversion of reactant. Considering a non-volatile liquid phase reactant, substitution of equation (D.15) into (D.16) produces

$$-K_{o,L}C_L m_{cat} = F_o X (D.17)$$

If the conversion is low (less than 0.2), equation (D.17) is useful since it allows one to estimate $K_{o,L}$ from three measurable quantities. Furthermore, one is able to determine which process (mass transfer or surface reaction) is the slowest (i.e., the rate determining step), by comparison with mass transfer data or correlations. If mass transfer is not the rate determining step, then the surface reaction rate constant can be calculated from $K_{o,L}$, provided the effectiveness factor η is known. An estimate of the intrinsic rate constant is given in Appendix E by this method.

Steady Operation Integral or PFR Design Equation Using the Overall Rate Constant

The approach used in the previous section can be applied to an integral design equation. The utility of such an approach is that the restriction to low conversions is not necessary. For a catalytic fixed-bed reactor the design equation can be written as

$$F_o dX = R_o dm_{cat} (D.18)$$

where m_{cat} is the mass of catalyst [g]. Again for a non-volatile liquid phase reactant, substitution of (D.15) into (D.18) gives

$$F_o dX = -K_{o,L} C_L dm_{cat} (D.19)$$

For a constant liquid flowrate F_o can be written as

$$F_0 = C_{I,0} v_I \tag{D.20}$$

Substituting (D.20) into (D.19) gives

$$C_{Lo}v_L dX = -K_{o,L}C_L dm_{cat}$$
 (D.21)

Conversion X can be expressed in terms of C_L and C_{Lo} by

$$C_L = C_{Lo}(1 - X)$$
 (D.22)

Substituting (D.22) into (D.21) gives

$$\frac{dX}{1-X} = \frac{-K_{o,L}}{v_I} dm_{cat} \tag{D.23}$$

Integration of equation (D.23) gives

$$\int_{0}^{X} \frac{dX}{1-X} = \int_{0}^{m_{cat}} \frac{-K_{o,L}}{v_L} dm_{cat}$$

$$\ln\left(\frac{1}{1-X}\right) = \frac{K_{o,L}}{v_L} m_{cat} \tag{D.24}$$

which can be rearranged to give

$$K_{o,L} = \frac{v_L}{m_{cat}} \ln \left(\frac{1}{1 - X} \right) \tag{D.25}$$

From the conversion, X, the liquid volumetric flow rate, and the mass of catalyst in the reactor, m_{cat} , $K_{o,L}$ can be calculated. The same procedure as in the previous section can be used to determine the surface reaction rate constant, provided mass transfer is not the rate determining process for the overall rate. As an example of this calculation, the surface reaction rate constant is calculated in Appendix E.

APPENDIX

E

Sample Calculation of the Surface Reaction Rate Constant Estimation of k and E₂ using the CSTR Form of the Reaction Equation

$$R_0 = F_{A0}X$$

$$F_{A0} = C_{A0} \nu_0$$

Steady-state trickle-bed experimental data are given below

Liquid Flow [mL/min]	Conversion	Rate [mol/min]	Temperature [°C]	Pressure [atm]
475.4	0.00500	8.48×10^{-6}	2.5	11
447.3	0.22016	3.52×10^{-4}	50	11

Also

$$C_L = 3.57\text{E}-06 \text{ mol/mL } (250 \text{ ppmw})$$
 $\rho_p = 1.0943 \text{ g/cm}^3$ $R_o = 2.36\text{E}-10 \text{ mol/(g cat s)}$ $d_p \cong 4.06 \text{ mm}$ $k_c a_c = 0.03807 \text{ 1/s (at } 25^\circ\text{C})$ $k_c a_c = 0.06247 \text{ 1/s (at } 50^\circ\text{C})$

Example: Estimate the reaction rate constant k for 25°C

$$R_0 = 8.48 \cdot 10^{-6} \cdot \frac{\text{mol}}{\text{min}} \cdot \frac{1}{410.08 \cdot \text{g}_{\text{cat}}} \cdot \frac{\text{min}}{60 \cdot \text{s}}$$

$$R_0 = 3.446 \cdot 10^{-10} \cdot \frac{\text{mol}}{\text{g}_{\text{cat}} \cdot \text{s}}$$

$$R_0 \left(\frac{m}{k_c a_c} + \frac{\rho_p}{k \eta} \right) = C_L$$

$$k = \left[\left(\frac{C_L}{R_0} - \frac{m}{k_c a_c} \right) \frac{\eta}{\rho_p} \right]^{-1}$$

APPENDIX E 161

$$k = \left[\sqrt{3.57 \cdot 10^{-6} \cdot \frac{\text{mol}}{\text{mL}} \cdot \frac{\text{g cat's}}{3.446 \cdot 10^{-10} \cdot \text{mol}} - \frac{631.4 \cdot \text{g cat}}{1000 \cdot \text{cm}^3} \cdot \frac{\text{s}}{0.03807}} \cdot \frac{\text{cm}^3}{1.0943 \cdot \text{g cat}}} \right]^{-1}$$

$$k = 1.058 \cdot 10^{-4} \cdot \text{s}^{-1}$$

Example: Estimate the reaction rate constant k for 50°C

$$R_0 = 3.52 \cdot 10^{-4} \cdot \frac{\text{mol}}{\text{min}} \cdot \frac{1}{410.08 \cdot \text{g}_{\text{cat}}} \cdot \frac{\text{min}}{60 \cdot \text{s}}$$

$$R_0 = 1.431 \cdot 10^{-8} \cdot \frac{\text{mol}}{\text{g}_{\text{cat}} \cdot \text{s}}$$

$$k_{c}a_{c}=0.06247 \text{ s}^{-1}$$

$$k = \left[\left(3.57 \cdot 10^{-6} \cdot \frac{\text{mol}}{\text{mL}} \cdot \frac{\text{g cat} \cdot \text{s}}{1.431 \cdot 10^{-8} \cdot \text{mol}} - \frac{631.4 \cdot \text{g cat}}{1000 \cdot \text{cm}^3} \cdot \frac{\text{s}}{0.04416} \right) \cdot \frac{\text{cm}^3}{1.0943 \cdot \text{g cat}} \right]^{-1}$$

$$k = 4.653 \cdot 10^{-3} \cdot \text{s}^{-1}$$

Estimate Activation Energy

$$E_{a} = -R \ln \left(\frac{k_{1}}{k_{2}}\right) \left(\frac{1}{T_{1}} - \frac{1}{T_{2}}\right)^{-1}$$

$$E_{a} = \frac{-8.314 \cdot J}{\text{mol} \cdot K} \cdot \left(\ln \left(\frac{1.058 \cdot 10^{-4} \cdot \text{s}^{-1}}{4.653 \cdot 10^{-3} \cdot \text{s}^{-1}}\right)\right) \cdot \left[\frac{1}{(25 + 273.15) \cdot \text{K}} - \frac{1}{(50 + 273.15) \cdot \text{K}}\right]^{-1}$$

$$E_{a} = 1.212 \cdot 10^{5} \cdot \frac{J}{\text{mol}}$$

$$E_{a} = 121.235 \cdot \frac{kJ}{\text{mol}}$$

F

Sample Calculation of the Surface Reaction Rate Constant Estimation of k and E₄ using the Integral Form of the Reaction Equation

Given the integral form of the reactor equation

$$X = 1 - \exp\left(\frac{-K_s}{v_L}m_{cat}\right)$$

where

$$K_{S} = \left(\frac{m}{k_{c}a_{c}} + \frac{\rho_{p}}{k\eta}\right)^{-1}$$

Steady-state trickle-bed experimental data are given below

Liquid Flow	Conversion	Rate	Temperature	Pressure
[mL/min]		[mol/min]	[°C]	[atm]
475.4	0.00500	8.48×10^{-6}	2.5	11
447.3	0.22016	3.52×10^{-4}	50	11

Also

$$C_L = 3.57\text{E}-06 \text{ mol/mL } (250 \text{ ppmw})$$
 $\rho_p = 1.0943 \text{ g/cm}^3$ $R_o = 2.36\text{E}-10 \text{ mol/(g cat s)}$ $d_p = 4.06 \text{ mm}$ $h_c a_c = 0.03807 \text{ 1/s } (\text{at } 25^{\circ}\text{C})$ $h_c a_c = 0.06247 \text{ 1/s } (\text{at } 50^{\circ}\text{C})$

Example: Estimate the reaction rate constant k for 25°C

$$K_S = -\ln(1 - 0.00500) \cdot \left(475.3 \cdot \frac{\text{cm}^3}{\text{min}} \cdot \frac{1}{446.33 \cdot \text{g}} \cdot \frac{\text{min}}{60 \cdot \text{s}}\right)$$

$$K_S = 8.896 \cdot 10^{-5} \cdot \frac{\text{cm}^3}{\text{g} \cdot \text{s}}$$

$$k = \left(\frac{1}{K_S} - \frac{m}{k_c a_c}\right)^{-1} \frac{\rho_p}{\eta}$$

$$k = \left(\frac{s \cdot g}{8.896 \cdot 10^{-5} \cdot \text{cm}^3} - \frac{0.6872 \cdot g}{\text{cm}^3} \cdot \frac{s}{3.66 \cdot 10^{-2}}\right)^{-1} \cdot \frac{1.0943 \cdot g}{\text{cm}^3}$$

$$k = 9.751 \cdot 10^{-5} \cdot \text{s}^{-1}$$

Example: Estimate the reaction rate constant k for 50°C

$$K_{S} = -\ln(1 - 0.22016) \cdot \left(447.3 \cdot \frac{\text{cm}^{3}}{\text{min}} \cdot \frac{1}{446.33 \cdot \text{g}} \cdot \frac{\text{min}}{60 \cdot \text{s}}\right)$$

$$K_{S} = 4.153 \cdot 10^{-3} \cdot \frac{\text{cm}^{3}}{\text{g} \cdot \text{s}}$$

$$k = \left(\frac{1}{K_{S}} - \frac{m}{k_{c}a_{c}}\right)^{-1} \frac{\rho_{p}}{\eta}$$

$$k = \left(\frac{\text{s} \cdot \text{g}}{4.153 \cdot 10^{-3} \cdot \text{cm}^{3}} - \frac{0.6872 \cdot \text{g}}{\text{cm}^{3}} \cdot \frac{\text{s}}{5.98 \cdot 10^{-2}}\right)^{-1} \cdot \frac{1.0943 \cdot \text{g}}{\text{cm}^{3}}$$

$$k = 4.772 \cdot 10^{-3} \cdot \text{s}^{-1}$$

Estimate Activation Energy

$$E_{a} = -R \ln \left(\frac{k_{1}}{k_{2}}\right) \left(\frac{1}{T_{1}} - \frac{1}{T_{2}}\right)^{-1}$$

$$E_{a} = \frac{-8.314 \cdot J}{\text{mol} \cdot K} \cdot \left(\ln \left(\frac{9.751 \cdot 10^{-5} \cdot \text{s}^{-1}}{4.772 \cdot 10^{-3} \cdot \text{s}^{-1}}\right)\right) \cdot \left[\frac{1}{(25 + 273.15) \cdot \text{K}} - \frac{1}{(50 + 273.15) \cdot \text{K}}\right]^{-1}$$

$$E_{a} = 1.247 \cdot 10^{5} \cdot \frac{J}{\text{mol}}$$

APPENDIX F 164

$$E_a = 124.658 \cdot \frac{kJ}{mol}$$

Comparison of calculated reaction rate constants

Temperature	Differential	Integral PFR	Percent Difference
[°C]	Estimate [s ⁻¹]	Estimate [s ⁻¹]	[%]
25	1.058×10^{-4}	9.751 × 10 ⁻⁵	8.5
50	4.653×10^{-3}	4.772×10^{-3}	2.5

Comparison of calculated activation energies

CSTR Estimate 121.24 kJ/mol Integral Estimate 124.66 kJ/mol

Percent Difference 2.7 %

Calculation of effect of pressure on gas-liquid mass transfer

For gas pressure to have an effect on the gas-liquid mass transfer coefficient, the inequality

$$\left(\frac{r_{hydrogenation}}{P_{H_1}}\right)_{1,1,MP_d} > \left(\frac{r_{hydrogenation}}{P_{H_1}}\right)_{0,1,MP_d}$$

or

$$\left(\frac{X}{P_{H_1}}\right)_{1.1\,MPa} > \left(\frac{X}{P_{H_2}}\right)_{0.1\,MPa}$$

must be satisfied.

Given the data at 50°C (note that there is about a 10% difference in the liquid velocity at which these data were obtained):

Pressure [MPa]	X	v_L [mL/min]
0.1	0.0555	495.0
1.1	0.2202	447.3

APPENDIX F 165

$$\left[\left(\frac{X}{P_{H_1}} \right)_{1.1 \text{ MPa}} = 0.20 \right] < \left[\left(\frac{X}{P_{H_1}} \right)_{0.1 \text{ MPa}} = 0.56 \right]$$

Therefore pressure does not affect the gas-liquid mass transfer coefficient.

Estimating the order of reaction assuming a hydrogen pressure effect

The reaction rate law is assumed to have the form

$$-r_{CRHO} = kC_{CRHO,s}C_{H_1}^n$$

where the concentrations are at the catalyst surface. If conversions are low, estimates of the catalyst surface concentrations can be made utilizing equations (D.1) through (D.3)

$$R_o = k_G a_G \frac{(C_G - C_{iG})}{m} \tag{D.1}$$

$$R_o = k_L a_G \frac{(C_{iL} - C_L)}{m} \tag{D.2}$$

$$R_o = k_C a_C \frac{(C_L - C_S)}{m} \tag{D.3}$$

and a modified form of equation (D.4)

$$R_o = \frac{k\eta C_{CRHO,s} C_{H_2}^n}{\rho_P} \tag{F.1}$$

with $\eta = 1$.

The reaction order can then be estimated by taking a ratio of equation (F.1) at two different pressures

$$\frac{(R_0)_{0.1 \text{ MPa}}}{(R_0)_{1.1 \text{ MPa}}} = \frac{(kC_{CRHO,S}C_{H_2}^n)_{0.1 \text{ MPa}}}{(kC_{CRHO,S}C_{H_1}^n)_{1.1 \text{ MPa}}}$$
(F.2)

APPENDIX F 166

Solving for n gives

$$n = \frac{\ln\left(\frac{R_{0,0.1 MPa}C_{CRHO,S,1.1 MPa}}{R_{0,1.1 MPa}C_{CRHO,S,0.1 MPa}}\right)}{\ln\left(\frac{C_{H_1,0.1 MPa}}{C_{H_2,1.1 MPa}}\right)}$$
(F.3)

Given the values below (using data from previous table at 50°C) and calculated surface concentrations

	0.1 MPa	1.1 MPa
X	0.0555	0.2202
C _{CRHO,s} [mol/L]	3.517×10^{-3}	3.372×10^{-3}
$C_{H_2,S}$ [mol/L]	6.035×10^{-4}	7.528×10^{-3}

the value of n is 0.523 which is approximately $\frac{1}{2}$.

G

Trickle-bed reactor resistance analysis to determine the contribution of various processes to the overall rate of reaction

The overall rate of reactant consumption or product formation in a trickle-bed reactor consists of various steps each of which takes a certain length of time. Those which take the longest time are often termed rate determining. These rate determining steps can also be viewed as a resistance to the overall rate of reactant consumption or product formation. In general a resistance impedes the movement of some quantity and it is the gradient of the quantity or some other potential quantity which provides the driving force which moves the quantity through the resistance. For example Ficks law of diffusion expresses this physical situation mathematically

$$J_r = -D\frac{dC}{dr} \tag{G.1}$$

The diffusivity D is a conductivity while 1/D represents a resistance.

A similar approach can be used for the analysis of a trickle-bed reactor. Consider the equations (D.1) through (D.4) from Appendix D. These equations can be written in a form of

Rate = Gradient / Resistance
$$(G.2)$$

$$R_o = k_G a_G \frac{(C_G - C_{iG})}{m} \tag{D.1}$$

$$R_o = k_L a_G \frac{(C_{iL} - C_L)}{m} \tag{D.2}$$

$$R_o = k_C a_C \frac{(C_L - C_S)}{m} \tag{D.3}$$

$$R_o = \frac{k\eta C_S}{\rho_P} \tag{D.4}$$

In each of the above equations, the gradient represents a concentration difference and the resistance for each equation is then given by APPENDIX G 168

$$R_G = \frac{m}{H^* k_G a_G} \tag{G.3}$$

$$R_{GL} = \frac{m}{k_L a_G} \tag{G.4}$$

$$R_{LS} = \frac{m}{k_C a_C} \tag{G.5}$$

$$R_{R} = \frac{\rho_{p}}{k\eta} \tag{G.6}$$

Note that equations (G.3) and (G.4) arise because of Henry's law. In the case in which the limiting reactant is in the liquid phase, the resistances which are compared are equations (G.5) and (G.6).

Example: Estimate the relative resistance of liquid-solid mass transfer to surface reaction given

$$C_L = 3.57\text{E}-06 \text{ mol/mL} (250 \text{ ppmw})$$
 $\rho_p = 1.0943 \text{ g/cm}^3$ $R_o = 2.36\text{E}-10 \text{ mol/(g cat s)}$ $d_p \cong 4.06 \text{ mm}$ $\eta \cong 1$ $k_c a_c = 0.03807 \text{ 1/s (at 25°C)}$ $k = 7.25\text{E}-05 \text{ s}^{-1}$ $k_c a_c = 0.06247 \text{ 1/s (at 50°C)}$

$$R_{LS} = \frac{m}{k_C a_C}$$

$$R_{LS} = 0.6 \cdot \frac{g}{cm^3} \cdot \frac{s}{0.03807}$$

$$R_{LS} = 1.576 \cdot 10^4 \cdot \text{kg} \cdot \text{m}^{-3} \cdot \text{s}$$

$$R_R = \frac{\rho_p}{k\eta}$$

$$R_{R} = \frac{1.0943 \cdot \frac{g}{cm^{3}}}{\left(7.25 \cdot 10^{-5} \cdot s^{-1} \cdot 1\right)}$$

$$R_R = 1.509 \cdot 10^7 \cdot \text{kg} \cdot \text{m}^{-3} \cdot \text{s}$$

H

Axial Dispersion Sample Calculations

Mears (1971) criterion for neglecting axial dispersion is given by:

$$\frac{L}{d_p} > \frac{20m}{Pe_L} ln \frac{C_i}{C_o} \tag{H.1}$$

Since conversion X, is given by:

$$X = \frac{C_i - C_o}{C_i} \tag{H.2}$$

Mears' equation can be cast into the form:

$$\frac{L}{d_p} > \frac{20m}{Pe_L} ln \frac{1}{1 - X} \tag{H.3}$$

As an estimate of Pe_L the correlation of Furzer and Mitchell (1970) is used

$$Pe_L = 13 Re_L^{0.4} Ga_L^{-0.333}$$
 (H.4)

where Pe_L is defined as

$$Pe_L = \frac{u_L d_p}{D_{EL}} \tag{H.5}$$

and

$$Ga_L = \frac{d_p^3 g \rho_L^2}{\mu_L^2} \tag{H.6}$$

and

$$Re_L = \frac{u_L d_p \rho_L}{\mu_L} \tag{H.7}$$

APPENDIX H 171

Example: Determine if Mears criterion is satisfied given the data below.

Data:

$$d_p = 3 \text{ mm}$$
 $\mu_L = 1.129 \text{ cP}$ $L = 30 \text{ cm}$ $\rho_L = 1 \text{ g/cm}^3$ $d_T = 2.067 \text{ in}$ $\nu_L = 450 \text{ cm}^3/\text{min}$ $\lambda = 0.01$

Assume the reaction is first order (m = 1).

$$d_{p} = 3 \cdot \text{mm} \cdot \frac{\text{m}}{1000 \cdot \text{mm}} \qquad d_{p} = 3 \cdot 10^{-3} \cdot \text{m}$$

$$\rho_{L} = 1.0 \cdot \frac{\text{g}}{\text{cm}^{3}} \cdot \frac{\text{kg}}{1000 \cdot \text{g}} \cdot 10^{6} \cdot \frac{\text{cm}^{3}}{\text{m}^{3}} \qquad \rho_{L} = 1 \cdot 10^{3} \cdot \text{kg} \cdot \text{m}^{-3}$$

$$\mu_{L} = 1.129 \cdot \text{cP} \cdot \frac{\frac{\text{kg}}{(\text{m} \cdot \text{s})}}{1000 \cdot \text{cP}} \qquad \mu_{L} = 1.129 \cdot 10^{-3} \cdot \text{kg} \cdot \text{m}^{-1} \cdot \text{s}^{-1}$$

$$A_{x} = \frac{\pi}{4} \cdot \left(2.067 \cdot \text{in} \cdot 2.54 \cdot \frac{\text{cm}}{\text{in}}\right)^{2} \qquad A_{x} = 2.165 \cdot 10^{-3} \cdot \text{m}^{2}$$

$$u_{L} = \frac{v_{L}}{A_{x}} \qquad u_{L} = 3.464 \cdot 10^{-3} \cdot \text{m} \cdot \text{s}^{-1}$$

$$Re_{L} = \frac{u_{L} \cdot d_{p} \cdot \rho_{L}}{\mu_{L}} \qquad Re_{L} = 9.206$$

$$Ga_{L} = \frac{d_{p}^{3} \cdot \text{gr} \rho_{L}^{2}}{\mu_{L}^{2}} \qquad Ga_{L} = 2.076 \cdot 10^{5}$$

$$Pe_{L} = 13 \cdot Re_{L}^{0.4} \cdot Ga_{L}^{-0.333} \qquad Pe_{L} = 0.536$$

$$\frac{L}{d_p} = 100$$

Since the reaction is assumed first order, m = 1, therefore

$$\frac{20}{Pe_L} \cdot ln \left(\frac{1}{1 - X} \right) = 0.375$$

Since

$$\frac{L}{d_p} > \frac{20m}{Pe_L} ln \frac{1}{1 - X}$$

for this combination of liquid flow rate and conversion, Mears criterion is satisfied.

Catalyst External Wetting Correlations

The Mills-Dudukovic equation for catalyst wetting is

$$f = \sqrt{\frac{(D_{EO})_{app}}{(D_{EO})_{LF}}} = 1.0 - exp \left(-1.35 Re_L^{0.333} Fr_L^{0.235} We_L^{-0.170} \left(\frac{a_t d_p}{\varepsilon_B^2} \right)^{-0.0425} \right)$$
 (I.1)

Although a second form of the Mills-Dudukovic equation for catalyst wetting is given by

$$f = \sqrt{\frac{(D_{EO})_{app}}{(D_{EO})_{LF}}} = tanh \left(0.664 Re_L^{0.333} Fr_L^{0.195} We_L^{-0.171} \left(\frac{a_t d_p}{\varepsilon_B^2} \right)^{-0.0615} \right)$$
 (I.2)

only (I.1) is used, with

$$Re_L = \frac{u_L d_p \rho_L}{\mu_L} \tag{I.3}$$

$$Fr_L = \frac{u_L^2}{gd_p} \tag{I.4}$$

$$We = \frac{u_L^2 \rho_L d_p}{\sigma_L} \tag{I.5}$$

$$a_t = \frac{S_{ex}(1 - \varepsilon_B)}{V_b} \tag{I.6}$$

Example: Determine the catalyst external wetting, given the data below.

Data:

$$\rho_L = 1 \text{ g/cm}^3$$
 $\mu_L = 1.129 \text{ cP}$
 $\sigma_L = 70 \text{ mN/m}$
 $\nu_L = 450 \text{ cm}^3/\text{min}$
 $d_p = 3 \text{ mm}$
 $\varepsilon_B = 0.372$

APPENDIX I 174

$$d_{p} = 3 \cdot \text{mm} \cdot \frac{\text{m}}{1000 \cdot \text{mm}} \qquad d_{p} = 3 \cdot 10^{-3} \cdot \text{m}$$

$$r_{p} = \frac{d_{p}}{2} \qquad r_{p} = 1.5 \cdot 10^{-3} \cdot \text{m}$$

$$S_{ex} = 4 \cdot \pi \cdot r_{p}^{2} \qquad S_{ex} = 2.827 \cdot 10^{-5} \cdot \text{m}^{2}$$

$$V_{p} = \frac{4}{3} \cdot \pi \cdot r_{p}^{3} \qquad V_{p} = 1.414 \cdot 10^{-8} \cdot \text{m}^{3}$$

$$\rho_{L} = 1 \cdot \frac{\text{g}}{\text{cm}^{3}} \cdot \frac{\text{kg}}{1000 \cdot \text{g}} \cdot 10^{6} \cdot \frac{\text{cm}^{3}}{\text{m}^{3}} \qquad \rho_{L} = 1 \cdot 10^{3} \cdot \text{kg} \cdot \text{m}^{-3}$$

$$\rho_{L} = 1.129 \cdot \text{cP} \cdot \frac{\frac{\text{kg}}{(\text{m} \cdot \text{s})}}{1000 \cdot \text{cP}} \qquad \mu_{L} = 1.129 \cdot 10^{-3} \cdot \text{kg} \cdot \text{m}^{-1} \cdot \text{s}^{-1}$$

$$\sigma_{L} = 70 \cdot \frac{\text{mN}}{\text{m}} \cdot \frac{\text{N}}{1000 \cdot \text{mN}} \qquad \sigma_{L} = 0.07 \cdot \text{kg} \cdot \text{s}^{-2}$$

$$A_{x} = \frac{\pi}{4} \cdot \left(2.067 \cdot \text{in} \cdot 2.54 \cdot \frac{\text{cm}}{\text{in}}\right)^{2} \qquad A_{x} = 2.165 \cdot 10^{-3} \cdot \text{m}^{2}$$

$$a_{t} = \frac{S_{ex} \cdot (1 - \varepsilon_{B})}{V_{p}} \qquad a_{t} = 1.256 \cdot 10^{3} \cdot \text{m}^{-1}$$

$$\nu_{L} = 450 \cdot \frac{\text{cm}^{3}}{\text{min}} \qquad \nu_{L} = \frac{\nu_{L}}{A_{x}}$$

$$\nu_{L} = 3.464 \cdot 10^{-3} \cdot \text{m} \cdot \text{s}^{-1}$$

$$Re_{L} = \frac{u_{L} \cdot d_{p} \cdot \rho_{L}}{\mu_{L}} \qquad Re_{L} = 9.206$$

APPENDIX I 175

$$Fr_{L} = \frac{u_{L}^{2}}{g \cdot d_{p}} \qquad Fr_{L} = 4.082 \cdot 10^{-4}$$

$$We_{L} = \frac{u_{L}^{2} \cdot \rho_{L} \cdot d_{p}}{\sigma_{L}} \qquad We_{L} = 5.144 \cdot 10^{-4}$$

$$\int_{-1.35 \cdot Re_{L}}^{0.333} \cdot Fr_{L}^{0.235} \cdot We_{L}^{-0.170} \cdot \left(\frac{a_{l} \cdot d_{p}}{\epsilon_{B}^{2}}\right)^{-0.0425}$$

$$f = 0.759$$

Therefore, the catalyst external wetting is about 76%.

J

Estimation of Binary Liquid Diffusion Coeffcients at Infinite Dilution Using the Wilke-Chang Correlation

The Wilke-Chang correlation is given by (Reid, Prausnitz and Poling, 1987, p. 598)

$$D_{AB}^{\circ} = \frac{7.4 \times 10^{-8} (\phi M_B)^{1/2} T}{\eta_B V_A^{0.6}}$$
 (J.1)

where

 D_{AB}° = diffusion coefficient of solute A at very low concentration in solvent B, cm²/s M_{B} = molecular weight of solvent B, g/mol

T = temperature, K

 η_B = viscosity of solvent B, cP

 V_A = molar volume of solvent A at its normal boiling temperature, cm³/mol

 ϕ = association factor of solvent B, dimensionless

Example: Calculate the diffusion coefficient of crotonaldehyde (A) in water (B) at 25°C.

Given: For water: $\phi = 2.6$, $\eta_B = 0.894$ cP at 25°C, $M_B = 18$ g/mol

First estimate V_A by LeBas method for estimation of specific volume at the boiling point from Table 3-8 (Reid, Prausnitz and Poling, 1987, p. 53) volume increments are C = 14.8, O = 7.4, H = 3.7

$$V_A = 4(14.8) + 7.4 + 6(3.7) = 88.8 \text{ cm}^3/\text{mol}$$

$$D_{AB}^{\circ} = \frac{7.4 \times 10^{-8} \left(2.6 \times 18 \frac{g}{\text{mol}}\right)^{1/2} (298.15 \text{K})}{\left(0.894 \text{ cP}\right) \times \left(88.8 \text{ cm}^3\right)^{0.6}}$$

$$D_{AB}^{\circ} = 1.14 \times 10^{-5} \text{ cm}^2/\text{s}$$

Example: Calculate the diffusion coefficient of hydrogen (A) in water (B) at 50°C.

Given: $D_{AB}^{\circ} = 4.8 \times 10^{-5}$ cm²/s for hydrogen in water at 298 K, for water $\eta_B = 0.894$ cP at 25°C and $\eta_B = 0.549$ cP at 50°C

Since one experimental point is given the following expression can be written

$$\frac{D_{AB,50^{\circ}C}^{\circ}}{D_{AB,298K}^{\circ}} = \frac{\frac{7.4 \times 10^{-8} (\phi M_{B})^{1/2} (273.15 + 50) K}{\eta_{B,50^{\circ}C} V_{A}^{0.6}}}{\frac{7.4 \times 10^{-8} (\phi M_{B})^{1/2} (298) K}{\eta_{B,298K} V_{A}^{0.6}}}$$

which can simplified to

$$\frac{D_{AB,50^{\circ}C}^{\circ}}{D_{AB,298K}^{\circ}} = \frac{\frac{(273.15 + 50)K}{\eta_{B,50^{\circ}C}}}{\frac{(298)K}{\eta_{B,298K}}} = \frac{323.15K}{298K} \times \frac{\eta_{B,298K}}{\eta_{B,50^{\circ}C}}$$

solving for D_{AB}° at 50°C gives $D_{AB}^{\circ} = 8.476 \times 10^{-5}$ cm²/s for hydrogen in water at 50°C.

K

Experimental Results for Trickle-bed Experiments with Light Distillate

All experiments were conducted at 25°C and 1.1 MPa. The ratio G/L is the ratio of gas volumetric flow rate to liquid volumetric flow rate.

			Cor	version of CR	CHO
Experiment #	Liquid Flow	Space time	G/L [(mL/min)/(mL/min)]		/min)]
	[mL/min]	[min]	5	10	15
5	116.2	5.589	0.576	0.558	0.558
6	233.8	2.777	0.396	0.381	0.365
7	721.6	0.900	0.153	0.154	0.147

Table K.1 Steady state results from steady operation - 30 cm bed length experiments

			Con	version of CF	NHO OHA
Experiment #	Liquid Flow	Space time	G/L [G/L [(mL/min)/(mL/min)]	
	[mL/min]	[min]	5	10	15
1	120.4	5.396	0.790		
2	228.3	2.845	0.557	0.545	0.536
3	113.3	5.734	1.000		
4	126.8	5.121	0.979	0.954	0.941

Table K.2 Steady state results from steady operation - 60 cm bed length experiments

Experiment #	Liquid Flow	Conversion of CRHO Space Time G/L [(mL/min)/(mL/min)			
Experiment #	. •	• 1	<u> </u>	(11112/111111)/(11112	
	[mL/min]	[min]	5	10	15
2	228.3	2.845	0.557	0.545	0.536
5	116.2	5.589	0.576	0.558	0.558
6	233.8	2.777	0.396	0.381	0.365
7	721.6	0.900	0.153	0.154	0.147
4	126.8	5.121	0.979	0.954	0.941

Table K.3 Steady state results from steady operation - space time comparison

APPENDIX K 179

Periodic	Liquid Flow	Space time		version of CR (mL/min)/(mL	
Operation	[mL/min]_	[min]	5	10	15
30s / 1 min	411.9	1.5767			0.179
30s / 10 min	147.1	4.4149			0.423
30s / 2 min	264.8	2.4527			0.268
30s / 3 min	215.8	3.0101			0.329
30s / 5 min	176.5	3.6790			0.355

Table K.4 Periodic operation results, effect of period length - 30 cm bed length experiments

Periodic	Liquid Flow	Space time		version of CF (mL/min)/(mL	
Operation	[mL/min]	[min]	5	10	15
1 min / 5 min	235.4	2.7593	0.156	0.183	0.267
2 min / 5 min	353.1	1.8395	0.083	0.136	0.178
3 min / 5 min	470.8	1.3796	0.073	0.098	0.151

Table K.5 Periodic operation results, effect of flush duration - 30 cm bed length experiments

Flush	Cycle	Time Average	Xqss
Duration	Period	Liquid Flow	G/L = 15
(min)	(min)	[mL/min]	
0.5	1	411.9	0.2081
0.5	2	264.8	0.2915
0.5	3	215.8	0.3445
0.5	5	176.5	0.4082
0.5	10	147.1	0.4783

Table K.6 Quasi-steady state results, effect of period length - 30 cm bed length experiments

Flush	Cycle	Liquid Flow	Space time	Con	version of CR	HO
Duration	Period	[mL/min]	[min]	G/L [((mL/min)/(mL	/min)]
(min)	(min)			5	10	15
1	5	235.4	2.759	0.343	0.344	0.321
2	5	353.1	1.840	0.256	0.257	0.233
3	5	470.8	1.380	0.212	0.213	0.189

Table K.7 Quasi-steady state results, effect of flush duration - 30 cm bed length experiments

Quasi-steady state results are calculated assuming:

Concentration crotonaldehyde in feed (steady-state): 1.8×10^{-5} mol/mL

Concentration butyraldehyde at 117.7 mL/min (steady-state):

G/L	[mol/mL]
5	1.09×10^{-5}
10	1.09×10^{-5}
15	1.05×10^{-5}

Concentration butyraldehyde at 706.1 mL/min (steady-state):

G/L	[mol/mL]	
5	3.03×10^{-6}	
10	3.05×10^{-6}	
15	2.62×10^{-6}	

Minimum liquid flow rate: 117.7 mL/min Maximum liquid flow rate: 706.1 mL/min

Experimental Results for Trickle-bed Experiments with Water

Liq Flow	Conversion	Space time	Rate
[mL/min]		[min]	[mol/min]
3.4	0.3772	176.76	4.63×10^{-6}
4.7	0.2206	128.82	3.72×10^{-6}
13.3	0.0956	45.65	4.55 × 10 ⁻⁶
23.5	0.0495	25.92	4.15×10^{-6}
42.9	0.0442	14.19	6.77×10^{-6}
76.9	0.0364	7.90	1.00×10^{-5}
106.5	0.0267	5.71	1.01×10^{-5}
108.6	0.0307	5.60	1.19×10^{-5}
135.4	0.0186	4.49	8.98×10^{-6}
205.0	0.0180	2.97	1.32×10^{-5}
207.9	0.0124	2.93	9.20×10^{-6}
245.4	0.0146	2.48	1.28×10^{-5}
371.8	0.0067	1.64	8.90 × 10 ⁻⁶
377.6	0.0068	1.61	9.20×10^{-6}
475.4	0.0050	1.28	8.48×10^{-6}

Table L.1 Steady operation data 25°C and 1.1 MPa

Liq Flow	Conversion	Space time	Rate
[mL/min]		[min]	[mol/min]
7.3	0.2681	83.0	7.01×10^{-6}
10.1	0.1914	60.3	6.89 × 10 ⁻⁶
12.2	0.1897	49.9	8.25×10^{-6}
19.3	0.0856	31.5	5.90 × 10 ⁻⁶
47.0	0.0446	12.9	7.49×10^{-6}

Table L.2 Periodic operation data 25°C, 1.1 MPa, 5 min period, 0.1 split

Liq Flow	Conversion	Space time	Rate
[mL/min]		[min]	[mol/min]
36.7	0.0686	16.5	8.99×10^{-6}
118.7	0.0198	5.1	8.39 × 10 ⁻⁶
234.8	0.0098	2.6	8.25×10^{-6}

Table L.3 Periodic operation data 25°C, 1.1 MPa, 5 min period, 0.5 split

Liq Flow	Conversion	Space time	Rate
[mL/min]		[min]	[mol/min]
5.02	0.3812	121.13	6.83×10^{-6}
7.46	0.1996	81.54	5.31 × 10 ⁻⁶
12.07	0.1571	50.39	6.77×10^{-6}
23.17	0.0634	26.25	5.24×10^{-6}
47.27	0.0371	12.86	6.26×10^{-6}
47.78	0.0391	12.73	6.67 × 10 ⁻⁶

Table L.4 Periodic operation data 25°C, 1.1 MPa, 20 min period, 0.1 split

Liq Flow	Conversion	Space time	Rate
[mL/min]		[min]	[mol/min]
34.67	0.0571	17.54	7.07×10^{-6}
60.73	0.0382	10.01	8.29 × 10 ⁻⁶
111.21	0.0227	5.47	9.03 × 10 ⁻⁶
122.75	0.0171	4.95	7.48×10^{-6}
123.07	0.0191	4.94	8.41 × 10 ⁻⁶
183.50	0.0089	3.31	5.82 × 10 ⁻⁶
211.67	0.0090	2.87	6.81 × 10 ⁻⁶
131.00	0.0295	4.64	1.38×10^{-5}
178.50	0.0553	3.41	3.52×10^{-5}

Table L.5 Periodic operation data 25°C, 1.1 MPa, 20 min period, 0.5 split

Liq Flow	Conversion	Space time	Rate
[mL/min]		[min]	[mol/min]
5.1	0.917	118.5	1.68×10^{-5}
14.8	0.925	41.1	4.89×10^{-5}
29.2	0.789	20.8	8.22×10^{-5}
61.3	0.734	9.9	1.61 × 10 ⁻⁴
112.7	0.613	5.4	2.47×10^{-4}
195.2	0.447	3.1	3.11 × 10 ⁻⁴
195.4	0.302	3.1	2.11 × 10 ⁻⁴
220.7	0.517	2.8	4.07 × 10 ⁻⁴
447.3	0.220	1.4	3.52×10^{-4}

Table L.6 Steady operation data 50°C and 1.1 MPa

Liq Flow	Conversion	Space time	Rate
[mL/min]		[min]	[mol/min]
3.2	0.891	191.4	1.01×10^{-5}
7.6	0.794	80.5	2.14×10^{-5}
11.8	0.686	51.5	2.89×10^{-5}
18.3	0.587	33.2	3.84×10^{-5}
45.0	0.417	13.5	6.70×10^{-5}

Table L.7 Periodic operation data 50°C, 1.1 MPa, 5 min period, 0.1 split

Liq Flow	Conversion	Space time	Rate
[mL/min]		[min]	[mol/min]
6.5	0.886	93.5	2.06×10^{-5}
20.0	0.742	30.4	5.30×10^{-5}
58.5	0.504	10.4	1.05 × 10 ⁻⁴
64.2	0.458	9.5	1.05 × 10 ⁻⁴
103.6	0.370	5.9	1.37 × 10 ⁻⁴
195.3	0.267	3.1	1.86 × 10 ⁻⁴
231.2	0.242	2.6	1.99 × 10 ⁻⁴

Table L.8 Periodic peration data 50°C, 1.1 MPa, 5 min period, 0.5 split

Liq Flow	Conversion	Space time	Rate
[mL/min]		[min]	[mol/min]
3.5	0.729	175.8	9.00×10^{-6}
12.0	0.490	50.7	2.10×10^{-5}
19.7	0.414	30.9	2.91×10^{-5}
46.8	0.279	13.0	4.66 × 10 ⁻⁵

Table L.9 Periodic operation data 50°C, 1.1 MPa, 20 min period, 0.1 split

Liq Flow	Conversion	Space time	Rate
[mL/min]		[min]	[mol/min]
6.6	0.825	92.7	1.93 × 10 ⁻⁵
20.6	0.665	29.5	4.89 × 10 ⁻⁵
56.5	0.450	10.8	9.27 × 10 ⁻⁵
100.9	0.333	6.0	1.20 × 10 ⁻⁴
199.6	0.226	3.0	1.61 × 10 ⁻⁴
234.7	0.241	2.6	2.02 × 10⁴

Table L.10 Periodic operation data 50°C, 1.1 MPa, 20 min period, 0.5 split

Liq Flow	Conversion	Space time	Rate
[mL/min]		[min]	[mol/min]
2.7	0.929	223.5	9.02×10^{-6}
7.5	0.757	81.1	2.03×10^{-5}
18.6	0.350	32.7	2.32×10^{-5}
59.0	0.228	10.3	4.80×10^{-5}
79.6	0.218	7.6	6.21×10^{-5}
137.3	0.134	4.4	6.56×10^{-5}
148.7	0.120	4.1	6.38×10^{-5}
495.0	0.056	1.2	9.81×10^{-5}

Table L.11 Steady operation data 50°C and 0.1 MPa

Liq Flow	Conversion	Space time	Rate
[mL/min]		[min]	[mol/min]
22.2	0.275	27.4	2.17×10^{-5}
14.8	0.468	41.0	2.48×10^{-5}
10.7	0.581	57.0	2.21×10^{-5}
48.6	0.263	12.5	4.57 × 10 ⁻⁵
1.5	0.932	396.8	5.10×10^{-6}

Table L.12 Periodic operation data 50°C, 0.1 MPa, 5 min period, 0.1 split

Liq Flow	Conversion	Space time	Rate
[mL/min]		[min]	[mol/min]
242.5	0.080	2.5	6.88×10^{-5}
30.2	0.459	20.2	4.94×10^{-5}
74.4	0.236	8.2	6.26×10^{-5}
103.3	0.164	5.9	6.07×10^{-5}
26.6	0.477	22.8	4.53 × 10 ⁻⁵

Table L-13 Periodic operation data 50°C, 0.1 MPa, 5 min period, 0.5 split

Liq Flow	Conversion	Space time	Rate
[mL/min]		[min]	[mol/min]
23.1	0.212	26.3	1.75×10^{-5}
9.3	0.478	65.5	1.58×10^{-5}
50.4	0.152	12.1	2.73×10^{-5}
15.4	0.388	39.5	2.13×10^{-5}
5.3	0.595	115.8	1.12×10^{-5}

Table L.14 Periodic operation data 50°C, 0.1 MPa, 20 min period, 0.1 split

Liq Flow	Conversion	Space time	Rate
[mL/min]		[min]	[mol/min]
253.5	0.055	2.4	4.95×10^{-5}
18.9	0.484	32.1	3.27×10^{-5}
120.9	0.135	5.0	5.83×10^{-5}
50.0	0.198	12.2	3.54×10^{-5}
43.0	0.217	14.1	3.33×10^{-5}

Table L.15 Periodic operation data 50°C, 0.1 MPa, 20 min period, 0.5 split

M

Sample Gas Chromatograph Analysis Data and Calculations

For the system being studied the organic compounds of interest are listed in Table M.1.

Common Name	IUPAC Name	Formula	Normal Boiling Point [°C]
butyraldehyde	1-butanal	CH ₃ CH ₂ CH ₂ CHO	75.7
crotonaldehyde	2-butenal	CH ₃ CH=CHCHO	104.5
n-butanol	1-butanol	CH ₃ CH ₂ CH ₂ CHOH	117.3
crotyl alcohol	2-buten-1-ol	CH₃CH=CHCHOH	121.2

Table B.1 Organic Compounds of Interest in the TBR system

During the experiments, samples are collected in bottles for later analysis. To each sample a internal standard is added. A 1 μ L sample is then manually injected into an Hewlett-Packard 5890 Series II Gas Chromatograph (GC) for analysis. The operating conditions of the GC are given in Table B.2.

Operating Parameter	Value/Condition
Injector Temperature	250 °C
Column Head Pressure	140 kPa
Column	DB Wax 30 m × 0.53 mm ID
	Megabore
Oven Conditions and	35 °C, 4 min; 10°C/min to 80°C;
Temperature Program	80°C, 15°C/min to 120 min;
	120°C, 3 min;
	total time 14.2 min
Detector	Flame Ionization (FID)
Detector Temperature	250 °C
Carrier Gas	Helium (Linde Ultra High Purity)
FID Makeup Gas	Helium (Linde Ultra High Purity)

Table M.2 GC Operating Parameters

The signal from the GC is sent to an HP 35900D data acquisition card installed in a IBM compatible PC. The signal data is collected, processed and integrated by the HP Chemstation software running under Microsoft Windows 3.1. Computer hardware and software specifications are listed in Table B.3.

Hardware/Software Component	Specification
Computer	IBM compatible PC
Processor (CPU)	Intel 80386-25
Coprocessor (FPU)	Intel 80387-25
Random Access Memory (RAM)	4 MB
Hard Disk	Western Digital 40 MB (formatted)
Operating System	MS-DOS 6.2 and Windows 3.1

Table M.3 Computer Hardware and Software Specifications

Tabular summary data for a sample chromatogram are given in Table B.4. A sample chromatogram is given in Figure B.1. All components exit the column after about 4½ minutes. A period of about 1½ to 2 minutes is allowed to elapse before injection of the next sample.

Calibration curves were obtained by preparation of several aqueous solutions of each component and an internal standard (acetone). All solutions were prepared on a weight basis. From the calibration curves, response factors for each chemical species were determined and are listed in Table M.4.

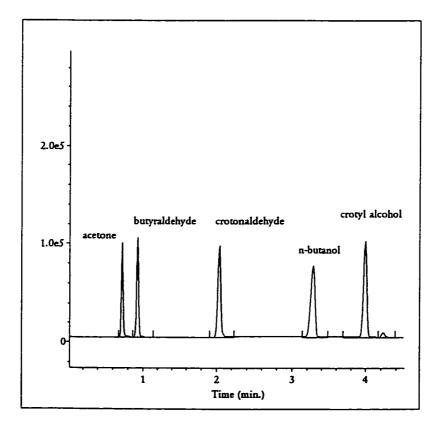


Figure M.1 Sample Gas Chromatograph

APPENDIX M 189

Chemical species	Response factor
butyraldehyde	0.727
crotonaldehyde	0.642
n-butanol	0.548

Table M.4 Response factors for chemical species.

The concentration of each component in a reactor sample was determined by injection of a fixed volume of the internal standard acetone into a fixed volume of sample. The concentration of each species was calculated as

$$C_i = R_i C_{aetone} \frac{A_i}{A_{acetone}} \tag{M.2}$$

where C_i is the concentration of species i, $C_{acetone}$ is the concentration of acetone in the sample, R_i is the response factor for species i, A_i is the peak area of species i, and $A_{acetone}$ is the peak area for the internal standard, acetone.

The conversion was calculated as

$$X_{CRHO} = 1 - x_{CRHO} \tag{M.1}$$

where X_{CRHO} is the conversion of crotonaldehyde and x_{CRHO} is the mole fraction of crotonaldehyde in the sample.

N

Reaction Thermodynamics

The free energy of combustion for crotonaldehyde and butyraldehyde at 25°C are listed in Table N.1.

Compound	Free Energy of Combustion -ΔG _c ° (kcal/mol)
crotonaldehyde (l)	546.12 ± 0.09†
butyraldehyde (l)	591.53 ± 0.17 [†]
carbon dioxide (g)	94.26 [‡]
water (g)	54.6351‡

[†] Tjebbes (1967) ‡ Perry and Green (1984)

Table N.1 Free Energies of Combustion

The free energies of formation can be calculated noting that

$$CH3CH = CHCHO + 5O2 \rightarrow 3H2O + 4CO2$$
 (N.1)

$$CH_3(CH_2)_2CHO + \frac{11}{2}O_2 \rightarrow 4H_2O + 4CO_2$$
 (N.2)

The free energies of formation for crotonaldehyde and butyraldehyde are then 5.17 kcal/mol and -4.05 kcal/mol respectively. Therefore the overall free energy of crotonaldehyde hydrogenation to butyraldehyde is -9.22 kcal/mol.



Simulation code listings

The file listing below is a sample of the gPROMS code used for steady operation simulations.

```
# Trickle Bed Reactor Steady Operation Simulation
# gPROMS code executed with gPROMS 1.4C for DOS
# David Stradiotto
# April 1, 1997
declare
          DimConcentration = 0.0 : 0.0 : 1000.0 unit = "gmol/gmol"
DimTemperature = 0.0 : -1000.0 : 1000.0 unit = "K/K"
NOType = 0.0 : 0.0 : 1.0
end
model TBR # start model TBR
parameter
                                            real
                                                                                    reaction rate constant
                                                                                    liquid-solid mass transfer external catalyst wetting
     ksas
                                   as
                                            real
                                            real
                                                                                    bed porosity
catalyst bulk density
liquid superficial
     bed_porosity
                                   as
                                            rea?
     density_catalyst as
                                                               [kg/m3]
                                            real
     u_liq
                                                               [m/s]
                                                                                    velocity
diffusivity in liquid
                                            real
                                                               [m/s]
    mu_Liq
mu_Liq_SI
                                                               [P]
[kg/(m s)]
                                                                                    liquid viscosity
liquid viscosity
                                            real
                                            real
                                                                                   parameter for ksas
parameter for ksas
liquid density
liquid mass flux
liquid phase Re number
liquid phase Fr number
liquid phase We number
     alpha_s
                                  as
                                            real
                                                           ####
                                                               [kg/m3]
[kg/(m2 s)]
     rho_Liq
                                            real
    G_Liq
Re_Liq
Fr_Liq
We_liq
                                  as
                                            real
                                  as
                                            real
                                                              []
[]
[m]
[1/m]
[N/m]
[m/s2]
[m]
[m]
                                  as
                                            real
                                  as
                                            rea?
     d_particle
                                  as
                                            real
                                                                                    particle diameter
                                                                                    area per volume catalyst
liquid surface tension
                                  as
                                            real
     sigma_Liq
                                  as
                                            real
    g
ZLower
                                  as
                                            real
                                                                                    gravitational constant
                                  as
                                            real
                                                                                    top of bed
     zupper
                                  as
                                            real
                                                                                   bottom of bed
     ZPoints
                                  as
                                            integer
                                                                                   z axis grid points
distribution_domain
                             (ZLower: ZUpper)
     axial
variable
                             distribution(axial) of DimConcentration distribution(axial) of DimConcentration
    C_Liq
C_Sol
boundary
# C_Liq(ZLower|)=1.0;
  C_Sol(ZLower|)=0.0;
partial(C_Sol(ZUpper|),axial)=0.0;
    C_Liq(ZLowerl) = 3.57;
```

```
# C_Liq(ZLower|) - C_Sol(Zlower|) = 0.0;
equation
  Mass Balance for Liquid Phase
    for z:=ZLower|+ to ZUpper| do
  $C_Liq(z) = -u_Liq * partial(C_Liq(z),axial)
  - ksas * (C_Liq(z) - C_Sol(z));
  Mass Balance for Solid Phase
    for z:=ZLower| to ZUpper| do
    $C_Sol(z) = -k * f * C_Sol(z)
    + ksas * (C_Liq(z) - C_Sol(z));
end # model TBR
process Simulation # start process Simulation
   unit MyTBR as TBR
        within MyTBR do
# domain boundary limits and grid definition
            ZLower := 0.0;
ZUpper := 0.3;
                                                            # grid points along z axis
            ZPoints := 30:
# other parameters for simulation
            bed_porosity := 0.37;
density_catalyst := 1.0943e3;
 parameters which must be set for the appropriate temperature
1) set the rate constant k
2) set the diffusivity of crotonaldehyde in water
 3) set the properties of water (use comments to select)
  reaction rate constant assuming first order rate law with respect to liquid phase reactant
   at 25°C k = 9.751e-5 [1/s] at 50°C k = 4.772e-3 [1/s]
            k := 9.751e-5;
                                                                # [1/s]
        liquid superficial velocity
   - the 1st number is the liquid flow rate in mL/min

    the 2nd is the catalyst bed cross-sectional area in cm2
    the 3rd is the conversion from cm/min to m/min
    the 4th is the conversion from m/min to m/s

            u_{Liq} := 3.4/21.65/100.0/60.0; # [m/s]
```

```
# diffusivity of crotonaldehyde in water
# at 25°C D_Liq = 1.14e-9 [m2/s]
# at 50°C D_Liq = 2.02e-9 [m2/s]
                            := 1.14e-9;
                                                      # [m2/s]
# properties of water at 25°C
          sigma_Liq := 0.0726;
rho_Liq := 997.1;
mu_Liq := 0.00894;
mu_Liq_SI := 0.000894;
                                                      # [N/m]
# [kg/m3]
# [P = g/(cm s)]
# [kg/(m s)]
  properties of water at 50°C
                                                      # [N/m]
# [kg/m3]
# [P = g/(cm s)]
# [kg/(m s)]
          sigma_Liq := 0.0682;
rho_Liq := 988.1;
mu_Liq := 0.00549;
mu_Liq_SI := 0.000549;
# constants for liquid-solid mass transfer coefficient
# Goto and Smith correlation
          alpha_S := 45.0;
n_S := 0.56;
# other parameters
                            G_Liq
          d_particle
# Dimensionless Numbers: Re, Fr, We
          Re_Liq := (u_Liq * d_particle * rho_liq) / mu_Liq_SI;
          Fr_Liq := u_Liq^2.0 / (g * d_particle);
          We_Liq := (u_Liq^2.0 * rho_Liq * d_particle) / sigma_Liq;
" Liquid-Solid Mass Transfer Coefficient # Goto and Smith (1975)
          # Catalyst External Wetting Factor
# Mills (1981)
# to simulate incomplete wetting comment
# the line f: = 0.0
          f := 0.2+(1.0 - exp(-1.35 * Re_Liq^0.333
    * Fr_Liq^0.235 * We_Liq^(-0.170)
    * (a_t * d_particle / bed_porosity^2.0)^(-0.0425)));
# complete wetting
```

APPENDIX O 194

```
# to simulate complete wetting comment
# the Mills correlation
        f := 1.0:
 axial discretization technique
        axial := [UFDM, 2, ZPoints];
     end
  initial
           steady_state
     within MyTBR do
        for z:=ZLower|+ to ZUpper| do 
C_Liq(z)=3.57;
        end
     end
  solutionparameters
     gplot := ON;
  schedule
     continue for 25000 # note that time is in seconds
end
```

The file listing below is a sample of the gPROMS code used for periodic operation simulations. Note that simulations up to 120 periods were done but only 4 periods are shown in this listing.

APPENDIX O

```
density_catalyst as
                                                         [kg/m3]
[m/s]
                                                                             catalyst bulk density
                                        real
     u_liq
                                         real
                                                                             liquid superficial
                                as
                                                                             velocity
diffusivity in liquid
                                                      #
                                                         [m/s]
[P]
[kg/(m s)]
     D_Liq
                                                      #
                                        real
                                                                             liquid viscosity
liquid viscosity
parameter for ksas
parameter for ksas
     mu_Liq
mu_Liq_SI
                                as
                                        real
                                                      #
                                as
                                        real
                                                      ***
     alpha_s
                                as
                                        real
                                as
                                        real
                                                                            parameter for ksas
liquid density
liquid mass flux
liquid phase Re number
liquid phase Fr number
liquid phase We number
particle diameter
area per volume catalyst
liquid surface tension
gravitational constant
ton of hed
    rho_Liq
G_Liq
Re_Liq
Fr_Liq
We_liq
                                                         [kg/m3]
[kg/(m2 s)]
                                as
                                        real
                                as
                                        real
                                as
                                        real
                                                         [m]
[1/m]
[N/m]
[m/s2]
[m]
                                                      #
                                as
                                        real
                                                      #
                                as
                                        real
     d_particle
                                        real
                               as
                                                      #
     a_t
                                as
                                        real
     sigma_Liq
                               as
                                        real
                                                      #
                                as
                                        rea]
     g
ZLower
                                                                            top of bed
bottom of bed
z axis grid points
                                        real
                               as
     ZUpper
                                as
                                        real
     ZPoints
                               as
                                        integer
#
   periodic operation model parameters
    holdup_LSE
                                        real
                                                         []
                                                                             external static liquid
                                                                             holdup
    V_reactor
                                        real
                                                                             reactor volume
    V_LSE
                                        real
                                                         [m3]
                                                                             external static liquid
                               as
                                                                             holdup volume
    A_cat_E
                               as
                                        real
                                                         [m2]
                                                                             catalyst external surface
                                                                             area
     film_thickness
                                                                            liquid film thickness
diffusion mass transfer
                               as
                                        real
     ksas_film
                                        real
                                                                             coefficient
   periodic operation simulation parameters
                                                                            period length fraction of period with
    period
                                        real
    split
                                        real
                               as
                                                                             liquid flow
                                                        [m/s]
[s]
                                                                            liquid pulse velocity duration of liquid flow
       _Liq_Amp
                               as
                                        real
    flush_time
                                        real
    dry_time
                               as
                                        real
                                                        [s]
                                                                            duration without liquid
distribution_domain
    axial
                      as
                               (ZLower: ZUpper)
variable
                               distribution(axial) of DimConcentration distribution(axial) of DimConcentration
    C_Liq
                      as
                      as
    ksas_eff
                      as
                               NoType
                                                          # [1/s]
# [m/s]
    u_Liq_Flow as
                               NoType
boundary
# C_Liq(ZLower|)=1.0;
   C_Sol(ZLower|)=0.0;
partial(C_Sol(ZUpper|),axial)=0.0;
    C_Liq(ZLower|) = 3.57;
# C_Liq(ZLower|) - C_Sol(Zlower|) = 0.0;
#==
equation
# Determination of ksas_eff
    if (u_Liq_Flow = 0.0) then
  ksas_eff = ksas_film;
    else
        ksas_eff = ksas:
```

```
end
   Mass Balance for Liquid Phase
     for z:=ZLower|+ to ZUpper| do
    $C_Liq(z) = -u_Liq_Flow * partial(C_Liq(z),axial)
    - ksas_eff * (C_Liq(z) - C_Sol(z));
     end
   Mass Balance for Solid Phase
     for z:=ZLower| to ZUpper| do
    $C_Sol(z) = -k * f * C_Sol(z)
    + ksas_eff * (C_Liq(z) - C_Sol(z));
end # model TBR
process Simulation # start process Simulation
     unit MyTBR as TBR
    monitor
         MyTBR.C_LIQ(31);
         within MyTBR do
   domain boundary limits and grid definition
              ZLower := 0.0;
ZUpper := 0.3;
                                                                   # [m]
# [m]
             ZPoints := 30;
                                                                   # grid points along z axis
# other parameters for simulation
             # parameters which must be set for the appropriate temperature
# 1) set the rate constant k
# 2) set the diffusivity of crotonaldehyde in water
# 3) set the properties of water (use comments to select)
# 3
    reaction rate constant assuming first order rate law with respect to liquid phase reactant
    at 25°C k = 9.751e-5 [1/s]
at 50°C k = 4.772e-3 [1/s]
             k := 4.772e-3;
                                                                       # [1/s]
         liquid superficial velocity

    the 1st number is the liquid flow rate in mL/min
    the 2nd is the catalyst bed cross-sectional area in cm2
    the 3rd is the conversion from cm/min to m/min
    the 4th is the conversion from m/min to m/s

    for periodic operation, this is the time average liquid
   flowrate
```

```
u_{Liq} := 6.6/21.65/100.0/60.0;
                                                      # [m/s]
# diffusivity of crotonaldehyde in water
# at 25°C D_Liq = 1.14e-9 [m2/s]
# at 50°C D_Liq = 2.02e-9 [m2/s]
          D_Liq
                          := 2.02e-9;
                                                # [m2/s]
  properties of water at 25°C
          sigma_Liq := 0.0726;
rho_Liq := 997.1;
mu_Liq := 0.00894;
mu_Liq_SI := 0.000894;
                                                      # [N/m]
# [kg/m3]
# [P = g/(cm s)]
# [kg/(m s)]
# properties of water at 50°C
                                                      # [N/m]
# [kg/m3]
# [P = g/(cm s)]
# [kg/(m s)]
                            := 0.0682;
           sigma_Liq
           rho_Liq := 988.1;
mu_Liq := 0.00549;
                           := 0.000549;
           mu_Liq_SI
# constants for liquid-solid mass transfer coefficient
# Goto and Smith correlation
           alpha_S
                             := 45.0;
                      := 0.56;
# other parameters
                                                                            # [kg/(m2 s)]
# [m]
# [m/s2]
# [1/m]
                             := u_Liq_Amp * rho_Liq;
:= 0.00406;
          G_Liq
           d_particle
                             := 9.8;
:= 6.0*(1 - bed_porosity)/d_particle;
           ă_t
# periodic operation model parameters
          # periodic operation simulation parameters
          period
                            := 20.0 * 60.0;
                          := 0.5;
:= u_Liq / split;
:= split * period;
:= (1.0 - split) * period;
          split
u_Liq_Amp
flush_time
          dry_time
# Dimensionless Numbers: Re, Fr, We
          Re_Liq := (u_Liq_Amp * d_particle * rho_liq) / mu_Liq_SI;
          Fr_Liq := u_Liq_Amp^2.0 / (g * d_particle);
          We_Liq := (u_Liq_Amp^2.0 * rho_Liq * d_particle) / sigma_Liq;
# Liquid-Solid Mass Transfer Coefficient
# Goto and Smith (1975)
```

```
# Catalyst External Wetting Factor # Mills (1981)
# to simulate incomplete wetting comment
# the line f: = 0.0
         # complete wetting
# to simulate complete wetting comment
# the Mills correlation
         f := 1.0;
# axial discretization technique
         axial := [UFDM, 2, ZPoints];
# initialize liquid velocity
   assign
within MyTBR do
        u_Liq_Flow := u_Liq_Amp;
# initialize bed to uniform crotonaldehyde concentration
  initial
           steady_state
      within MyTBR do
         for z:=ZLower|+ to ZUpper| do
_C_Liq(z)=3.57;
         for z:=ZLower| to ZUpper| do
    C_Sol(z)=3.57;
         end
# set solution and data output parameters
  solutionparameters
     gplot := ON;
  schedule
     continue for 25000
# note that time is in seconds
      sequence
        continue for MyTBR.flush_time
reset MyTBR.u_Liq_Flow := 0.0e0; end
            reset MyTBR.u_Liq_Flow := 0.0e0; end
```

end

```
continue for MyTBR.dry_time
    reset MyTBR.u_Liq_Flow := MyTBR.u_Liq_Amp; end  # 1 period
continue for MyTBR.flush_time
    reset MyTBR.u_Liq_Flow := 0.0e0; end
continue for MyTBR.dry_time
    reset MyTBR.u_Liq_Flow := MyTBR.u_Liq_Amp; end
continue for MyTBR.flush_time
    reset MyTBR.u_Liq_Flow := 0.0e0; end
continue for MyTBR.dry_time
    reset MyTBR.u_Liq_Flow := MyTBR.u_Liq_Amp; end
continue for MyTBR.flush_time
    reset MyTBR.u_Liq_Flow := 0.0e0; end
continue for MyTBR.flush_time
    reset MyTBR.u_Liq_Flow := 0.0e0; end
continue for MyTBR.dry_time
end
```

Liquid Holdup Data

Liquid	Wet bed mass [g]				
flow rate		Gas flow rate [mL/min]			
[mL/min]	0.0	29.5	129.6	230.1	1567.0
35.5		2533.0	2535.0		
37.0					2534.0
72.0	2533.0				2532.0
73.0		2534.0		2534.0	
74.0			2534.5		2531.0
146.0	2535.5				
222.5	2534.0	2533.5		2535.5	2533.0
335.0	2534.5	2535.0	2535.0		2534.0
480.0	2535.5		2534.5		2531.5
482.5				2536.5	
482.5				2533.5	
520.0		2534.0	2533.0		2535.0

Table P.1 Wet bed mass measurements

Liquid	Liquid Mass [g]				
flow rate		Gas flow rate [mL/min]			
[mL/min]	0.0	29.5	129.6	230.1	1567.0
35.5		291.0	293.0		
37.0					292.0
72.0	291.0				290.0
73.0		292.0		292.0	
74.0			292.5		289.0
146.0	293.5				
222.5	292.0	291.5		293.5	291.0
335.0	292.5	293.0	293.0		292.0
480.0	293.5		292.5	i.	289.5
482.5				294.5	
482.5				291.5	
520.0	_ ,	292.0	291.0		293.0

Table P.2 Total static liquid holdup mass

Liquid	Total static liquid holdup					
flow rate		Gas flow rate [mL/min]				
[mL/min]	0.0	29.5	129.6	230.1	1567.0	
35.5		0.460	0.463			
37.0		ļ			0.462	
72.0	0.460				0.459	
73.0		0.462		0.462		
74.0			0.463		0.457	
146.0	0.464					
222.5	0.462	0.461		0.464	0.460	
335.0	0.463	0.463	0.463		0.462	
480.0	0.464		0.463		0.458	
482.5				0.466		
482.5				0.461		
520.0		0.462	0.460		0.463	
average	0.463	0.462	0.463	0.463	0.460	

Table P.3 Total static liquid holdup

Gas Flow [mL/min]	Total static liquid holdup	Total static liquid holdup	External static liquid holdup
	[mL]		•
0.0	292.5	0.463	0.032
29.5	291.9	0.462	0.031
129.6	292.4	0.463	0.032
230.1	292.9	0.463	0.033
1567.0	290.9	0.460	0.030
average	292.1	0.462	0.032

Table P.4 Data summary

Notes:

Catalyst bed length dry: 29.7 cm Catalyst bed length wet: 29.2 cm

Column mass: 1825 g Catalyst mass: 417 g Bed volume: 632.15 cm³ Internal static holdup: 0.4304

APPENDIX

Q

Statistical Analyses for First Order Plug Flow Models for Steady and Periodic Operation

Regression Significance

The significance of regression on a statistical basis can be tested by means of an F-test on the mean square due to regression and the mean square due to residual variation (Draper and Smith, 1981, pp. 31-33), where

$$F = \frac{MS_{reg}}{s^2} \tag{Q.1}$$

If the value of F calculated above is greater than F(1, n-2) then the variation about the mean is due mostly as a result of regression and not random variation (i.e. the regression is significant).

Example: Steady operation regression for 0 to 450 L/min data.

From the regression calculations F = 1823.74. From F tables F(1, 13, 0.95) = 4.67.

Since F = 1823.74 > F(1, 3, 0.95) = 4.67, the regression is significant.

A similar comparison was made for steady and periodic operation data given below in Table Q.1.

Trickle-bed Operation	Apparent k [s ⁻¹]	Regression F	F Distribution from Table Significance of Regress	
Steady, 0 to 50 mL/min	0.00249	62.14	F(1, 3, 0.95) = 10.13	yes
Steady, 50 to 450 mL/min	0.00487	148.47	F(1, 8, 0.95) = 5.32	yes
Periodic (split, period)				
0.1, 5 min	0.00391	95.14	F(1, 3, 0.95) = 5.32	yes
0.5, 5 min	0.00440	3684.80	F(1, 1, 0.95) = 161.4	yes
0.1, 20 min	0.00383	85.78	F(1, 4, 0.95) = 7.71	yes
0.5, 20 min	0.00342	201.82	F(1, 5, 0.95) = 6.61	yes

Table Q.1 Regression Statistics for Plug Flow Models of Steady and Periodic Operation Data

From Table Q.1 the regression of each set of data is statistically significant.

APPENDIX Q 203

Testing Pairs of Apparent Rate Constants

Slopes (apparent rate constants) estimated from the regression analyses can be treated as random variables. For a given set of data, the regression analysis provides an estimated value of the slope and a standard deviation (or standard error) representing the error associated with the estimate. As Draper and Smith (1981, pp. 24 - 27) suggest, a t-test may be performed to determine if the slope is significantly different (in the statistical sense) from a certain value. The test of two slopes with each other is comparable to testing two means, with each mean having an associated standard deviation. Such an analysis is given by Perry et al. (1984, p. 2-86). The t-statistic is calculated by

$$t = \frac{\overline{x}_2 - \overline{x}_1}{\sqrt{\frac{s_1^2}{n_1} + \frac{s_2^2}{n_2}}}$$
 (Q.2)

where the degrees of freedom (d.f.) are

$$d.f. = \frac{\left[\frac{s_1^2}{n_1} + \frac{s_2^2}{n_2}\right]^2}{\left(\frac{s_1^2}{n_1}\right)^2 + \left(\frac{s_2^2}{n_2}\right)^2}$$

$$\frac{\left(\frac{s_1^2}{n_1}\right)^2 + \left(\frac{s_2^2}{n_2}\right)^2}{n_2 - 1}$$
(Q.3)

Example: Compare regression statistics for 0.1 split and 5 minute period experimental data at 25°C and 1.1 MPa, with data for steady operation at 25°C and 1.1 MPa and 0 to 50 mL/min liquid flow rate.

Given: $1 \equiv$ steady operation, $2 \equiv$ periodic operation

$$n_1 = 5$$
 $\bar{x}_1 = 0.002499285$ $s_1 = 0.000317057$
 $n_2 = 5$ $\bar{x}_2 = 0.003913802$ $s_2 = 0.000401254$

t = 6.184

$$\frac{s_1^2}{n_1} = 2.01051\text{E}-08$$
 $\frac{s_2^2}{n_2} = 3.22009\text{E}-08$ $d.f. = 7.594 = 7$

t(7,0.975) = 2.365 (2 sided, 95% confidence level)

Since t = 6.184 > t(7, 0.975) = 2.365, the two slopes can be said to significantly different at the 95% confidence level.

APPENDIX Q 204

Table Q.2 lists regression statistics, while Table Q.3 summarizes the results of the above analysis for the other periodic operation results.

Data Set	Apparent	Standard	Sample	R ²
	k [s ⁻¹]	Error	Size	
Steady, 0 to 50 mL/min	0.00249	3.17×10^{-4}	5	0.954
Periodic, 0.1, 5 min	0.00391	4.01×10^{-4}	5	0.969
Periodic, 0.1, 20 min	0.00383	4.14×10^{-4}	6	0.955
Steady, 50 to 450 mL/min	0.00487	4.00×10^{-4}	10	0.949
Periodic, 0.5, 5 min	0.00440	7.26×10^{-5}	3	0.999
Periodic, 0.5, 20 min	0.00342	2.41×10^{-4}	7	0.976

Table Q.2 Regression Statistics

Periodic	Steady Operation, 0 to 50 mL/min		Steady Operation, 50 to 450 mL/min		Statistically Significant
Operation	t-statistic eq. (Q.2)	t-statistic*	t statistic eq. (Q.2)	t-statistic*	Difference
0.1, 5 min	6.184	2.365			yes
0.1, 20 min	6.045	2.306			yes
0.5, 5 min			3.554	2.228	yes
0.5, 20 min			7.208	2.179	yes

^{*} two sided t-statistic at the 95% confidence level

Table Q.3 Statistical Difference Tests

Classification of Trickle-bed Reactor System and Periodic Operation

In Chapter 2, Table 2.6 showed criteria, used to determine if periodic operation can improve performance compared to steady operation.

System $\dot{y} = \frac{dy}{dt} = f(y, u)$	Linear Control $\frac{\partial f}{\partial u} = B$	Nonlinear Control $\frac{\partial f}{\partial u} = B(y, u)$
Linear System $\frac{\partial \mathbf{f}}{\partial \mathbf{y}} = \mathbf{A}(\mathbf{u})$	$\Delta = 0$ no improvement possible	Δ≠0 improvement possible
Nonlinear System $\frac{\partial f}{\partial y} = A(y, \mathbf{u})$	Δ≠0 improvement possible	Δ ≠ 0 improvement possible

Table 2.6 Classification of periodic operation control problems

To classify the trickle-bed system, steady operation model A is used since it produced reasonable results when compared to experimental data. The differential equations for model A are given below without initial or boundary conditions.

$$\frac{\partial C_L}{\partial t} = -u_L \frac{\partial C_L}{\partial z} - k_s a_s (C_L - C_s) = f_1 \tag{7.1}$$

$$\frac{dC_s}{dt} = -kfC_s + k_s a_s (C_L - C_s) = f_2$$
 (7.3)

APPENDIX R 206

The state variables are C_L and C_s and the controlled variable is u_L . The state variables C_L and C_s are functions of z, axial position, and t time. The parameters f and $k_s a_s$ are typically nonlinear functions of u_L given below (these were defined more precisely by equations (2.26) and (2.21) respectively).

$$f \approx f\left(u_L^{1/3}\right) \tag{R.1}$$

$$k_s a_s \approx k_s a_s \left(u_L^{1/2} \right) \tag{R.2}$$

From Table 2.6, periodic operation cannot result in an improvement if the system is linear and the control scheme is also linear. The system of differential equations f, is differentiated with respect to each state variable and the controlled variable, and these partial derivatives are then compared with Table 2.6 for classification of the type of system and control.

Differentiation of equation (7.1) with respect to u_L gives

$$\frac{\partial f_1}{\partial u_L} = \frac{\partial}{\partial u_L} \left(u_L \frac{\partial C_L}{\partial z} - k_s a_s \left(C_L - C_s \right) \right)$$

$$\frac{\partial f_1}{\partial u_L} = u_L \frac{\partial}{\partial u_L} \left(\frac{\partial C_L}{\partial z} \right) + \frac{\partial C_L}{\partial z} - k_s a_s \frac{\partial}{\partial u_L} \left(C_L - C_s \right) - \left(C_L - C_s \right) \frac{\partial k_s a_s}{\partial u_L}$$

$$\frac{\partial f_1}{\partial u_L} = -\left(C - C_s \right) \frac{\partial k_s a_s}{\partial u_L} + \frac{\partial C_L}{\partial z} = B(C_L, C_s, u_L)$$
(R.3)

Differentiation of equation (7.1) with respect to C_L gives

$$\frac{\partial f_1}{\partial C_L} = \frac{\partial}{\partial C_L} \left(u_L \frac{\partial C_L}{\partial z} - k_s a_s (C_L - C_s) \right)$$

$$\frac{\partial f_1}{\partial C_L} = u_L \frac{\partial}{\partial C_L} \left(\frac{\partial C_L}{\partial z} \right) + \frac{\partial u_L}{\partial C_L} \frac{\partial C}{\partial z} - k_s a_s \frac{\partial}{\partial C_L} (C_L - C_s) - (C_L - C_s) \frac{\partial k_s a_s}{\partial C}$$

$$\frac{\partial f_1}{\partial C_L} = u_L \frac{\partial}{\partial C_L} \left(\frac{\partial C_L}{\partial z} \right) - k_s a_s = A(C_L, u_L)$$
(R.4)

Differentiation of equation (7.1) with respect to C_s gives

APPENDIX R 207

$$\frac{\partial f_1}{\partial C_s} = \frac{\partial}{\partial C_s} \left(u_L \frac{\partial C_L}{\partial z} - k_s a_s (C_L - C_s) \right)$$

$$\frac{\partial f_1}{\partial C_s} = -k_s a_s \frac{\partial}{\partial C_s} (C_L - C_s) = -k_s a_s = A(u_L)$$
(R.5)

When the same procedure is repeated with equation (7.3) the results below are obtained

$$\frac{\partial f_2}{\partial u_L} = \frac{\partial}{\partial u_L} \left(k_s a_s \left(C_L - C_s \right) - k \eta f C_s \right)$$

$$\frac{\partial f_2}{\partial u_L} = \left(C_L - C_s \right) \frac{\partial k_s a_s}{\partial u_L} - k \eta C_s \frac{\partial f}{\partial u_L} = B \left(C_L, C_s, u_L \right)$$

$$\frac{\partial f_2}{\partial C_L} = \frac{\partial}{\partial C_L} \left(k_s a_s \left(C_L - C_s \right) - k \eta f C_s \right)$$

$$\frac{\partial f_2}{\partial C_L} = k_s a_s = A \left(u_L \right)$$
(R.7)

$$\frac{\partial f_2}{\partial C_s} = \frac{\partial}{\partial C_s} \left(k_s a_s \left(C_L - C_s \right) - k \eta f C_s \right)$$

$$\frac{\partial f_2}{\partial C_s} = k_s a_s - k \eta f = A(u_L)$$
(R.8)

Equations (R.3) to (R.8) show based on the criteria of Table 2.6 that the trickle-bed reactor system can be classified as a nonlinear system under nonlinear control. Therefore improvement may be possible under periodic operation.

Calculation of Catalyst External Wetting from Tracer Experimental Data

The relationship between catalyst external wetting and liquid flow rate was determined using the technique described by Colombo et al. (1976). The procedure involved tracer experiments in a trickle-bed replica, followed by the determination of the first and second moments of concentration vs. time profiles generated from the tracer experiments. A typical concentration vs. time profile is shown in Figure S.1.

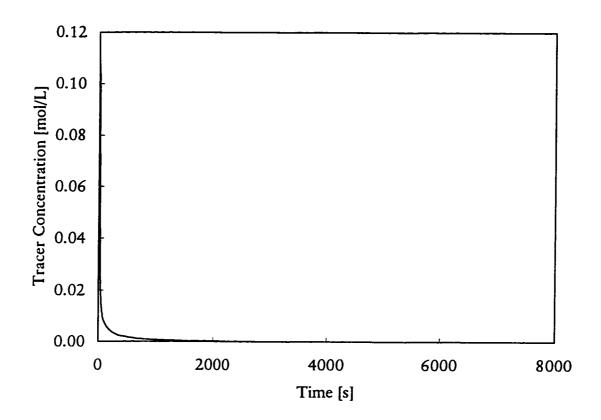


Figure S.1 Typical concentration vs. time profile from a tracer experiment; liquid flow rate: 480 mL/min

Two types of experiments were conducted - liquid upflow where it could be assumed that catalyst external wetting was complete, and trickle flow (downward liquid flow) where the external surface of the catalyst could be partially wetted.

To model the tracer concentration in the packed bed, Colombo et al. (1976) used two mass balances, one for the tracer in the flowing liquid and another for the tracer in the particle. The zeroth and first moments were then determined to be

APPENDIX S 209

$$M_0 = 1 + \frac{A}{3} \varepsilon_i \left(1 + \rho_L \beta \frac{1 - \varepsilon_i}{\varepsilon_i} \right)$$
 (S.1)

$$M_{1} = \left[\frac{1}{2} + \frac{1}{Pe} - \frac{1}{Pe^{2}} \left(1 - e^{-Pe}\right)\right] M_{0}^{2} + A \frac{r_{\rho}^{2} u \varepsilon_{i}}{D_{i} L} \left(1 + \rho_{L} \beta \frac{1 - \varepsilon_{i}}{\varepsilon_{i}}\right)^{2} \left(\frac{1}{45} + \frac{D_{i}}{9k_{s} r_{p}}\right)$$
(S.2)

where D_i is the internal diffusivity (diffusivity in the catalyst particles), β is the adsorption equilibrium constant of the tracer, r_p is the particle radius, u is the liquid effective velocity defined as

$$u = \frac{u_L}{\varepsilon} \tag{S.3}$$

for the liquid full reactor and

$$u = \frac{u_L}{\omega \varepsilon} \tag{S.4}$$

for the trickle-bed reactor.

The parameter A is defined as

$$A = \frac{3(1-\varepsilon)}{\varepsilon} \tag{S.5}$$

for the liquid full reactor and

$$\Lambda = \frac{3(1-\varepsilon)}{0\varepsilon} \tag{S.6}$$

By calculating the moments for the liquid-full reactor and the trickle-bed reactor, the diffusivity D_i is estimated for each. The ratio of the two can then be used to estimate the external catalyst wetting. That is

$$f = \frac{D_{i,TBR}}{D_{i,LF}} = \frac{D_{i,app}}{D_i}$$
 (S.7)

REFERENCE LIST

Bailey, J.E., and F.J.M. Horn, "Improvement of the Performance of a Fixed-Bed Catalytic Reactor by Relaxed Steady State Operation", AIChE J., 17, 550 (1971).

Bailey, J.E., F.J.M. Horn, and R.C. Lin, "Cyclic Operation of Reaction Effects of Heat and Mass Transfer Resistance", AIChE J., 17, 818 (1971).

Bailey, J.E., "Periodic Operation of Chemical Reactors: A Review", Chem. Eng. Commun., 1, 111 (1973).

Castellari, A.T. and P.M. Haure, "Experimental Study of the Periodic Operation of a Trickle-Bed Reactor", AIChE J., 41, 1593 (1995).

Colombo, A.J., G. Baldi, and S. Sicardi, "Solid-Liquid Contacting Effectiveness in Trickle Bed Reactors", *Chem. Eng. Sci.*, 31, 1101 (1976).

Cordova, W.A., and P. Harriot, Chem. Eng. Sci., 30, 1201 (1975).

Davis, M.E., Numerical Methods & Modeling for Chemical Engineers, John Wiley & Sons, New York, NY, pp. 128-156, 1984.

Daubert, T.E., Physical and Thermodynamic Properties of Pure Chemicals: Data Compilation, Hemisphere Publishing Corporation, New York, NY, 1989.

Draper, N., and H. Smith, Applied Regression Analysis, 2nd ed., John Wiley & Sons, New York, NY, p. 144, 1981.

Dudukovic, M.P., "Catalyst Effectiveness Factor and Contacting Efficiency in Trickle-Bed Reactors", AIChE J., 23, 940 (1977).

Dudukovic, M.P., and P.L. Mills, "Chemical and Catalytic Reactor Modeling", ACS Symposium Series, 237, 37 (1984).

Fogler, H.S., Elements of Chemical Reaction Engineering, Prentice-Hall, Englewood Cliffs, New Jersey, pp. 610-622, 1986.

Frye, C.G., and J.F. Mosby, "Kinetics of Hydrodesulfurization", Chem. Eng. Prog., 63, 66 (1967).

Furzer, I.A., and R.W. Michell, "Liquid-Phase Dispersion in Packed Beds with Two-Phase Flow", AIChE J., 16, 380 (1970).

REFERENCE LIST 211

Gates, B.C., J.R. Katzer, and G.C.A. Schuit, *Chemistry of Catalytic Processes*, McGraw-Hill Inc., New York, NY (1979).

Gianetto, A., and P.L. Silveston, Multiphase Chemical Reactors: Theory, Design, Scale-up, Hemisphere Publishing Corporation, Washington, D.C., pp. 289-349, 1986.

Gianetto, A., and V. Specchia, "Trickle-Bed Reactors: State of Art and Perspectives", Chem. Eng. Sci., 47, 3197 (1992).

Goto, S., and J.M. Smith, "Trickle-Bed Reactor Performance Part I. Holdup and Mass Transfer Effects", AIChE J., 21, 706 (1975a).

Goto, S., and J.M Smith, "Trickle-Bed Reactor Performance Part II. Reaction Studies", AIChE J., 21, 714 (1975b).

Goto, S., S. Watanabe, and M. Matsubara, Can. J. Chem. Eng., 54, 551 (1976).

Hasokowati, W., R.R. Hudgins, and P.L. Silveston, "Loading, Draining and Hold-up in Periodically Operated Trickle-Bed Reactors", Can. J. Chem. Eng., 7, 405 (1994).

Haure, P., R.R. Hudgins, and P.L. Silveston, "Periodic Operation of a Trickle-Bed Reactor," AIChE J., 35, 1437 (1989).

Herskowitz, M., and J.M. Smith, "Trickle-Bed Reactors: A Review", AIChE J., 29, 1 (1983).

Hochman, J.M., and E. Effron, "Two-phase cocurrent downflow in packed beds", *I&EC Fund.*, 8, 63 (1969).

Hofmann, H., in Gianetto, A., and Silveston, P.L. (editors), Multiphase Chemical Reactors, p. 257, 1986.

Kenney, C.N., and W. Sedriks, "Effectiveness factors in a three-phase slurry reactor: the reduction of crotonaldehyde over a palladium catalyst", *Chem. Eng. Sci.*, 27, 2029 (1972).

Koros, R.M., in Proceedings of the 4th International 16th European Symposium on Chemical Reaction Engineering, p. 372, Heidelberg, April, 1976.

Lange, R., Hanika, D., Stradiotto, D., Hudgins, R.R., and P.L. Silveston, "Investigations of Periodically Operated Trickle-Bed Reactors", Chem. Eng. Sci., 49, 5615 (1995).

Lannus, A., and L.S. Kershenbaum, "On the Cyclic Operation of Tubular Reactors", AIChE J., 16, 329 (1970).

Larachi, F., A. Laurent, N. Midoux, and G. Wild, "Experimental Study of a Trickle-bed Reactor Operating at High Pressure: Two-phase Pressure Drop and Liquid Saturation", Chem. Eng. Sci., 46, 1233 (1991).

Lee, C.K., and J.E. Bailey, "Modification of Consecutive-Competitive Reaction Selectivity by Periodic Operation", *Ind. Eng. Chem. Process Des. Dev.*, 19, 160 (1980).

Mears, D.E., "The role of axial dispersion in trickle-flow laboratory reactors", Chem. Eng. Sci., 26, 1361 (1971).

Mills, P.L., and M.P. Dudukovic, "Evaluation of Liquid-Solid Contacting in Trickle-Bed Reactors by Tracer Methods", AIChE J., 27, 893 (1981).

Mills, P.L., and M.P. Dudukovic, "A Comparison of Current Models for Isothermal Trickle-bed Reactors: Application to a Model Reaction System", in "Chemical and catalytic reactor modeling", ACS Symp. Series, 185th Meeting, (1984), pp. 37-59.

Michell, R.W., and I.A. Furzer, "Mixing in trickle flow through packed beds", Chem. Eng. J., 4, 53, 1972.

Myers, E.C., and K.K. Robinson, "Multiphase Kinetic Studies with a Spinning Basket Reactor", 5th International Symposium on Chemical Reaction Engineering, 447 (1978).

Perry, R.H., D.W. Green, and J.O. Maloney (eds.), Perry's Chemical Engineer's Handbook 6th Edition, McGraw-Hill, New York, NY, p. 3-102, 1984.

Press, W.H., B.P. Flannery, S.A. Teukolsky, W.T. Vetterling, *Numerical Recipes in C The Art of Scientific Computing*, Cambridge University Press, New York, NY, pp. 648-649, 1990.

Ramachandran, P.A., and Chaudhari, R.V., *Three-phase Catalytic Reactors*, Gordon Breach and Science Publishers, New York, NY, pp. 200-255, 1983.

Reid, C.R., J.M. Prausnitz, and B.E. Poling, *The Properties of Gases and Liquids*, 4th ed., McGraw-Hill, New York, NY, p. 598, 1986.

Rylander, P.N., Catalytic hydrogenation over platinum metals, Academic Press, New York, NY, 1967.

Sater, V.E., and O. Levenspiel, "Two-phase flow in packed beds", *I&EC Fund.*, 5, 86 (1966).

REFERENCE LIST 213

Satterfield, C.N., "Trickle-Bed Reactors", AIChE J., 21, 209 (1975).

Satterfield, C.N., Heterogeneous Catalysis in Industrial Practice, 2nd ed., McGraw-Hill Inc., New York, NY, p. 491, 1991.

Satterfield, C.N., Mass Transfer in Heterogeneous Catalysis, M.I.T. Press, Cambridge, Massachusetts, p. 20, 1970.

Schädlich, K., U. Hoffman, and H. Hoffman, "Periodical Operation of Chemical Processes and Evaluation of Conversion Improvements," *Chem. Eng. Sci.*, 38, 1375 (1983).

Schiesser, W.E., The Numerical Method of Lines: Integration of Partial Differential Equations, Academic Press Inc., San Diego, CA, pp. 97-141, 1991.

Schneider, G.E., Introduction to Finite Element Analysis, ME 559 Course Notes, 1996.

Sedriks, W., and C.N. Kenney, "Partial wetting in trickle bed reactors - the reduction of crotonaldehyde over a palladium catalyst", *Chem. Eng. Sci.*, 28, 559 (1973).

Shah, Y.T., Gas-Liquid-Solid Reactor Design, McGraw-Hill Inc., New York, NY, pp. 180-229, 1979.

Silebi, C.A., and W.E. Schiesser, Dynamic Modeling of Transport Process Systems, Academic Press Inc., San Diego, CA, pp. 202-244, 1992.

Silveston, P.L., Unpublished work, (1994).

Streeter, V.L., and E.B. Wylie, Fluid Mechanics First SI Metric Edition, McGraw-Hill Ryerson Limited, Toronto, ON, p. 534, 1981.

Sylvester, N.D., K.K. Kulkami, and J.J.Carberry, Can. J. Chem. Eng., 53, 313 (1975).

Thullie, J., L. Chiao, and R.G. Rinker, "Production Rate Improvement in Plug-Flow Reactors with Concentration Forcing", *Ind. Eng. Chem. Res.*, 26, 945 (1987).

Tjebbes, J., "Heats of Combustion of Butanal and Some Related Compounds", Pure Appl. Chem., 2, 129 (1961).

Wakao, N., and Kaguei, S., Heat and Mass Transfer in Packed Beds, Gordon and Breach Science Publishers, New York, NY, 1982.

NOMENCLATURE

Roman symbols

```
A
         amplitude of a pulse
a_i, a_i
         interfacial area [m²/m³]
a_c, a_s liquid-catalyst (liquid-solid) contact area [m<sup>2</sup>]
         catalyst external surface area [m<sup>2</sup>]
A_{CE}
Во
         Bodenstein number
C_e
         concentration at reactor exit [mol/L]
C_f
         concentration at reactor entrance [mol/L]
        concentration of species i at the gas side of the gas-liquid interface [mol/L]
C_{i,Gi}
        concentration of species i at the liquid side of the gas-liquid interface [mol/L]
C_{i,Li}
        concentration of species i at the liquid side of the liquid solid interface [mol/L]
C_{i,S}
D_L
        liquid phase diffusivity [m<sup>2</sup>/s]
d_p
         effective particle diameter [mm]
D_r
         radial dispersion coefficient [m²/s]
D_z
        axial dispersion coefficient [m<sup>2</sup>/s]
E_{a}
        activation energy [J/mol]
        catalyst external wetting factor
Fr
        Froude number
G
        superficial gas mass velocity [kg m<sup>-2</sup> s<sup>-1</sup>]
G_{L}
        superficial liquid mass velocity [kg m<sup>-2</sup> s<sup>-1</sup>]
H
        Henry's law constant [atm/mol frac.]
k_{app}
        apparent rate constant [s<sup>-1</sup>]
k_L
        gas-liquid mass transfer coefficient [s<sup>-1</sup>]
k_o, k_s
        liquid-solid mass transfer coefficient [s-1]
k,
        reaction rate constant [s<sup>-1</sup>]
L
        reactor length [cm]
L
        superficial liquid mass velocity [kg m<sup>-2</sup> s<sup>-1</sup>]
n
        reaction rate order
P
        pressure [MPa]
Pe
        Peclet number
        radial position [cm]
        crotonaldehyde reaction rate [mol m<sup>-3</sup> s<sup>-1</sup>]
r<sub>CRHO</sub>
Re
        Reynolds number
        cycle split in periodic operation
SV
        space velocity [s<sup>-1</sup>]
T
        temperature [°C]
        time [s]
и
        superficial velocity [cm/s]
        time-average volumetric liquid flow rate [cm<sup>3</sup>/s]
v_L
        trickle-bed reactor volume [m3]
V_{TRR}
        Weber number
We
```

NOMENCLATURE 215

- X conversion
- X_{P} conversion under periodic operation
- X_{ss} conversion at steady-state
- z axial position [cm]

Greek letters

- β_{LD} dynamic liquid holdup
- β_s total static liquid holdup
- δ path length for diffusion [m]
- ΔH_R heat of reaction [kJ/mol]
- ε_B bed porosity [m³/m³]
- η catalyst internal effectiveness factor
- η_c catalyst external wetting factor
- λ_{eff} effective bed thermal conductivity [W/m·K]
- ν reaction species stoichiometric coefficient
- ρ_P catalyst skeletal density [g/cm³]
- μ_L absolute viscosity [Pa·s]
- τ space-time [s]

Subscripts

- A species A
- app apparent
- a activation
- B bed; species B
- c catalyst
- CE catalyst external
- *eff* effective
- eo based on total cross-sectional area of catalyst
- G gas
- L liquid
- LD liquid dynamic
- LF liquid full
- LSE liquid static external
- P periodic operation
- r radial direction
- S solid
- SS steady-state
- TBR trickle-bed reactor
- z axial direction